



Universitetet
i Stavanger

FACULTY OF SCIENCE AND TECHNOLOGY

MASTER'S THESIS

Study programme/specialisation: Konstruksjoner og materialer – Maskinkonstruksjoner	Spring semester, 2017 Open/ Confidential
Author: Mats Røed Jørgensen (signature of author)
Programme coordinator: Vidar Hansen Supervisor(s): Cathrine Hartung	
Title of master's thesis: Evaluation of Ductile Iron for Offshore Application	
Credits: 30	
Keywords: <i>Ductile iron</i> <i>Welded steel</i> <i>Fracture surface</i> <i>Charpy impact test</i> <i>Fracture toughness</i>	Number of pages: 102 + supplemental material/other: 8 Stavanger, 15.06.2017



Universitetet
i Stavanger

Master Thesis

**Evaluation of Ductile Iron for
Offshore Application**

Mats Røed Jørgensen

*Dept. of Mechanical and Structural Engineering and
Materials Science*

University of Stavanger

15th June 2017

Acknowledgment

This master thesis is written during the spring of 2017, as a part of my studies for a Master of Science degree at the University of Stavanger.

I would like to thank Cathrine Hartung at Elkem Foundry Products, for the opportunity to work on this subject, and providing highly appreciated knowledge and support during this work. She is also to thank for involving me in the professional everyday life of a engineer, by inviting me to meetings and foundry visits. The process of working together with Elkem on this thesis has been a valuable learning experience. I would also like to thank Jan Kåre Helle and the boys at Mandal Castings, for providing me with the sufficient materials and showing me, hands-on, the art of producing cast iron.

My gratitude does also go to Professor Vidar Folke Hansen for his support, and for sharing his knowledge and experience regarding this type of work.

I would like to thank my fellow students and friends, for valuable motivation, sharing of knowledge, late hours and good laughs. Not only for the last couple of months, but throughout all 5 years at the University of Stavanger.

Finally I would give special gratitude to my family and girlfriend, for their love and support that has kept me going through challenging times.

Mats Røed Jørgensen

Stavanger, 15th June 2017

Abstract

The possibility of using ductile iron as a construction material for offshore applications have been investigated. If ductile iron is considered as being a substitute material for welded steel, it can create a larger freedom for engineers in a design process as well as provide benefits regarding strength and cost. The issue of getting ductile iron approved as a reliable substitute material for steel is a statement made by DNV GL, being that cast irons normally should not be used with minimum design temperature below 0°C. This statement is mostly based on the perception of cast iron being brittle i lower temperatures.

Based on this statement ductile iron has been evaluated with regard to toughness properties determined by both a Charpy impact test and a fracture toughness test. This is mainly done to investigate whether the values gathered from a impact test give a realistic picture of ductile irons toughness, when compared to a selected grade of steel. This is done of three materials, named 400-18LT, 500-14, and 500-7. Included is also a study concerning fracture behavior in various ductile irons microstructures. To declare ductile iron as sufficient for offshore applications have a value of minimum fracture toughness been set.

The results show that mechanical properties in ductile iron is highly dependent on microstructural mechanics and chemical composition. Achievable by a well planned and correctly performed production process, especially when it comes to quality and holding time of inoculants. It is also apparent that the Charpy impact test is not suitable when evaluating ductile irons, mainly due to the material's notch- and strain rate sensitivity.

It is concluded that the 500-14 material is the only material declared being sufficient according to the listed requirements. This result clearly illustrates the positive effects of using Silicon as a ferrite strengthener. Pearlite was observed being damaging to toughness properties, especially at lower temperatures, and should be kept at a minimum for the reviewed area of use. 400-18LT displayed lower than expected fracture toughness results, despite performing well regarding impact energy. The reason for this has been concluded being connected to a degenerated inoculation effect.

Contents

1	Introduction	1
1.1	Background	2
1.2	Objective	3
1.3	Outline of Thesis	4
2	Theory	5
2.1	Cast iron	5
2.1.1	Fe-C Phase Diagram	6
2.1.2	Fe-C-Si	7
2.1.3	Carbon Equivalent	8
2.1.4	Types of Cast Iron	8
2.2	Ductile Iron	9
2.2.1	Spherodization	10
2.2.2	Inoculation	11
2.2.3	Microstructure	12
2.2.4	Chemical Composition of Ductile Iron	17
2.3	Offshore Application	20
2.3.1	Ductile Iron vs. Steel	21
2.3.2	Casting vs. Welding	23
2.3.3	Ductile-to-brittle Transition Temperature	25
2.4	Fracture Mechanics	26
2.4.1	Fracture Behavior	27
2.4.2	Fracture toughness	31
2.5	Test Methods	32
2.5.1	Mechanical Properties	32
2.5.2	Microstructure	37
2.5.3	Chemistry	38
2.5.4	Scanning Electron Microscope	38

3 Literature study	41
3.1 Evaluation of Charpy Impact Testing on Ductile Iron	41
3.2 Fracture Toughness	44
3.3 Effect of Silicon	47
3.4 Effect of Ferrite and Pearlite on Impact and Fracture Properties	49
3.5 Mechanical Behavior of Graphite Nodules	51
4 Fracture Surface Study	53
4.1 Materials	53
4.2 Experimental	56
4.3 Results	56
4.3.1 Microstructure	56
4.3.2 Fracture Surface	58
4.4 Discussion	61
5 Materials	63
5.1 Mechanical properties	64
5.2 Chemical composition	64
5.3 Microstructure	65
6 Experimental	67
6.1 Casting	67
6.2 Machining	69
6.3 Tensile testing	70
6.4 Charpy Testing	70
6.5 Fracture Toughness Testing	71
6.6 Microstructural Analysis	72
7 Analysis	73
7.1 Mechanical, Chemical and Microstructural Properties	73
7.2 Charpy Impact Test	76
7.2.1 V-notched Test Samples	77
7.2.2 Unnotched Test Samples	79

7.3	Fracture Toughness	81
7.3.1	Relationship Between Charpy-V and Fracture Toughness	86
8	Discussion	89
8.1	EN-GJS-400-18LT	89
8.2	EN-GJS-500-14	90
8.3	EN-GJS-500-7	92
8.4	Offshore Application	93
9	Conclusion	95
10	Further Work	97
	Bibliography	98
A	Microstructural Reports	103
A.1	EN-GJS-400-18LT	103
A.2	EN-GJS-500-14	104
A.3	EN-GJS-500-7	105
B	Chemical Analysis Reports	106
B.1	EN-GJS-400-18LT	106
B.2	EN-GJS-500-14	107
B.3	EN-GJS-500-7	108
C	Tensile Testing Reports	109
C.1	EN-GJS-400-18LT	109
C.2	EN-GJS-500-14	110

List of Figures

2.1	Iron-Carbon phase diagram	6
2.2	Difference between uninoculated and inoculated ductile iron	11
2.3	Image of a well developed graphite nodule in a ferritic matrix with traces of pearlite	13
2.4	Distributions of ferrite and pearlite in ductile iron	15
2.5	Tables illustrating the correlation between mechanical properties and nodularity	17
2.6	Trace elements effect on the Fe_3C eutectic temperature	19
2.7	Typical ductile-to-brittle transition diagram for a ferritic material	25
2.8	Modes of loading and corresponding fracture	27
2.9	Illustration of the two brittle fracture modes	28
2.10	Ductile and brittle fracture mode in tensile bars	29
2.11	Image showing both ductile and brittle fracture features	30
2.12	Through-thickness crack in an infinite plate	31
2.13	Charpy V-notch specimen and testing machine	34
2.14	SE(B) test specimen geometry	35
2.15	Load vs crack opening displacement curves showing three types of fracture behavior	36
2.16	SE(B) test rig	36
2.17	Positioning of clip gauge in a SE(B) specimen	37
3.1	Schematic illustration of notch sensitivity in ductile iron	42
3.2	Fracture toughness of various ductile irons	44
3.3	Relationship between impact energy and fracture toughness for steels	45
3.4	Relationship between impact energy and fracture toughness for welded S355 steel	46
3.5	Influence of Si content on Charpy V impact energy of ferritic ductile iron	48
3.6	Impact properties on ductile iron with increasing volume of ferrite	50

3.7	Decohesion of graphite nodule and matrix during tensile test	52
4.1	4 tensile bars used in fracture surface study	55
4.2	Fracture surface of the 4 cut tensile bars	55
4.3	Representative image of microstructure	57
4.4	Fracture surface at a magnification of 200x	59
4.5	Fracture surface at a magnification of 1000x	60
6.1	Sketch illustrating placement of the given number of samples in the cast mould	68
6.2	Finished cast sample	69
6.3	Model for machining the different test specimens	69
6.4	Fracture toughness test setup	72
7.1	Representative image of the microstructure of the three materials	75
7.2	V-notched test results	77
7.3	Image of the V-notched impact test specimens	78
7.4	Unnotched test results	80
7.5	Image of the Unnotched impact test specimens	81
7.6	Fracture toughness at the two temperatures	82
7.7	Load vs. displacement curve of 400-18 at two temperatures	84
7.8	Load vs. displacement curve of 500-14 at two temperatures	85
7.9	Load vs. displacement curve of 500-7 at two temperatures	85
7.10	Comparison of fracture toughness and impact energy at 20°C	86

List of Tables

2.1	Difference in the carbon-rich phase of cast irons	9
2.2	Damaging graphite structure	14
2.3	Comparison between ferrite and pearlite in ductile iron	15
2.4	Comparison of ductile iron and cast steel	22
2.5	Comparison of ductile iron and structural steel	23
3.1	Test results with increasing wt% Si	47
4.1	Mechanical properties of tensile tested materials	54
4.2	Chemical composition of tensile tested materials	54
4.3	Mircostructural characteristics of the FR-materials	57
5.1	3 different grades of ductile iron	63
5.2	Minimum requirements for given materials	64
5.3	Standard amount of Si and C	65
7.1	Results from tensile test	73
7.2	Chemical analysis	74
7.3	Microstructural analysis	74
7.4	V-notched impact test results	77
7.5	Unnotched impact test results	79
7.6	Fracture toughness test results	82
7.7	Percentage difference between Charpy-V impact values and K_{Ic}	87
8.1	Evaluation of mechanical properties to be evaluated for offshore application	93

Nomenclature

Acronyms

CE	Carbon Equivalent
CTOD	Crack Tip Opening Displacement
HAZ	Heat Affected Zone
SEM	Scanning Electron Microscope
wt%	Weight Percentage

Elements

Ba	Barium
Bi	Bismuth
Ca	Calcium
C	Carbon
Ce	Cerium
Co	Cobalt
Cr	Cromium
Cu	Copper
Fe	Iron
Mg	Magnesium
Mn	Manganese
Mo	Molybdenum
Ni	Nickel
O	Oxygen
Pb	Lead
P	Phosphorus
Sb	Antimony
Se	Selenium
Si	Silicon
Sn	Tin
Sr	Strontium
S	Sulphur

Ti	Titanium
V	Vanadium
Y	Yttrium
Zn	Zinc
Zr	Zirconium

1. Introduction

The engineering industry is constantly evolving. New requirements, demands and challenges arise every day. Products always need to improve, get better, lighter, cheaper and greener. Optimization is what drives technology, and what paints the future of engineering. The offshore industry today is dependent on optimization, now more than ever. The innovative ability of evolving designs that is lightweight, efficient and sustainable, is crucial to succeed. The engineer's challenge is to find the solutions that will optimize a process. To design the products that will cost less to manufacture, and to study the materials that can contribute to optimization without negatively affect the structural integrity of a component.

The pressing optimization demands in the industry, necessitates and motivates an expand of material selection. Choosing the most suitable material when designing a new mechanical component defines what production process should be used, at what cost, and ultimately, the final design of the component. When it comes to the offshore industry, where steels are the dominant and preferred construction material, an optimization solution could be to find a substitute material, providing benefits regarding strength, weight and production cost.

Today many offshore components are produced by welded steel. Some qualities of steel used in specific applications has comparable properties of strength as some ductile cast iron grades available. However, cast irons is usually not considered as a substitute for steel because of the common perception of cast being a brittle material.

1.1 Background

The background for this thesis is that Elkem Foundry Products, who develop, produce and sell speciality ferroalloys for production of cast iron worldwide, are providing consultation regarding getting ductile iron approved as being a sufficient construction material intended to be used for crane sheaves. One of the strategic goals of Elkem Foundry Products is to promote cast iron as construction material. To facilitate this they look for potential new segments where cast iron can be used successfully, and for partners that are interested in evaluating cast iron in new applications. In one of these partnerships, the potential to qualify ductile cast iron as a replacement of welded steel in crane sheaves was identified.

In the case of the crane sheaves the combination of ductile iron grade 500-7 and casting as production method offered a solution with higher strength properties compared to the steel equivalent, allowing for thinner and lighter component, easier production and simplified quality assurance. The only obstacle left was to get the ductile cast iron accepted as a substitution by the end customer and standardization body for the component, was to demonstrate that it complies with the applicable standard and rule, in this case, DNV GL and DNVGL-OS-E101.

DNVGL-OS-E101, which is applicable to drilling facilities located on floating offshore units and on fixed offshore installations of various types(quote), states in [2.5.1] that:

"Cast iron shall not be used for critical parts with MDT below 0° C unless specifically justified and agreed between all parties."

This statement demonstrates the established perception that cast iron is a brittle material. While it does open for the possibilities of ductile iron being evaluated, it does not clearly present any minimum requirements.

The common perception of ductile cast iron being insufficient for low temperature working environments is likely connected to the low values of impact energy observed from a Charpy-V test method. A test method developed for determining toughness and ductile-to-brittle behavior of steel, giving a energy value often being used as a qualification requirement for steels. However, this test method does not give a mechanical property usable in a design process, nor does it provide a realistic description of toughness, or crack growth, in ductile irons.

1.2 Objective

The objective of this thesis is to highlight the mechanical properties and fracture behavior in ductile irons, with a focus on microstructural features and toughness properties.

The main evaluation will be based on three types of ductile iron:

1. 400-18LT which is a material already being used in the offshore wind turbine industry
2. 500-7 being supplied by a crane producers to be evaluated for use as a construction material for sheaves
3. 500-14 being a material solution strengthened by Silicon that can potentially, due to its higher strength expand the use of ductile iron and which is under consideration as replacement for 400-18LT in wind turbine applications

The purpose of the study is to provide a basis for evaluating the 3 materials as potential substitution for welded steel in offshore application and in relation to the requirements in DNVGL-OS-E101.

Theoretical background and a literature study of the related topic will provide the necessary knowledge sufficient to make a correct interpretation and evaluation of the results.

Another area of focus will be to evaluate the perception of brittleness and fracture behavior between the two test methods, Charpy impact test and fracture toughness, to highlight the notch sensitivity present in ductile iron, as well as the general accuracy of the Charpy impact test when evaluating ductile iron.

In addition, the purpose is also to achieve a greater understanding of solution strengthened ductile iron's fracture behavior. This will be done by studying fracture surfaces from torn tensile bars. As the production of test materials took longer time than expected this study was conducted on equivalent material samples.

1.3 Outline of Thesis

Chapter 1 is an introduction to the thesis work conducted, with motivation, background and the objective of the work.

Chapter 2 introduces the relevant background theory sufficient for the further discussion.

Chapter 3 presents relevant studies to create a larger understanding of mechanics of ductile iron.

Chapter 4 presents and discuss fracture surface mechanics, to highlight effect of Silicon, matrix and graphite structure.

Chapter 5 introduces a overview of the three material being evaluated.

Chapter 6 describes the processes of production and testing procedures.

Chapter 7 presents the results gathered form the various tests and analyses.

Chapter 8 discuss the results presented in Chapter 7, based on the objective.

Chapter 9 presents the conclusion based on the scope of the project and the discussed results.

Chapter 10 presents suggestions of future studies needed for a larger understanding of the present objective.

2. Theory

This chapter consist of sections describing and explaining the relevant background theory, being sufficient for the basic understanding og the following study, results and discussion.

2.1 Cast iron

Cast iron is defined as a Fe-C-Si alloy with Carbon (C) contents above 2.14 wt%. However, most of cast irons contain between 2.5 and 4% C. This high C content makes cast irons take advantage of eutectic solidification that similar materials, such as steel, does not. This solidification process makes cast iron excellent for production through casting, hence the name. Cast iron, when molted, possess a high fluidity and the ability to fill intricate moulds. These properties make cast iron a good material when producing complex components, in all sizes. Most casted components require little finishing and post-production treatment, which can make cast iron casting preferable against other materials and fabrication techniques.

Cast iron is the general name of a large family of materials, differentiated by how the carbon forms during solidification. Consistent in all types of cast iron is the microstructural formation of a carbon-rich phase existing in a metallic matrix. The two most common types are gray iron and ductile iron, where the main difference between the two is the graphite structure. In gray iron the graphite appears as flakes in the metallic matrix, whereas in ductile iron the graphite forms spherical nodules (Callister and Rethwisch, 2011).

Cast iron is produced by melting scrap iron, pig iron or steel scrap in a cupola- or an induction furnace. It is mostly the composition of alloying elements in the melt as well as the cooling rates that define the microstructure and mechanical properties of the resulting cast iron.

2.1.1 Fe-C Phase Diagram

Cast irons are similar to steels in the way that they are both an iron-carbon system. The biggest difference between the two materials is the carbon content. The amount of carbon in steels are rarely greater than 1.0 wt%. As seen in the iron-carbon phase diagram (Figure 2.1), face centered cubic austenite phase exist at maximum 2.1 % carbon. If the carbon content is above this percentage, the structure changes into both the austenitic phase as well as a carbon-rich phase consisting of either stable graphite or the metastable phase cementite (Fe_3C). This specific structure is what makes cast iron.

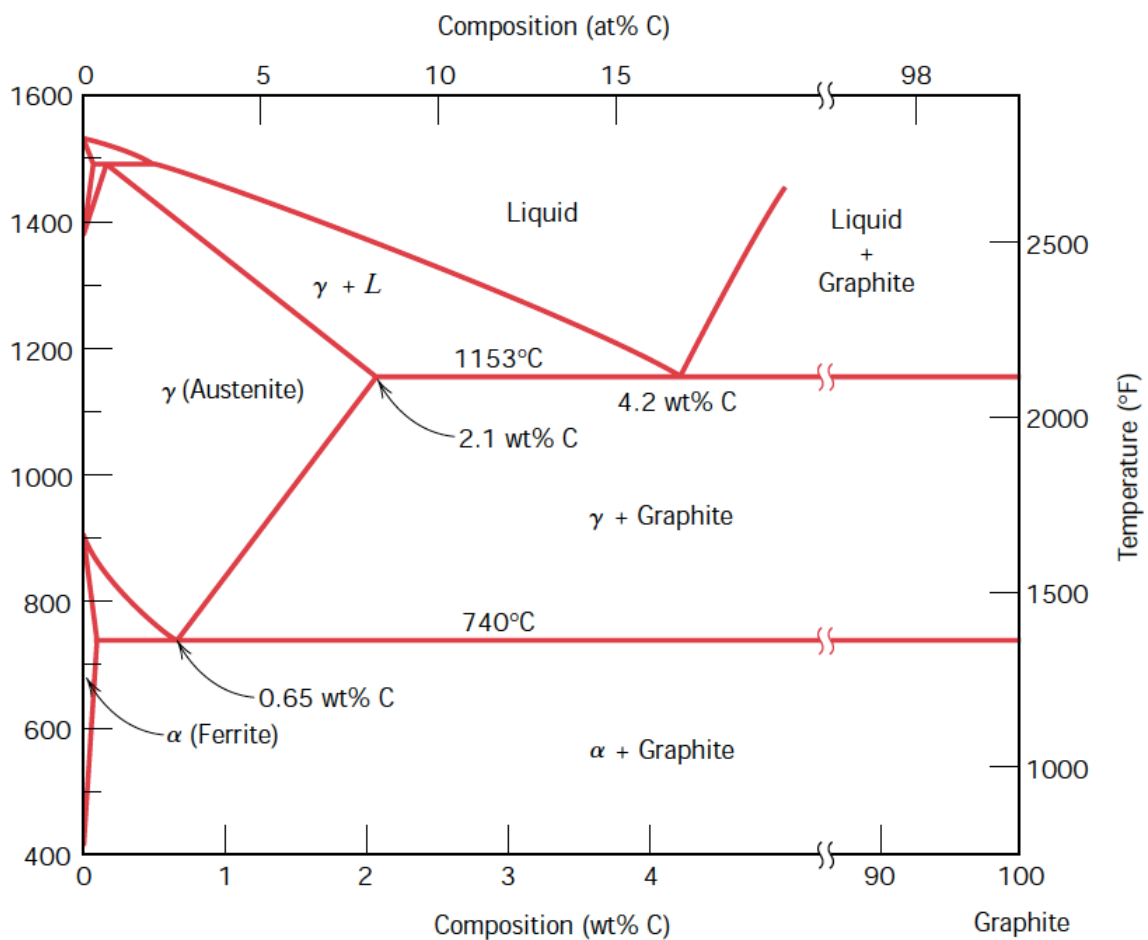


Figure 2.1: Iron-Carbon phase diagram (Callister and Rethwisch, 2011)

The eutectic point, which is the lowest temperature of solidification for a mixture of materials, is at 4.26 wt% C and 1148 °C for cast iron. Higher C percentage increases the temperature of solubility of graphite in liquid iron. When the liquid iron is poured into a cast and cools down, the solidification process starts. The phase diagram show that liquid iron with

higher carbon content than 2.1 wt% starts to solidify below the liquidus line, which varies with increasing carbon content. In this phase the formation of austenite dendrites starts (also called proeutectic austenite). The newly formed austenite grains have the ability to eject excess carbon, meaning that the carbon content in the remaining liquid increases until the melt reaches the eutectic temperature. Cast irons characteristic carbon-rich phase solidifies either to thermodynamically stable graphite or metastable cementite (Fe_3C), depending on the composition, cooling rate and melt treatment. The eutectic temperature for graphite is 1154°C while the temperature for cementite is 1148°C . This means that the phase-structure of cast iron in this temperature range is either a mixture of Fe_3C carbide in austenite or a mixture of graphite in austenite. After further cooling below the eutectoid temperature, which is 738°C for graphite and 727°C for cementite, the austenite transforms into ferrite and/or pearlite.

Whether the cast irons carbon-rich phase transforms into graphite or cementite defines if the resulting iron is characterized as gray or white cast irons. These two types of cast iron are different materials with different properties. The name originates from the color of the fracture surface. Cast iron with austenite-graphite eutectic has a gray fracture surface appearance while the austenite- Fe_3C structure has a white color. The process of creating gray or white iron is amongst other factors defined by cooling rates. The graphite in gray iron forms with slow cooling rates from the eutectic temperature. If the cooling is too rapid, the graphite will not have sufficient time to form and the result will be a cementite structure. (Reardon, 2011)

2.1.2 Fe-C-Si

In addition to consisting of a high value of C, cast irons are also greatly affected by the addition of Silicon (Si). Normal Si contents in cast irons are so substantial that cast irons need to be regarded as a Fe-C-Si alloy. Adding Si to a Fe-C alloy material will result in the following outcomes(Elkem AS, 2017):

- The eutectic and eutectoid temperatures change from a single value to a temperature range
- Decreased stability of cementite

- Increased stability of ferrite
- Decreasing eutectic and eutectoid C content
- Increased eutectic and eutectoid temperature

2.1.3 Carbon Equivalent

The carbon equivalent (CE) is an important value to be considered when producing cast iron. It immediately indicates whether a iron is hypoeutectic, eutectic or hypereutectic based on the calculated value being < 4.3 , equal to 4.3 or > 4.3 , respectively. The CE value are calculated by the relationship in Eq. 2.1.

$$CE = \%C + \frac{1}{3}(\%Si + \%P) \quad (2.1)$$

This is an important feature to define, because as well as determining the solidification point of the melt, it is also a contributor in whether the final cast iron solidifies into gray, white or mottled eutectic. The CE relationship is based on three elements being crucial to control in order to achieve proper solidification and performance.

2.1.4 Types of Cast Iron

General processing of cast iron will normally result in either gray or white iron depending on the resulting structure of the carbon-rich phase in the melt. Graphite in the shape of flakes gives gray iron, and cementite in a ferrite or pearlite matrix gives a white color and therefore white iron. Other compositions of common cast irons are ductile iron, malleable iron and compacted graphite iron. These compositions are differentiated by alloying elements that has an important effect on the resulting structure on the carbon. The individual microstructural properties of the carbon-rich phase of the different cast irons are listed in Table 2.1.

Table 2.1: Difference in the carbon-rich phase of cast irons

Type of cast iron	Carbon-rich phase
Gray iron	Lamellar graphite
White iron	Cementite (Fe_3C)
Ductile iron	Spherical graphite nodules
Compacted graphite iron	Vermicular graphite Intermediate between ductile and gray iron
Malleable iron	Temper graphite Irregularly shaped nodules of graphite

2.2 Ductile Iron

This thesis will mainly focus on ductile iron, also called nodular iron or spheroidal graphite iron. The main difference between gray and ductile iron is the formation of graphite in the matrix. In ductile iron graphite nucleates as spherical particles called nodules in a ferritic and/or pearlitic matrix. The formation of these nodules is accomplished by the addition of Magnesium (Mg) and/or Cerium (Ce) to the melted iron before casting. The Mg reacts with Sulfur (S) and the Oxygen (O) in the melt and changes the formation of graphite. This process will be discussed in Section 2.2.1.

Comparing gray and ductile iron it's clear that the nodular graphite structure has some advantages. The ductility of gray iron is low. With a tensile strength of 415 MPa the gray iron performs only with an elongation of 0.6%. This is because of the shape of the lamellar graphite which has a higher stress concentration factor due to its sharp angular boundaries. The shape of the nodular graphite in ductile iron makes its excellent ductility of up to 18% elongation with a tensile strength of 415 MPa. Ductile iron also possesses good machinability, high fatigue strength, high yield strength and a high modulus of elasticity. It also has a good wear resistance and are more shock resistant than gray iron. Ductile irons high strength and ductility makes it similar to some qualities of low alloy steels (Reardon, 2011)

2.2.1 Spherodization

The formation of graphite in the shape of nodules – spherodization – can be argued to be the most important process in the production of ductile iron. The spherical graphite feature has been proved to have a substantial effect on the mechanical properties, and is crucial to control in order for ductile iron to perform at its highest potential. The formation of this microstructural feature is, as mentioned, due to the addition of spheroidizers such as Mg. Theories of how the graphite nucleates in solidifying cast irons have been proposed in great numbers since the introduction of ductile iron. Theories include the gas bubble theory which states that bubbles of carbon monoxide in the melt act as nucleation sites for graphite, the graphite theory assuming that the nucleation occurs epitaxially from other graphite particles in the melt. Skaland (2005) concludes that the mechanisms of nucleation in ductile iron still needs further research and discussion, but they are all based on the assumption that graphite is formed by heterogeneous nucleation events, largely affected by minor trace elements.

One thing that is clear is that the graphite particles grow in volume with decreasing liquid iron carbon content, until the melt reaches the eutectic transformation temperature. When the liquid iron cools and the formation of austenite dendrites start, the austenite grains nucleates and grows around the graphite nodules, creating a austenitic shell. With decreasing temperature the carbon solubility decrease in the austenite. Diffusion of Carbon atoms towards the graphite nodules continues even after solidification until the eutectoid temperature. At this temperature the austenite transforms into ferrite which leads to more diffusion of Carbon atoms due to the negligible Carbon solubility in ferrite's body-centered cubic lattice (Di Cocco et al., 2010).

The spherical shapes of the graphite nodules have long been looked at as a unnatural state because it did not occur until a external addition of a spherodizing element was introduced. It was assumed that the lamellar structure existing in gray iron was the natural state of graphite in iron. However, a study of which molten gray iron was placed i a vacuum fro a long period of time, prior to casting, showed a reduction of surface active elements such as Oxygen (O), Phosphorus (P) and Sulphur (S). The reduction of these element resulted in a "clean" melt leading to graphite appearing as spherical shaped nodules. With this study it was concluded that flake graphite is actually a unnatural state of graphite and that it is the

surface active elements that creates this impurity. The addition of Mg in a cast iron melt will bind to these impurity elements and prevent them from affecting the graphite formation. This can be illustrated by a chemical analysis of a cast iron with flake graphite. This material will possess traces of O, S and P in the matrix as well as in the interface between metal and graphite. A chemical analysis of ductile magnesium inoculated iron will show no traces of Mg, O, S and P separately but rather in a combined form as Mg-S-P compounds (Double and Hellawell, 1995).

2.2.2 Inoculation

Inoculation is crucial in the production of cast iron. The purpose of inoculating ductile iron is to control the structure and properties of the material by increasing the number of nucleation sites. These nucleation sites give the graphite nodules in ductile iron higher growth potential. This will also cause a reduction of undercooling during the eutectic solidification process, which leads to a reduced risk of damaging carbide formation.

The most used inoculants are ferrosilicon alloys with a content of 50-75% Si and small amounts of one or more of Calcium (Ca), Barium (Ba), Strontium (Sr), Zirconium (Zr) and/or Ce. The amount of inoculant added to the melt is minimal – usually around 0.2 - 0.5 wt%. This does however sufficiently enough to achieve the wanted results. Figure 2.2 illustrates the microstructure of a uninoculated and a inoculated ductile iron, displaying the importance on inoculation (Elkem AS, 2011).

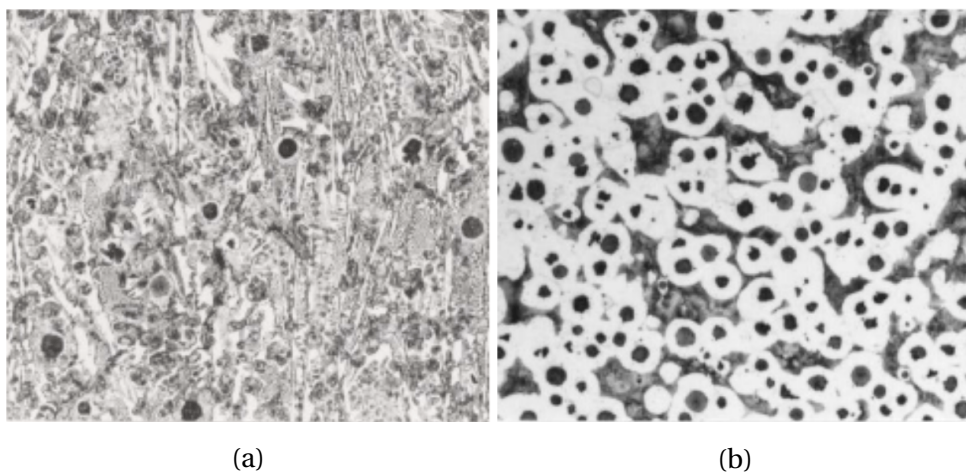


Figure 2.2: Difference between uninoculated and inoculated ductile iron (Elkem AS, 2011). (a) Uninoculated, (b) Inoculated.

2.2.3 Microstructure

Ductile irons microstructure, together with its chemical composition, is the main factors that define ductile iron's mechanical properties and behavior. Ductile irons microstructure are made up of a metallic matrix and a Carbon-rich phase, preferably is the shape of nodules. The consistency of the nodule size, distribution and round shape are imperative to achieve. Irregular shaped nodules will cause negative impact of the behavior and integrity of a ductile iron casting. Heat treatment of ductile iron will cause changes in the microstructure, but will not be covered in the present work. The following sections discuss the different microstructural features in as-cast ductile iron.

Graphite

Graphite is the name of the crystalline form of carbon. In ductile iron graphite does ideally consist as perfectly rounded nodules as illustrated in Figure 2.3. This round shape will cause less stress to concentrate in the connection between graphite and matrix. Graphite in the shape of flakes – imminent in gray iron – has poor fracture properties due to the shape of the graphite. The graphite flakes increase stress concentration and lowers toughness and fatigue strength of the material. In comparison, ductile iron does exhibit much higher toughness properties. The nodular graphite has a smaller effect on the concentration of internal stress in the material (Reardon, 2011). The direct effect the graphite nodules has on the mechanical properties will be discussed later.

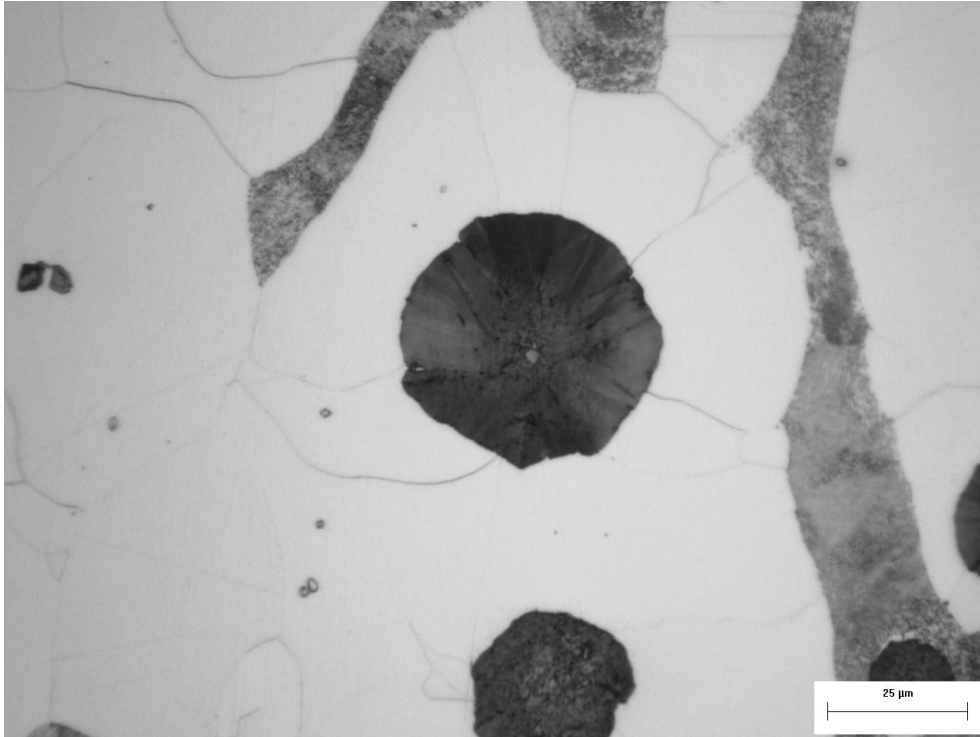


Figure 2.3: Image of a well developed graphite nodule in a ferritic matrix with traces of pearlite

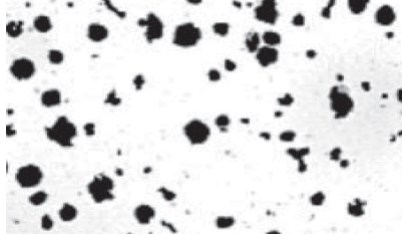
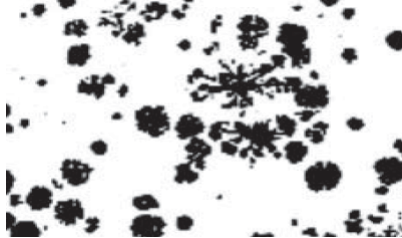


Deviation in Graphite Structure

The graphite structure formation is a sensitive process which can be affected by a number of factors. Cooling time, poor inoculation, high content of deleterious elements are just some factors that can cause irregular shaped graphite. Unwanted graphite structures are for example exploded, chunky or vermicular. These graphite structures deviating from the optimal nodular shape will cause a directly negative effect on the mechanical properties of ductile iron (Riposan et al., 2010). Table 2.2 shows the 4 mentioned unwanted shapes of graphite in ductile iron and the potential causes for these.

Another unwanted graphite formation not related to the generation of damaging nodular shapes, is the occurrence of flotation. Flotation is often a result of high CE and low cooling rates in large cross sectional castings. The slow cooling rate affects the graphite nodule formation by causing more carbon to precipitate towards the stable graphite phase. The resulting effect of this is a reduced nodule count, but increased nodule size. Flotation is the development of large nodules rising to the upper surface of the cast, due to lower density of graphite than iron, consequently leading to depletion of nodules in the lower parts of the

cast. This effect can lead to variation in mechanical properties at different depths of the cast and degradation of integrity of casting (Ductile Iron Society, 2013).

Table 2.2: Deviations from spheroidal graphite shape in ductile iron (Riposan et al., 2010)

Graphite	Potential Causes	Visual Structure
Irregular	<ul style="list-style-type: none"> • High holding temperature/time • Poor inoculation • Excessive fading • Anti-nodularising elements 	
Exploded	<ul style="list-style-type: none"> • Excessive rare earth elements • Particularly high purity charge • Large cross-section cast • High CE 	
Chunky	<ul style="list-style-type: none"> • Slow cooling rate • Excessive rare earths/charge purity • High Si, Ce, Ni, Ca • Poor inoculation 	
Vermicular	<ul style="list-style-type: none"> • Low residual Mg/RE • Excessive S, O • High temperature/Holding time • Antinodularising elements 	

Matrix

To achieve positive ductile properties in ductile iron, a ferritic matrix is necessary. Ferrite have a higher ability to deform plastically, making the material perform with a higher ductility. A pearlitic microstructure usually results in a higher strength and hardness naturally reducing the ductility. There is a general assumption that a 400 grade ductile iron normally have a fully ferritic matrix, 500 are predominantly ferritic in combination with pearlite (ferrite > 50%), 600 are predominantly pearlitic in combination with ferrite (pearlite > 50%) and 700 grade, and higher, is fully pearlitic. The material grade represents the minimum required tensile strength for the given material. The mechanical differences between different distributions the matrix structures are highlighted in Table 2.3.

Table 2.3: Mechanical comparison of pearlite and ferrite in ductile iron (Standard Norge, 2011)

Ductile iron grade	Matrix	Tensile strength [MPa]	Yield strength [MPa]	Elongation [%]
400	Ferrite	400	240	18
500	Ferrite - pearlite	500	320	7
600	Pearlite - ferrite	600	370	3
700	Pearlite	700	420	2

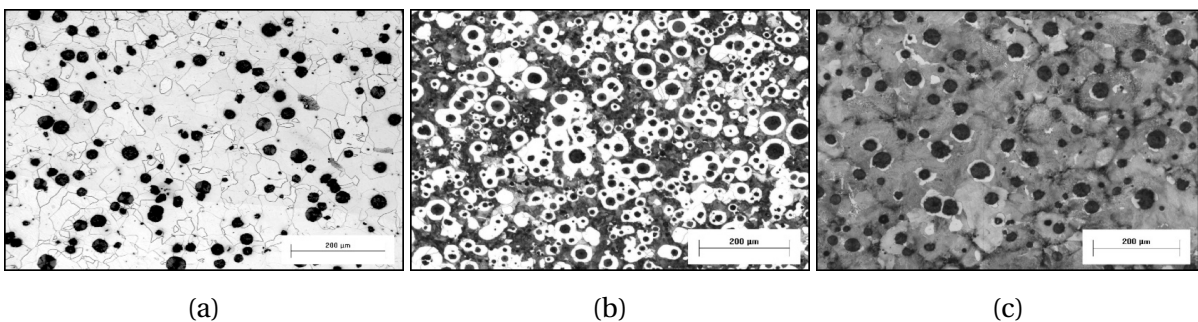


Figure 2.4: Microstructural image displaying different distributions of ferrite and pearlite. (a) Fully ferritic, (b) Pearlitic-ferritic, (c) fully pearlitic.

Characterization of Microstructure

To characterize the microstructural features in ductile iron, is important for quality assurance. It will also give a idea of how the material will behave regarding mechanical properties. The main features interesting to characterize is the graphite structure, nodule characteristics and matrix structure distribution. The most important nodule characteristics are described below.

Nodule density

The nodule density is the mean value of the number of nodules within a given area, usually per mm^2 . It is difficult to establish a optimal value of nodule density, however, keeping in mind the positive impact the nodules has on the mechanical properties, it would usually not be beneficial with a too low nodule density.

Nodularity

The nodularity is a percentage of how much of the graphite in the material that appears as spheres. If a ductile iron has 80% nodularity, it means that the remaining 20% of the graphite has a different shape, usually irregular shaped particles. The optimal nodularity of in ductile iron would be 100%, however, this is difficult to achieve.

Connection Between Microstructure and Mechanical Properties

The nodularity of ductile iron as a direct effect on its mechanical properties, shown by Al-Ghonamy et al. (2010). His study illustrated the effect different nodularities in ductile iron had on the mechanical properties. By mechanically testing 4 different ductile iron with varying nodularity. It shows that higher nodularity has a clear impact on the ductile and strength properties. This is illustrated in Figure 2.5.

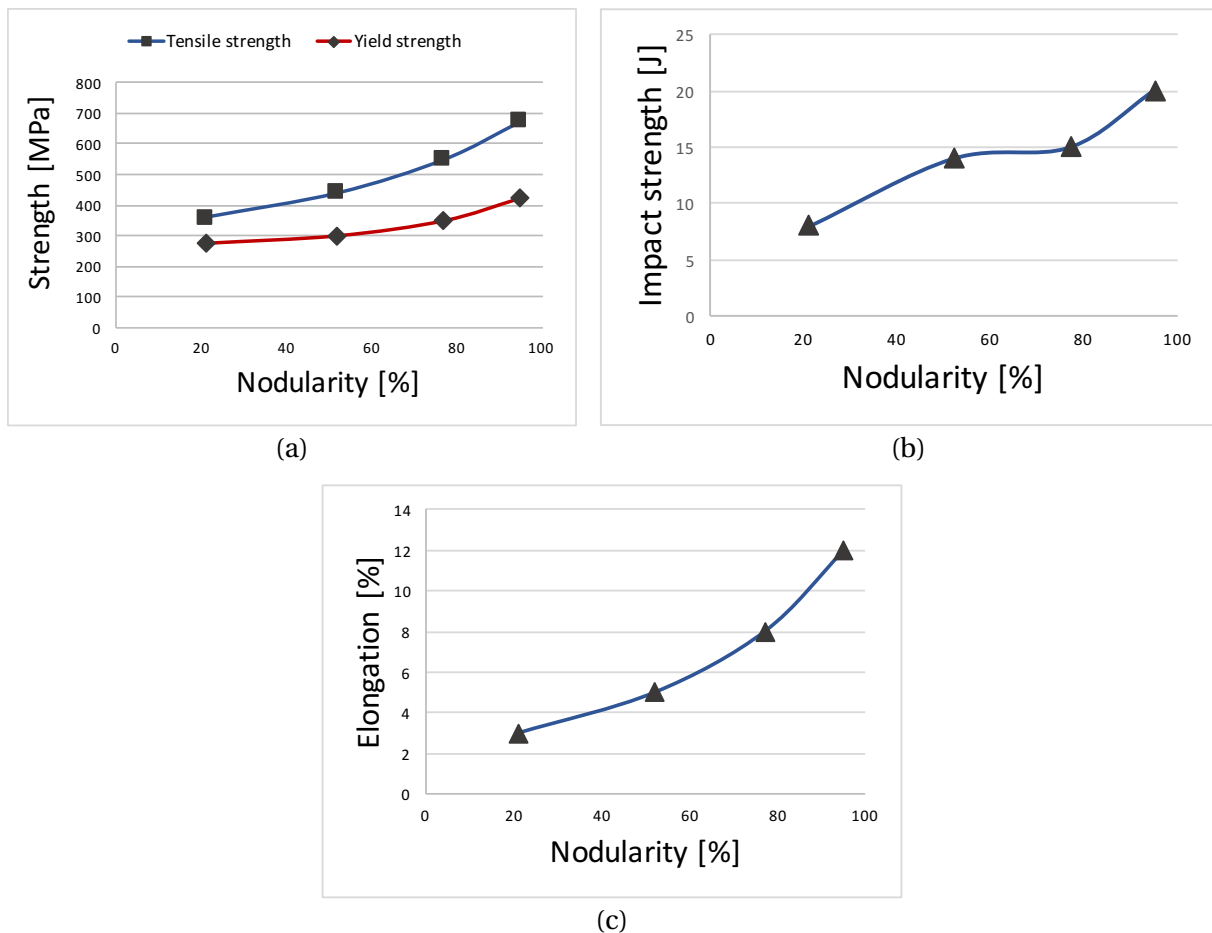


Figure 2.5: Tables illustrating the correlation between mechanical properties and nodularity (Al-Ghonamy et al., 2010)

The nodule count does also affect mechanical properties the same way that nodularity does. To achieve good ductility it is imperative to have a high nodule count, due to graphite's crucial role in achieving good ductile properties. Subsequently also affecting the properties strength and hardness negatively. High nodule count have been recorded to develop in sections experiencing faster cooling rate. This development is also relatable to nucleation and growth theories (Guo et al., 1998).

2.2.4 Chemical Composition of Ductile Iron

The chemical composition of ductile iron is one of the main factors which defines the distinct mechanical properties and microstructure of the metal. The general composition of ductile iron consist of five primary elements. These are Carbon (C), Silicon (Si), Manganese (Mn), Phosphorus (P), and Sulphur (S). All of these elements serves a specific purpose for

the final product. The main properties these elements apply to ductile iron are listed below (Elkem AS, 2017).

- Carbon - Reduces the melting temperature. It improves the castability and machinability, but can cause flotation, chunky or exploded graphite in high levels.
- Silicon - Improves graphitization and castability. Promotes ferrite and stable solidification. Increases strength and hardness of ferrite.
- Manganese - Promotes carbide and pearlite formation. Should be kept below 0.2% to achieve ferritic matrix.
- Phosphorus - Promotes pearlite formation and porosity. Increases fluidity, hardness and strength. Recommended value is max 0.03%.
- Sulphur - Reduced surface tension of graphite and refines grain size. Too low amount can cause nucleation problems. Recommended concentration is in the range 0.010-0.015%.

Together with these primary elements, there is always a need of spheroidizing elements, matrix controlling elements and other alloying elements to achieve a specific result. Other trace elements are always present in ductile iron. Some are damaging and should be kept at a minimum.

Graphitizers

Graphitizers are elements that promote the formation of graphite over carbide and ensures a more controlled cooling, ensuring the desired final microstructure. Known graphitizers are Silicon (Si), Nickel (Ni), Copper (Cu) and Cobalt (Co). These elements do also affect the Fe₃C eutectic by increasing the eutectic temperature upper and lower limit, as seen in Figure 2.6 (Elkem AS, 2017).

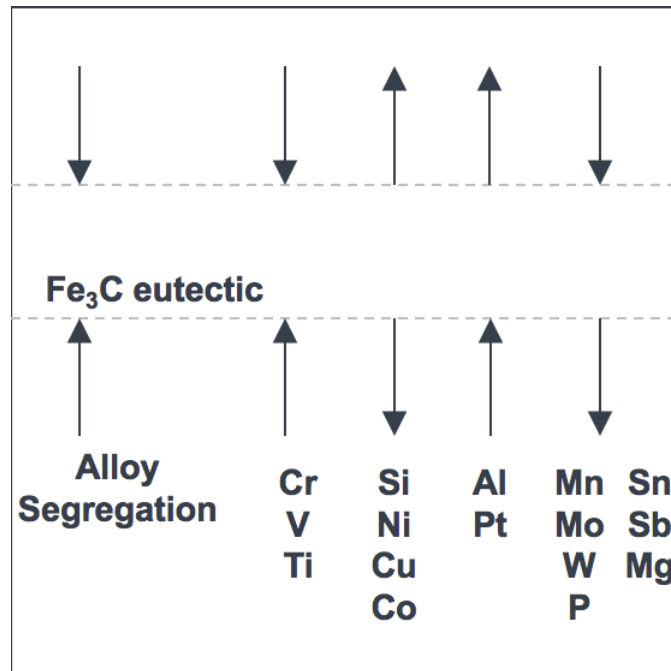


Figure 2.6: Trace elements effect on the Fe_3C eutectic temperature (Elkem AS, 2017)

Carbide promoters

Carbide promoting elements are elements that can cause the formation of damaging carbide rather than graphite. Carbide is a phase of Carbon unlike the preferable graphite phase. Carbide is damaging to the integrity of ductile iron castings, and will prevent the material to behave with the good mechanical properties that ductile irons are known for. Known carbide promoting elements are Chromium (Cr), Vanadium (V) and Tin (Ti). These elements will also cause a increase of Fe_3C eutectic temperature.

Pearlite Promoters

Pearlite promoting elements are alloys, or trace elements, that in large quantities will cause pearlite to develop during solidification of ductile iron. Known pearlite promoting elements are Selenium (Sn), Molybdenum (Mo), Phosphorus (P), Copper (Cu), Tin (Ti), Antimony (Sb), Manganese (Mn), Nickel (Ni) and Chromium (Cr), where Sn has the strongest pearlite promoting effect of them all. These alloying elements should be kept low if a ferritic matrix is wanted. This, however, does not mean that Sn are always damaging. In heavy section casting can Sn be used to control the formation of chunky graphite. The similari-

ties that these elements has, except being pearlite promoters is that they all affect the Fe_3C eutectic temperature, illustrated in Figure 2.6 (Elkem AS, 2017).

Spherodizers

Spherodizers are elements that promote the formation and nucleation of graphite nodules in ductile iron. The strongest spherodizer is Mg. Normal concentration of Mg in ductile iron is between 0.02 and 0.08%, but it's effectiveness is also related to the concentration of S and O in the iron. An exaggerated amount of Mg in the melt will result in the formation of carbide, which is undesirable. Controlled Mg amount is imperative to achieve a high nodule count and good nodularity. However, Mg is usually added in the iron together with other spheroidizing elements such as Ca, Yttrium (Y) or rare earth elements to improve the reliability of it's spheroidizing effect (Labrecque and Gagne, 1998).

Deleterious/Subversive Elements

Deleterious elements are unwanted trace elements which can cause damage to the optimal microstructure of ductile iron by for example promoting the development of unwanted graphite structures. A selection of these type of elements are Antimony (Sb), Bismuth (Bi), Lead (Pb), Titanium (Ti) and Zinc (Zn) (Elkem AS, 2017).

2.3 Offshore Application

The main objective of this report is to evaluate the use of ductile iron for offshore applications, with focus on lifting and drilling applications. Materials used offshore need to be able to withstand difficult working conditions and low temperatures. Many offshore components does also support heavy machinery that can cause a large amount of damage if failure occurs.

2.3.1 Ductile Iron vs. Steel

If ductile iron are to be considered as a reliable material for offshore applications, it will most likely be by substituting the use of steel. By introducing ductile iron with similar mechanical properties of steel, producers could experience a positive trend concerning cost. When comparing ductile iron and steel, they can seem like similar materials at first. They are both a iron-carbon alloy that can be modified regarding mechanical properties with the addition of alloying elements. Directly comparing mechanical properties is difficult due to the large variation of properties that can be achieved by altering the chemical composition or heat treating. With that said, there is several other physical differences between these materials.

The following comparison is limited to as-cast ductile iron and cast steel. The reason for this is that these materials have the most in common regarding cost, properties, production technique and areas of use. Regarding cost, the production of ductile iron will be most beneficial, mostly because of two factors: temperature required when pouring the melted material is higher for steel. And the need for adding risers in the melt to prevent shrinkage. The mechanical properties are similar, where the main difference in that steel possess better impact resistance and ductile iron perform better regarding vibration damping properties. Natural ductile iron also will provide better corrosion resistance than unalloyed steel, and even highly alloyed steels in certain environments (Penticiton Foundry, 2015). Oxidation will be generate faster in ductile iron, but this is mostly superficial, not affecting the structural integrity of the iron.

Penticiton Foundry (2015) have discussed the current topic in an article and generated a list comparing some of the physical properties of ductile iron and cast steel (Table 2.5). The list is constructed by listing what material has the preferred properties regarding the corresponding characteristic.

Table 2.4: Comparison of ductile iron and cast steel Penteciton Foundry (2015)

Characteristic	Ductile Iron	Cast Steel
Castability	X	
Ease of Machining	X	
Vibration Dampening	X	
Compressive Yield Strength	X	
Surface Hardenability	X	
Modulus of Elasticity		X
Impact Resistance		X
Corrosion Resistance	X	
Wear Resistance	X	X
Cost of Manufacture	X	

From Table 2.5 it clear that ductile iron possess a large amount of physical benefits over cast steel. Keep in mind that this is an as-cast material. A lot of steel used in todays construction are heat treated or high alloyed that mostly perform at a higher level.

When talking about mechanical properties, can ductile iron and structural steel exhibit similar values regarding strength. The main difference is values of elongation and Charpy impact energy. Impact energy in ductile irons are generally > 20 J and < 27 J (minimum) for steels. Steels does also have the advantage of a normally higher ductile-to-brittle transition temperature than ductile irons. These features will often have a large impact on material selection, especially for offshore applications with low design temperature. Using steel for both heavy duty and low stress applications have been sufficient for many years, and ductile iron could have been overlooked due to poor impact energy values and supposedly high transition temperature.

S355 is a versatile type of structural steel often being used in the most demanding environments, such as the offshore industry. It's name comes form it's average minimum yield strength of 355 MPa. This material does also possess mechanical properties similar to that of ductile irons, meaning it would be natural to compare these materials regarding areas of

use. Table 2.5 highlights the general mechanical properties of S355 steel and ductile irons, to illustrate the clear similarities between the two.

Table 2.5: Comparison of ductile iron and structural steel (Hechler et al., 2015)(Standard Norge, 2011).

Mechanical property	Tensile strength [MPa]	Yield strength [MPa]	Elongation [%]
S355	470-630	355	22
Ductile iron	350-900	220-600	2-22

One of the objectives of this report is to evaluate the use of Charpy-V impact energy for determination of ductile iron. This will be compared by studying the relationship between Charpy impact energy and fracture toughness, especially between as-cast ductile iron and welded steel. This relationship for welded S355 steel is presented in Section 3.2.

2.3.2 Casting vs. Welding

The following section is based on information from Blair and Monroe (2017). An engineer has to make a lot of critical decisions when designing a mechanical component. One of which is considering the best material to be used based on factors such as properties, cost and fabrication technique. When it comes to cast iron, there are not many options regarding fabrication techniques. Cast iron can be welded, but it is difficult and is mostly done only to correct damages and faults. Cast iron are produced by casting, and this is also one of the factors that can make this material favored for other materials. The two main ways to manufacture metals nowadays is casting or fabrication. Steel is usually fabricated by rolling, forging and/or welding. Rolled or forged steel’s mechanical properties are directly affected by this production technique in the way that makes the material anisotropic – the material exhibit different properties in the transverse and longitudinal direction. This anisotropic behavior is something designers need to take into account and base their design around, which gives rise to new challenges. Cast material does not express this feature and is considered isotropic.

Other benefits that casting provide is design flexibility. Standard fabricated parts are made out of several individual components, assembled to make a finished product. When pro-

ducing a component consisting of complex shapes, casting has a major advantage. Complexity and size are not an issue when casting. Mechanical components with a weight of up to 200 tons have been successfully produced by a casting process. These advantages give the engineer a larger freedom when constructing a component, making it easier to create a optimized design within the given design criteria.

There is no doubt that when constructing simple load bearing structures, consisting of steel beams and similar standardized components, fabrication with the use of welding is the easiest and most beneficial. On the other hand, when designing a optimized component with special requirements regarding size and are of use, casting would be more attractive. Casting does also provide tighter tolerances, giving the part a greater quality. Limiting the parts of a larger assembly will shorten the final assembly time as well as the cost of the project. Castings often weigh less due to the geometry that can be designed only restricted by the minimum component requirements rather than the capabilities of fabrication methods, bars and sheets (Blair and Monroe, 2017).

Welding is one of the most used fabrication methods for steels. By welding two mechanical pieces together, a weak point is introduced to the integrity of the construction. Even though a weld ideally should express the same material properties of the base material, this will not always be the case. Welding can be performed in a number of ways and techniques, but the main similarity between them all, is the use of heat. Materials welded together are all a product of fusion, where either melting of the base material or the addition of a separate melted material is introduced. Even though the material which are added to the welded construction during a fusion process are harder or stronger than the base material, will this not always strengthen the integrity of the material. Materials react different to the introduction of locally high temperature, and the result is often altering of the microstructure and mechanical properties at the weld and the heat affected zone (HAZ). Due to this, the material in a weld can be weaker than the base material. A HAZ is often a cause of embrittlement in the microstructure, hardening the material but at the same time weakening the toughness. Welds also require extensive testing and certification. Both non-destructive testing and destructive testing are used to evaluate the integrity of a weld due to the possibility of introducing an unwanted weak point to a structure.

2.3.3 Ductile-to-brittle Transition Temperature

This study is going to focus on the effect lower working temperature has on the mechanical properties of ductile iron. It is not desirable to get results that show the material suffering from major brittle properties at these temperatures. This is why the ductile-to-brittle transition temperature is of such importance. All ferrous metals have a critical ductile-to-brittle transition temperature, some higher than others. For each individual metal this critical temperature can vary depending on alloying elements, microstructure or heat treatment. The most used method of measure the brittle properties of a metal are impact tests. The resulting impact energy absorbed from this type of test in addition to microstructural analysis of the fracture surface will reveal the materials brittle property at the given temperature. Figure 2.7 shows a typical ductile-to-brittle behavior of a ferrous material.

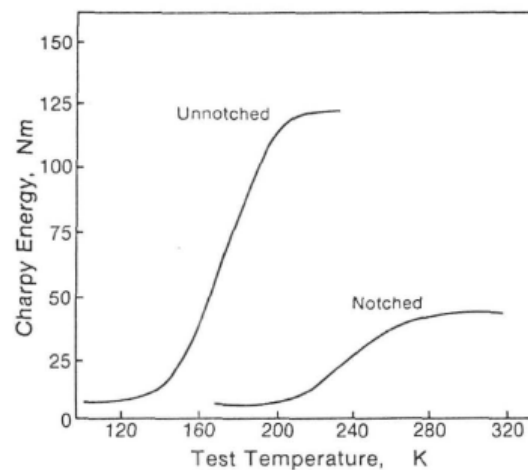


Figure 2.7: Typical ductile-to-brittle transition diagram for a ferritic material (Bradley and Srinivasan, 1990)

Forrest (2006) have studied the factors that affect the transition temperature of ductile iron.

The factors are:

- Pearlite – increasing amount of pearlite in the matrix decreases the impact strength
- Chemical composition – Increasing amounts of Si, P, Mn, etc. decreases the impact strength.
- The number and roundness of the graphite nodules.

These factors will be further discussed in Chapter 7 and 8.

2.4 Fracture Mechanics

Fracture mechanics can be defined as the study of crack formation and propagation in materials. It is a quantitative analysis used for evaluation of structural behavior in terms of applied stress, crack length and component geometry (Reardon, 2011). The fracture mechanics of a material is important to include in the design process. The traditional approach to structural design and material selection is defined by two variables; the strength of the material and the applied stress. By designing a component with higher strength than the inflicted stress, with an added safety factor, the component is assumed to be adequate. This approach is sufficient in many cases, but it does not take into consideration the possibility of an imposed weakness to material, such as a crack. Which is not unlikely to develop over time or through an unexpected event. If this scenario is a possibility, the design should be defined through the fracture mechanics approach. This approach is defined by three variables; Fracture toughness, flaw size and applied stress. The difference between the traditional approach and the fracture mechanics approach is that the strength of the material is substituted with fracture toughness and flaw size (Anderson, 2005).

Fracture mechanics analysis is based on two alternative approaches: the energy criterion and the stress intensity approach. The two approaches are equivalent in certain circumstances. This report will focus on the stress intensity approach, which is based on the theory of a critical stress intensity value at the tip of a crack, K (Anderson, 2005). Crack development in a component, according to the stress intensity approach, can be described by one of three modes of loading and resulting fracture, Illustrated in Figure 2.8. Mode I is called the opening mode and is the simplest and most used. It is these distinct modes that gives the characteristic subscript to the stress intensity factor K_I , K_{II} or K_{III} .

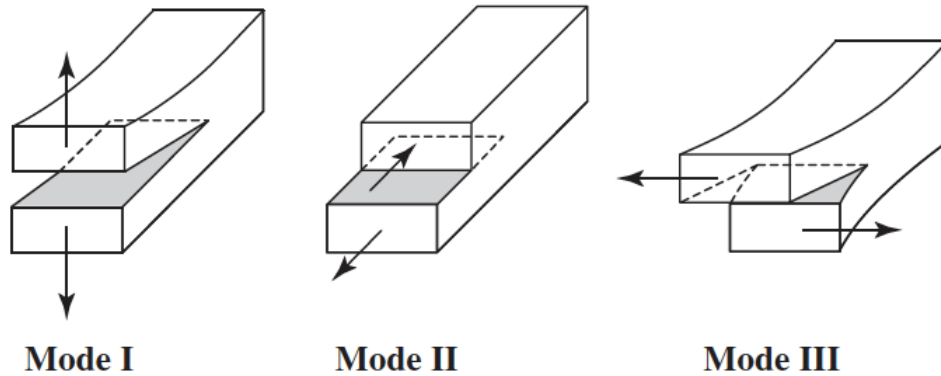


Figure 2.8: Modes of loading and corresponding fracture. Mode I: opening mode, Mode II: sliding mode, Mode III: tearing mode. (McEvily, 2013)

2.4.1 Fracture Behavior

Fractures of materials are generally categorized as being either of brittle or ductile nature. What defines the fracture behavior is the ability of a material to experience plastic deformation. A ductile material will experience a high energy absorption and a plastic deformation before fracture, which a brittle material will not. Ductility is known to be characterized by the value of elongation, however, in fracture behavior, ductile and brittle are relative terms that can be difficult to define (Callister and Rethwisch, 2011).

Brittle Fracture

The characteristic of a brittle fracture is that it exhibits minimal plastic deformation and a rapid crack propagation. The fracture surface is relatively flat and the direction of the crack motion is generally perpendicular to the direction of the applied tensile stress (Callister and Rethwisch, 2011). Crack propagation in a brittle metal is normally characterized as a cleavage fracture, i.e. repeated breaking of atomic bonds along the crystallographic plane. This type of fracture is called a transgranular/transcrystalline fracture because the crack passes through the grains, which in a ferritic material is along the (100) crystallographic plane. In a ferritic material, for which a transgranular brittle fracture has occurred, bright reflections can be observed on the fracture surface, by eye or a low-power microscope. These reflections is a result of the cleavage fracture leaving a somewhat flat surface of tearing the grains, called cleavage facets. By studying these facets with a 100x microscope it is pos-

sible to observe another characteristic of brittle fracture, named river patterns. The river patterns consist of several tear lines, created as the crack front passes from one grain to another. Neighboring planes is normally not aligned with each other, i.e. the crack changes direction within a grain, which requires a higher amount of energy, causing the tear lines to grow. These tear lines are a useful aid when determining the direction of crack propagation since they tend to occur perpendicular to the crack front (McEvily, 2013).

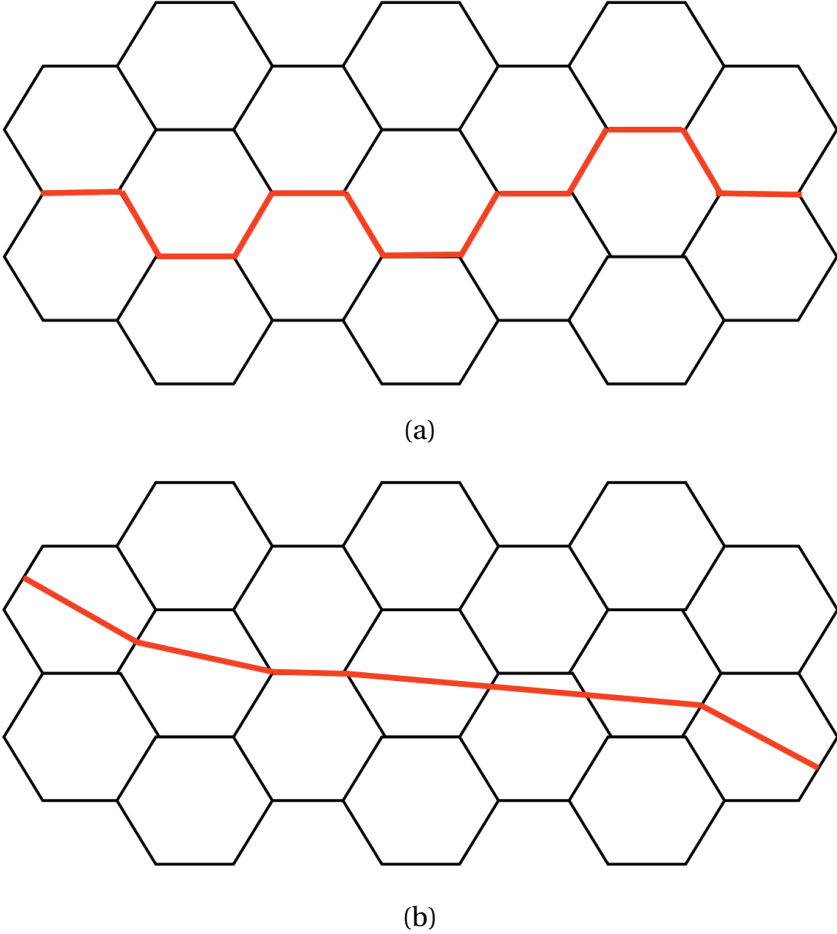


Figure 2.9: (a) Intergranular fracture, (b) Transgranular fracture

Crack propagation at grain boundaries can also occur in brittle materials, termed intergranular fracture. This type of fracture occurs due to weaknesses at the grain boundaries which of usually caused by segregation of impurity elements to the grain boundaries. A visual characteristic of this type of fracture is the rock candy, which appears as a crystal-like topography, that also appears bright at low magnification (McEvily, 2013).

Ductile Fracture

Ductile fractures will in most cases be preferable to brittle. This is first of all due to the often unexpected suddenness of a brittle fracture. It transpires without warning and is most of the time very damaging. All types of fractures are surely damaging, but one of ductile nature exhibits a warning beforehand in the shape of plastic deformation. This warning usually means that failure is imminent so that preventive actions can be taken. Secondly is more strain energy required to induce a ductile fracture, due to these materials higher toughness (Callister and Rethwisch, 2011).

A ductile tensile fracture, experience a visual characteristic feature termed necking, which represents the first stage of the plastic deformation of the material. From this stage to the point of fracture several processes is occurring. Including the formation of small microvoids, that enlarge, coalesce and forms an elliptical crack, whose longitudinal axis grow perpendicular to the stress direction. This leads to rapid crack propagation resulting in a fracture growing towards the outer perimeter of the neck. The final fracture leaves behind a cup-and-cone fracture (Figure 2.10(a)) due to the shear deformation, at the outer surface of the neck, which occurs at an angle of about 45° with the tensile axis. In contrast, will a tensile fracture profile of a brittle material have a relatively flat surface, illustrated in Figure 2.10(b).

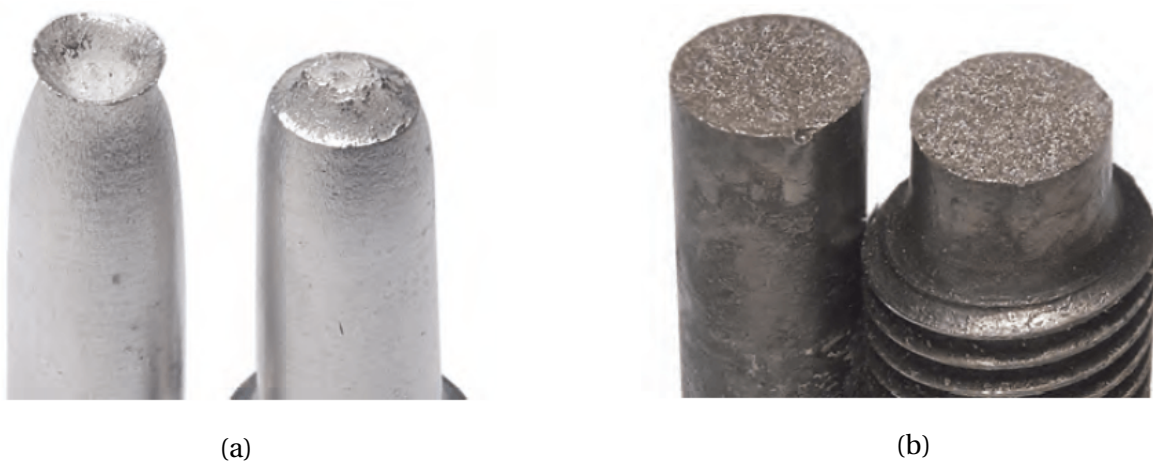


Figure 2.10: (a) Ductile cup-and-cone fracture. (b) Brittle fracture.

In contrast to brittle fracture is a ductile fracture categorized as noncrystallographic and takes place by plastic shear deformation. The microstructure at a microscopic level, in

the case of tensile tearing, has an appearance called dimples. This feature is created by the breaking of the ductile matrix. When the microvoids within the material link together they develop this characteristic feature, which is only visible when examined with a SEM (McEvily, 2013).

Ductile Iron Fracture Surface

Ductile iron is characterized as ductile in when comparing it to other types of cast iron. However, in a larger perspective, it does not compete with to most ductile materials. Regarding elongation, is there several types of steel that have a higher value. But then again, is ductile a relative term not defined by any specific value. A typical fracture surface of a ductile iron material will generally express features of both ductile and brittle nature. In Figure 2.11 microvoids are visible around the graphite nodules as well as the intergranular brittle fracture in the middle.

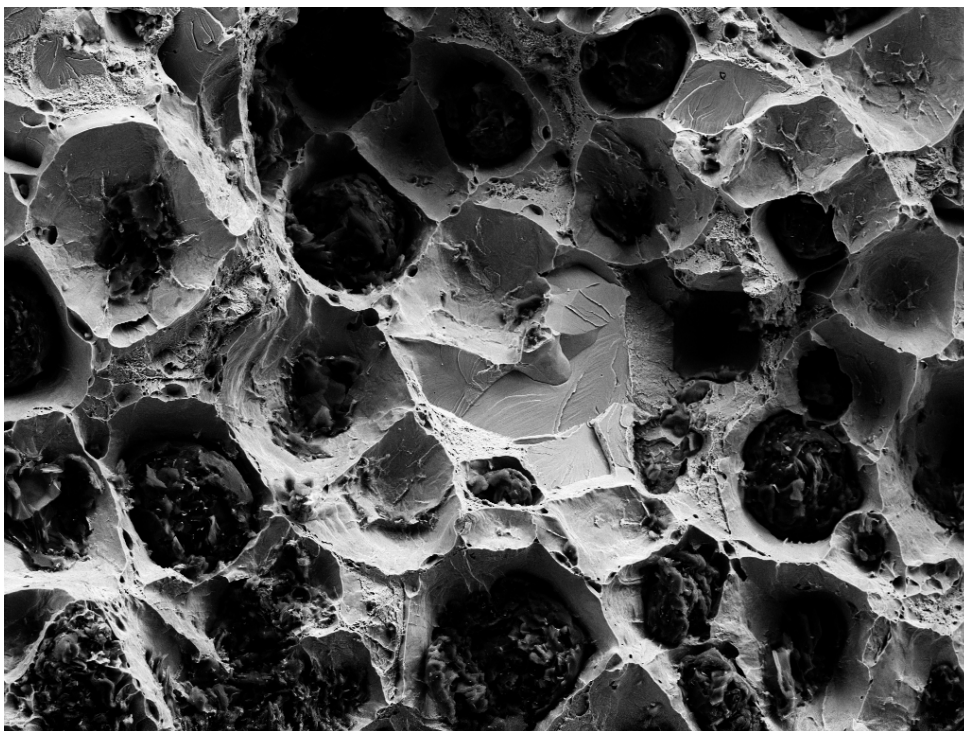


Figure 2.11: Image showing both ductile and brittle fracture features

2.4.2 Fracture toughness

Fracture toughness is defined as a material's ability to withstand force after a crack has been introduced. This test method results in a more describing property, that gives a more realistic value of toughness than the Charpy test; the critical stress intensity factor K_{Ic} . This factor is the critical limit of stress intensity required to initiate crack growth. The stress intensity factor (K) is a measured value used to determine the intensification of applied stress at the tip of a crack of known size and shape (Reardon, 2011). Failure will occur when $K_I = K_{Ic}$, showing that K_I can be described as the driving force of fracture and K_{Ic} is a measure of material resistance.

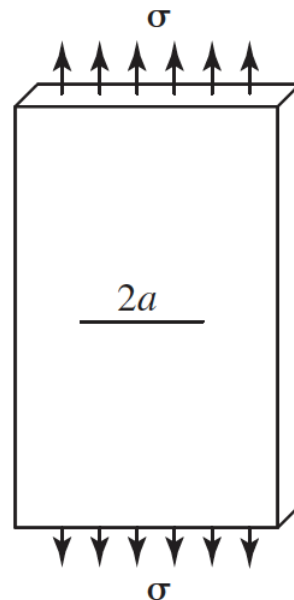


Figure 2.12: Through-thickness crack in an infinite plate (McEvily, 2013).

Figure 2.12 illustrates a through-thickness crack in an infinite plate subjected to tensile stress. In this case, a condition of plane strain exists, meaning that the value of K_I is not dependent on specimen thickness. K_I in this case is defined by Eq. 2.2.

$$K_I = \sigma \sqrt{\pi a} \quad (2.2)$$

Where σ is the applied stress and a is the half the crack length (Anderson, 2005).

2.5 Test Methods

This thesis will concentrate of four specific testing methods to determine mechanical properties and perform a microstructural analysis of the material.

- Tensile test
- Charpy test
- Fracture toughness test
- SEM, microstructural and chemical analysis

2.5.1 Mechanical Properties

Tensile test

The stress-strain test is one of the most used mechanical test operations for metals. It is a destructive test, meaning that the test specimen is permanently deformed and usually fractured. The test is performed in a tensile testing machine where a standard test specimen is experiencing a constant rate of elongation until it fails. The machine is measuring the load applied as well as the elongation of the material. The results are plotted in a stress-strain diagram. The stress-strain diagram gives an indication of several mechanical properties. This thesis will focus on three mechanical properties, gathered from the tensile test, highlighted in Callister and Rethwisch (2011):

- **Tensile strength** – is the value of stress at the highest point on the stress-strain curve. Corresponds to the maximum amount of stress that the material suffer from.
- **Yield strength** – the amount of stress that causes the material to suffer from plastic deformation. A material in tension will up to this point experience an elastic deformation. The unique property of elastic deformation is that by unloading the material, it will retract to its original shape. With stresses higher than the yielding point the material will be permanently deformed after unloading. The values of stress are determined by the force of the tensile test machine divided by the cross-sectional area of the test specimen.

$$\sigma = \frac{F}{A} \quad (2.3)$$

- **Elongation** – is a percentage of a materials change in length at fracture. More specifically, it is a value of the plastic deformation that has occurred upon fracture. This property is an indication of a materials ductility. The percentage is calculated by formula 2.4 where l_f is the fracture length and l_0 is the original length of the test specimen.

$$\%EL = \left(\frac{l_f - l_0}{l_0}\right) * 100 \quad (2.4)$$

Charpy test

Impact testing of materials is an important test of determining a materials impact energy. The most common impact test is the Charpy test, developed by a French scientist named G. Charpy. A standardized test specimen is placed in the path of a swinging pendulum. The pendulum drops and fractures the specimen. The resulting height of the pendulum after the fracture is what determines how much energy that has been absorbed by the material. The test was developed in 1901 when engineers became aware of the importance of material toughness in avoiding brittle fracture. The energy of separation that's measured with this test was believed to give an indication of the material's ability to resist brittle fracture (Anderson, 2005).

The standardized test specimen has the measurements of 10x10x55 mm with a V-shaped notch in the middle of one of the sides. The Charpy test is often done with several test specimens with varying temperatures to highlight the ductile-to-brittle transition that some materials exhibit at low temperatures. The energy impact energy measured are given in Joules (J).

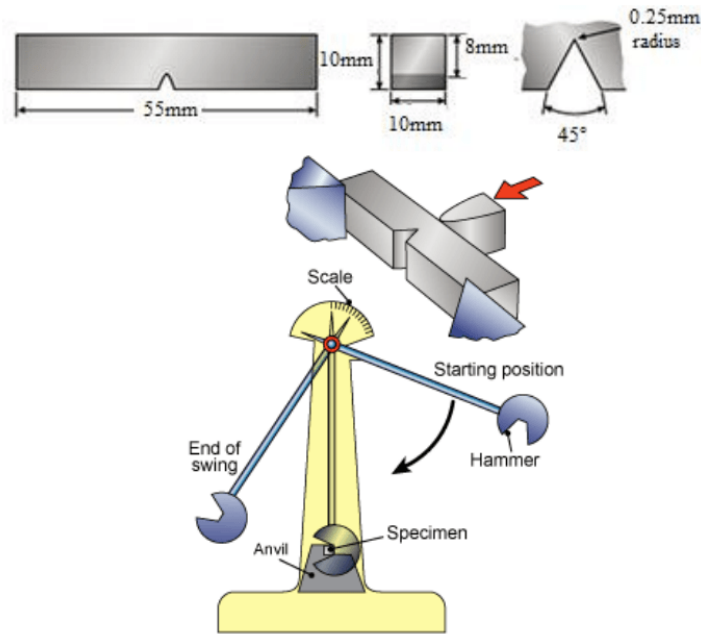


Figure 2.13: Charpy V-notch specimen and testing machine (TWI, 2017).

Even though the most used Charpy test method is done with a V-notch has several studies augmented that to get a reliable result of the properties of cast iron, the test should be performed without a notch. This statement will be further discussed later.

Plain-Strain Fracture Toughness

When determining a value of fracture toughness the method of plain-strain fracture toughness is most used. Using a standardized geometry a test specimen is loaded until failure. In this report, a three-point bend specimen (SE(B)) is used. The measured parameters is subjected force and the crack-tip opening displacement, measured with an attached clip gauge. The resulting force/displacement graph is used to calculate the stress intensity factor K_I . Fracture toughness is, as mentioned, a material's ability to withstand stress after a crack is already initiated. The way this is simulated is that the test specimen is fatigued until a crack of a specified length has developed. This process of pre-cracking can be time-consuming and is done before the actual test. The test specimen is machined according to requirements stated in (ISO, 2016), illustrated in Figure 2.14. The purpose of the machined notch in the middle is to hold the clip gauge used to measure displacement, as well as acting as a stress riser when creating the pre-crack.

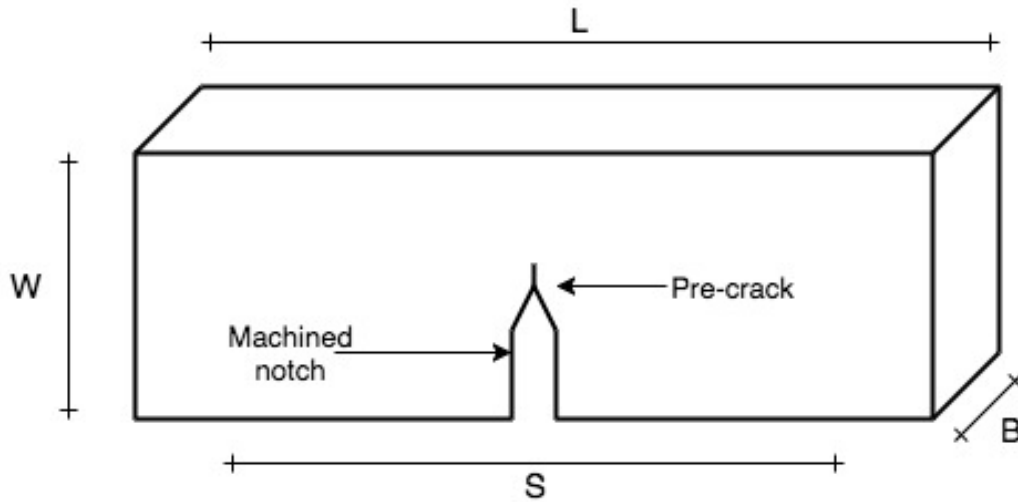


Figure 2.14: SE(B) test specimen geometry

The test method is completed by inflicting a constant force to the test specimen until a stable or unstable crack extension occurs. A value of F_Q is read from the resulting graph and used, along with geometrical constants, to calculate K_Q (see Eq 2.5).

$$K_Q = \frac{S}{W} * \frac{F_Q}{(BB_N W)^{0.5}} * g_1\left(\frac{a_0}{W}\right) \quad (2.5)$$

Where

- S is the span between the supporting rollers
- W is the width of the test specimen
- F_Q is a value of force determined from the force-displacement graph
- B is the thickness of the specimen
- B_N is the net thickness of the specimen, if no side grooves are used, $B_N = B$
- $g_1\left(\frac{a_0}{W}\right)$ is a stress intensity factor coefficient which takes into consideration the geometrical relationship between a_0 and W of the specimen. Values of $g_1\left(\frac{a_0}{W}\right)$ are given in (ISO, 2016) for specific values of a_0/W .

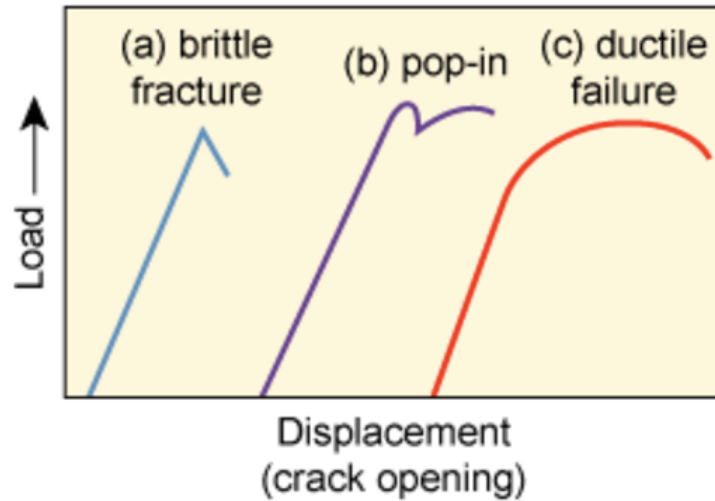


Figure 2.15: Load vs crack opening displacement curves showing three types of fracture behavior (Mathers, 2017).

If the calculated K_Q meet the requirements shown in Eq. 2.6 and Eq. 2.7 . Then K_Q is equal to K_{Ic} .

$$a_0, B, (W - a_0) \geq 2.5 \left(\frac{K_Q}{R_{p0.2}} \right)^2 \quad (2.6)$$

$$0.45 \leq \frac{a_0}{W} \leq 0.55 \quad (2.7)$$

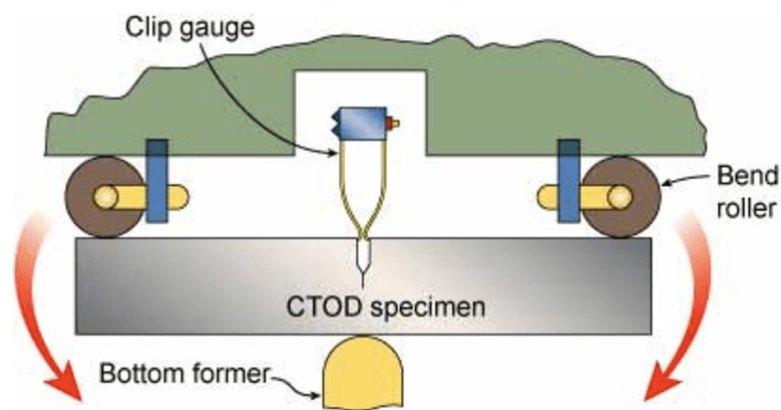


Figure 2.16: SE(B) test rig (Mathers, 2017).

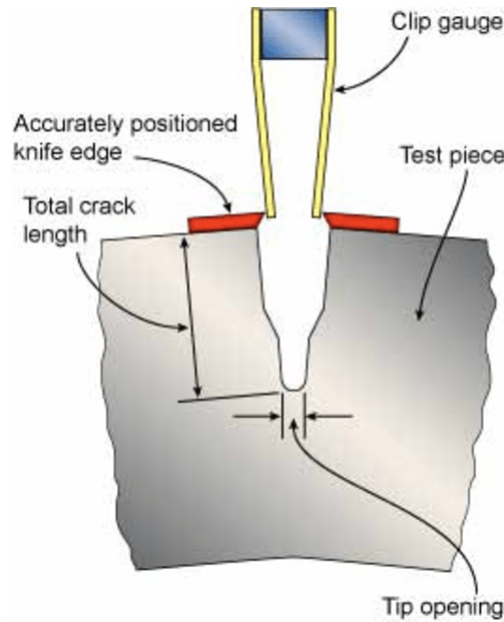


Figure 2.17: Positioning of clip gauge in a SE(B) specimen (Mathers, 2017).

2.5.2 Microstructure

The microstructural analysis is normally performed using a specific computer software to characterize the microstructural features visible in ductile iron. This analysis is completed using an optical light microscope and a computer software developed for this type of analysis. The software takes 25 representative pictures, with a magnification of 100x, of the material's surface and gathers information about microstructural features, specifically nodule characteristics and matrix composition. The material's microstructural features and adjacent values are calculated from the mean value of the 25 examined fields. The individual characteristics evaluated in this analysis are listed and described below:

- No. of particles – Number of total particles in all the 25 examined fields. Particles are defined as all graphite particles, from the spherical nodules to the chunky graphite that meet the minimum size criteria.
- No. of nodules – Number of total nodules in all the 25 examined fields that meet the minimum size and shape criteria. The shape criteria of a nodule is determined using a shape factor (SF). SF = 1 represent a perfect circle, SF=0 a straight line. To qualify a particle as being a nodule the required $SF \geq 0.6$. The shape factor is calculated as $SF = \frac{4A}{\pi * F_{max}^2}$ where F_{max} represents the minimum diameter of a particle for it be

included in the analysis. F_{\max} is usually $10\ \mu\text{m}$.

- Nodule density – Number of nodules per mm^2 .
- Nodularity – Percentage of graphite that occur in the shape of nodules.
- Graphite, ferrite and pearlite – Percentage of the specified structure in the examined area.
- Particle and nodule size – average particle and nodule size using a size limit $> 10\ \mu\text{m}$

2.5.3 Chemistry

The chemical analysis of ductile iron is usually completed using spark optical emission spectroscopy. The test specimen, usually measuring 1-2 cm, is prepared by grinding to secure a uniform and flat surface. The test sample is placed in the spark OES instrument and flooded with argon. A spark is created between a high powered electrode and the sample surface, reacting with the argon and creating a conductive plasma. Elements on the sample surface melt, evaporate and excites in contact with the spark. The excited atoms react with the plasma, emitting light at the characteristic wavelength. These wavelengths are detected, measured and compared to known standards to provide a qualitative result. This process will give a report on not just the different elements present in the examined material, but also the distribution of each element (Materials Evaluation and Engineering, Inc., 2017).

2.5.4 Scanning Electron Microscope

The Scanning Electron Microscope (SEM) is an important tool in the industry of microstructural analysis. Where a standard optical light microscope is restricted to a magnification of 1000x, will the SEM perform with a magnification of up to 50000x. An optical light microscope uses direct light to illuminate the sample, which together with the magnifying lenses creates a microscopic image. The SEM have no direct light source and uses only electrons to generate the image (Callister and Rethwisch, 2011).

Image Generation

The SEM emits electrons from an electron gun and the lenses focus the free flowing electrons onto the sample. These electrons interact with the atoms in the sample and result in new signals being emitted from the sample. The secondary and backscattered electrons make up the two most common signals used to form a SEM image. (Khursheed, 2011)

Other than the high magnification a SEM has exceptional resolution and great field depth. The reason for the high resolution is because of the small wavelength of electrons compared to light. The field of depth is achieved because of long working distances and the small aperture angles. When studying a fracture surface of a brittle material, the top and bottom of a torn structure will have a substantial height difference. With a SEM it is possible to achieve focus on both the top and bottom at the same time, due to small aperture angle and long working distance, making it ideal to study surfaces and defects of a material. In an optical light microscope, the lenses are made of glass. Electrons cannot pass through glass which is why the lenses in the SEM are electromagnetic, whose purpose is to lead the flowing electrons through the SEM and focus the electron beam on the specimen.

The purpose of using SEM in this report is to study the microstructural features and crack development visible in ductile iron. By using a SEM it is possible to get a larger understanding of the microscopic mechanics inherent in this material.

3. Literature study

This chapter will focus on the evaluation of theories and studies within the the topic of both ductile iron generally and the specific materials evaluated in the report.

3.1 Evaluation of Charpy Impact Testing on Ductile Iron

The Charpy impact test method was originally designed for steel. After the controversial failure of Americas liberty ships during World War II, the importance of this type of characterization became clear. At the time of the Liberty ships construction, there was no requirement of minimum impact energy as a design criterion. The investigations of the Liberty ships showed that the steel used met all the requirements regarding strength, chemical composition and microstructure. A report from this investigation made by Williams et al. (1949) suggested a minimum toughness requirement of 20 J and stated that “some criterion of notch sensitivity should be included in the specification requirements for the procurement of steels for use where structural notches, restraint, low temperatures, or shock loading might be involved.” This report led to a more acknowledged respect for the toughness of steels. The researched ductile-brittle behavior of steels led to the implementation of toughness values in codes and standards.

Even though the Charpy test where developed for steel, it has been used as a design requirement for cast irons. In DNVGL-OS-E101 “Drilling plant” it is stated that the minimum average Charpy V-notch energy absorption should not be lower that 10% of the yield strength. (DNV-GL, 2015)

Today, the Charpy test are still used to test the impact energy of steels, but also cast iron. By testing at varying temperatures, it is possible to construct impact energy vs. temperature curves. This curve is used to determine the ductile-to-brittle transition temperature. This temperature can also be determined where the fracture is 50% brittle, which is done by analyzing the fracture surface. This transition temperature is an interesting fact to highlight,

however, it is not a material property, and should not be used for design purposes (Oaks, 2012).

The Charpy impact test is still today the most commonly used test method for evaluating a material's fracture properties. It is clearly a beneficial test method, regarding price, time and simplicity. The most common test for ferritic steel is done with a V-notch carved into the test specimen. If the V-notch is not sufficient, some also use a U-notch or complete the test without a notch. The Charpy test method has been used to also categorize behavior of cast iron, but scientists argue that to transfer the Charpy requirements, that has been developed for steel, directly to nodular cast iron is not sufficient. A recent argument made by Meghan Oaks was that "Charpy impact testing is neither an accurate nor acceptable way to measure impact toughness in cast iron. It is inappropriate to use it as a means of comparison between cast iron and steel.". (Oaks, 2012) (Wallin, 2014)

Cast iron has commonly been characterized as notch insensitive and described as less affected by different notches than steel. However, this is proved to be wrong. Cast iron, and especially nodular cast iron, are very sensitive to notches. The reason for this is that a notch will create the properties of a small crack in the material. It's the graphite nodules in ductile iron that is the reason for this. These nodules can fail at small strains, creating a micro crack in front of the notch, making the notch sharper than what is normally experienced in steels. This effect is directly causing ductile iron to experience a lower Charpy-V energy for the same value of fracture toughness compared to steel. This shows clearly that Charpy-V values for ductile iron are insufficient when comparing to steel (Wallin, 2014).



Figure 3.1: Schematic illustration of notch sensitivity in ductile iron (Wallin, 2014)

Another problem with the Charpy test is the size of the test specimens. These are small in size, which is simple and economically favorable, but it does not represent the majority of real life applications. Stress experienced in these small geometries are complex and normally not directly applicable to in-service components (Oaks, 2012). The test method of applying a sudden impact force from a sharp object is not a realistic situation for most components either.

Research presented by Wallin shows a re-examination of the relevance of the Charpy-V test for ductile iron. He has proposed a new definition of an equivalent energy criterion for ductile iron. By taking into account for values of fracture toughness, which is a more realistic value of material toughness, he has come up with a table given equivalent values of impact energy from a Charpy-V test. He does, for instance, suggest that if a Charpy-V requirement for steel is 28 J, the corresponding requirement for ductile iron should be 13 J. This is however not studied extensively and should not be considered 100% valid (Wallin, 2014).

The fracture mechanics in ductile iron and steel is also of different nature. Fracture in steel develops through a consistent metallic matrix and the fracture surface on a Charpy specimen express what is known as shear lips, which is formed ahead of the crack tip at the boundary between the elastic zone and plastic zone. It has also been stated that the formation of these shear lips indicates plane stress behavior in the material. Fracture in ductile iron is a function of both the metallic matrix and the process of graphite de-bonding. Bradley and Srinivasan (1990) stated that Charpy-V results of ductile iron are only acceptable when the crack has sufficient matrix to travel through before it encounters a graphite nodule, which is correlated to a nodule count of less than 20mm². This value is very low and will result in decreasing mechanical properties. It can be said that there is not enough knowledge to juxtapose cast iron with steel, regarding impact energy values, taken from Charpy-V test.

3.2 Fracture Toughness

The mechanical property of fracture toughness is as mentioned a more qualitative value of toughness compared to Charpy impact values. Being a constant that can be used as a design requirement makes it an important property. In NS-EN1563 (Standard Norge, 2011) have some values of fracture toughness been listed for various grades of ductile irons (Figure 3.2).

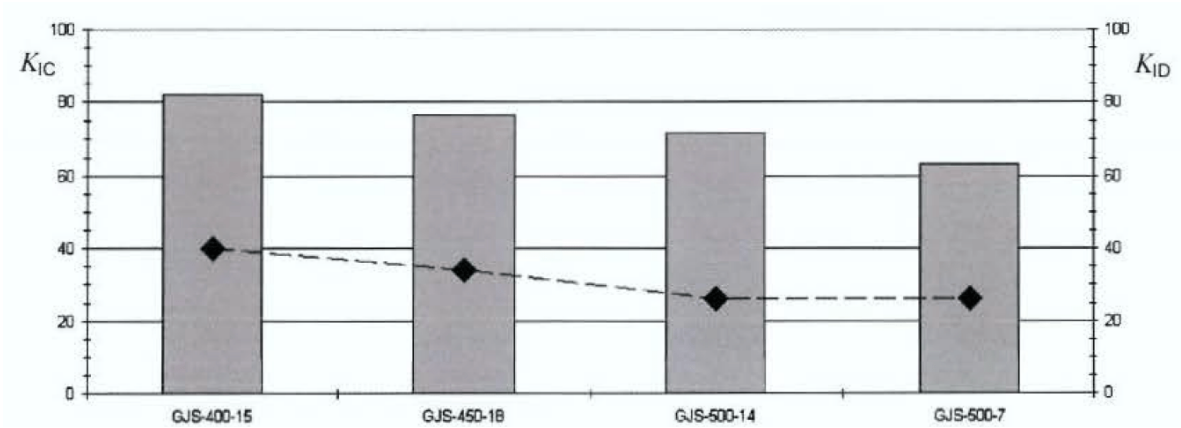


Figure 3.2: Fracture toughness of various ductile irons. Grey bars represent K_{IC} and black diamonds represent K_{ID} (Standard Norge, 2011)

These values are meant to act as a guiding value rather than a requirement for the stated grades of ductile iron.

One of the topics discussed in this report is the comparing of ductile iron and steel, with special attention towards on the relationship between toughness properties determined from impact test and fracture toughness test. A study presented by Bannister (1998) discuss the relationship between impact toughness and fracture toughness of steels. Figure 3.3 illustrates the correlating values of impact energy and fracture toughness for steels with varying yield strength.

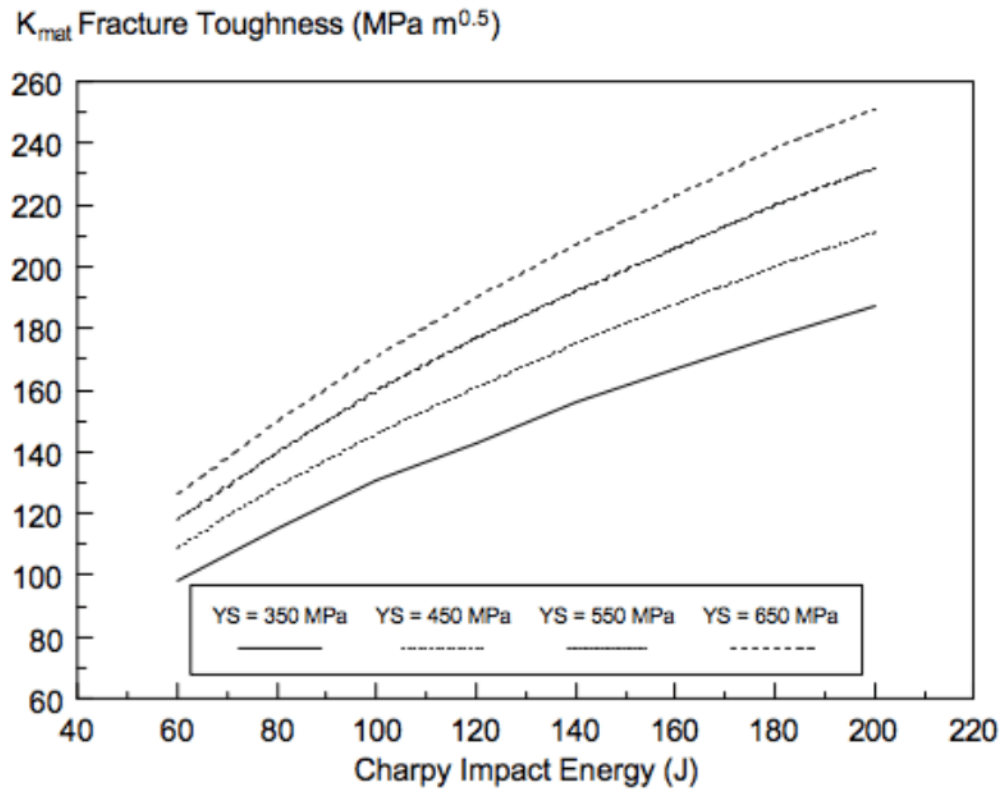


Figure 3.3: Relationship between impact energy and fracture toughness for steels (Bannister, 1998)

The general trend is that the fracture toughness value is slightly higher than the impact energy. An assumption can be made based on this statistics, that toughness values gathered from steel vary with an increment of 10-90% from impact energy values to fracture toughness values, depending on the yield strength. Keep in mind that these two values are not directly relatable and that the assumption is only based on the relationship between them. This relationship will, however, be differentiated with the resulting toughness values for ductile iron presented in Chapter 7.

The same relationship has been studied by Hesse et al. (2016), specifically targeting welded S355 steel. This result is appropriate to take into consideration in the present work due to the comparability of welded steel and cast iron. The relationship between impact value and fracture toughness for welded S355 steel is presented in Figure 3.4.

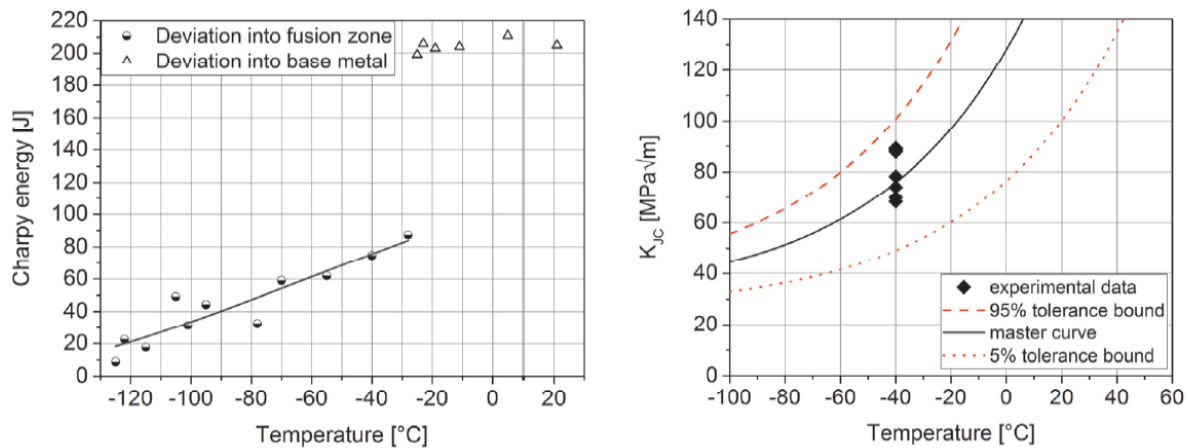


Figure 3.4: Relationship between impact energy and fracture toughness for welded S355 steel (Hesse et al., 2016)

It should be noted that the test results presented in Figure 3.4 is from S355 steel heat treated by normalization. This has been chosen due to the lack of available data for untreated S355.

When looking at the values at -20°C the Charpy impact energy is measured to be approximately 90 J the fracture toughness approximately $97 \text{ MPa}\sqrt{\text{m}}$. This results in an increment of 7.8% from the impact energy to fracture toughness. This percentage will be used as a basis of comparison with the materials studied later in this report.

A report published by Ko (2012), for Samsung Heavy Industries (SHI) take into consideration the issue of excluding ductile iron based on Charpy impact values. Two grades of ductile iron, 400-18LT and 350-18LT, have been used as construction material for hub, main frame and bearing housing in the wind turbine industry, in working conditions of -20°C and -40°C , respectively. The report highlights that predominant ferritic ductile iron is sufficient for being used in cold working environments. This statement is based on the requirements of a maximum pearlite content of 10%, at least 90% graphite nodules with the highest roundness (shape V and VI), and a minimum fracture toughness value of $50 \text{ MPa}\sqrt{\text{m}}$ at the specific working temperature. Ductile iron grades of 450 and 500 are have also been reported to be used in the wind turbine industry, provided that they meet the stated requirements. These requirements are being used by SHI to categorize ductile iron, and will also be the guiding requirements for the evaluation of the materials studied in this report.

3.3 Effect of Silicon

Silicon is, as mentioned, an essential element in the production of ductile iron. Several studies have documented positive effect with increasing amount of Si. Glavas et al. (2016) conducted a study on the effect of increasing amount of Si in ductile iron. The study focused on 6 types of ductile iron with wt% Si from 3.11 to 5.42. The properties regarding strength increased with a higher amount of Si, up to a certain specific amount. The same trend was observed on the nodule count and nodularity. These properties increased until the amount Si reached 4.22 wt%. At this point, the strength, nodule count and nodularity decreased slightly, but enough to conclude a decreasing negative trend after 4.22 wt%. Regarding other properties did the material experience decreasing values of both elongation and impact energy, and increasing values of hardness. The elongation did have a somewhat steady value until a negative drop at 4.22 wt% Si. The impact energy is often negatively correlated to the strength of a material, which is also the case in this example. The results from this study are illustrated in Table 3.1.

Table 3.1: Test results with increasing wt% Si (Glavas et al., 2016)

Si	Tensile strength	Yield strength	Elongation	Impact energy	Nodularity	Nodule count
[wt%]	[MPa]	[MPa]	[%]	[J]	[%]	
3,11	487	356	18.5	106	83.1	177
3,55	509	410	17.4	81	84.6	198
3,80	551	468	17.0	63	87.1	249
4,22	637	553	10.5	45	87.6	305
4,71	592	538	3.3	19	87.4	301
5,42	531	531	-	10	86.1	304

By studying the result it is clear that the Silicon is making the material harder and stronger, but also more brittle. This was not due to an increasing amount of pearlite, which is normally the reason for embrittlement of ductile iron. The ferrite content were at 98.1% at 3.11 wt% Si and reached 100 % at 3.80 wt% Si. The brittle behavior occurs due the increased embrittlement of ferrite. It has a minor but positive effect on the nodularity, however, the effect

on the nodule count it substantial. With this it can be assumed that the Silicon does not promote the nodularity of the graphite but that it makes the existing graphite exists smaller in size and larger in quantity. The study did also highlight that ductile irons strengthened by Si possess a higher yield/tensile strength ratio than other ferritic, ferritic/pearlitic and pearlitic ductile irons. With this, it can be assumed that the increased amount of Si has a greater effect on the yield strength than the tensile strength. It is clear from this report that ferritic ductile irons strengthened by Silicon possess a beneficial combination of mechanical properties (Glavas et al., 2016). According to this study, the maximum limit of Si, before it becomes damaging, is recorded to be at 4.22 %.

Regarding Silicon’s effect on the material at lower temperatures, there is a common assumption that the embrittled ferrite will affect the toughness properties of ductile iron by lowering the temperature. The effect is illustrated in Figure 3.5.

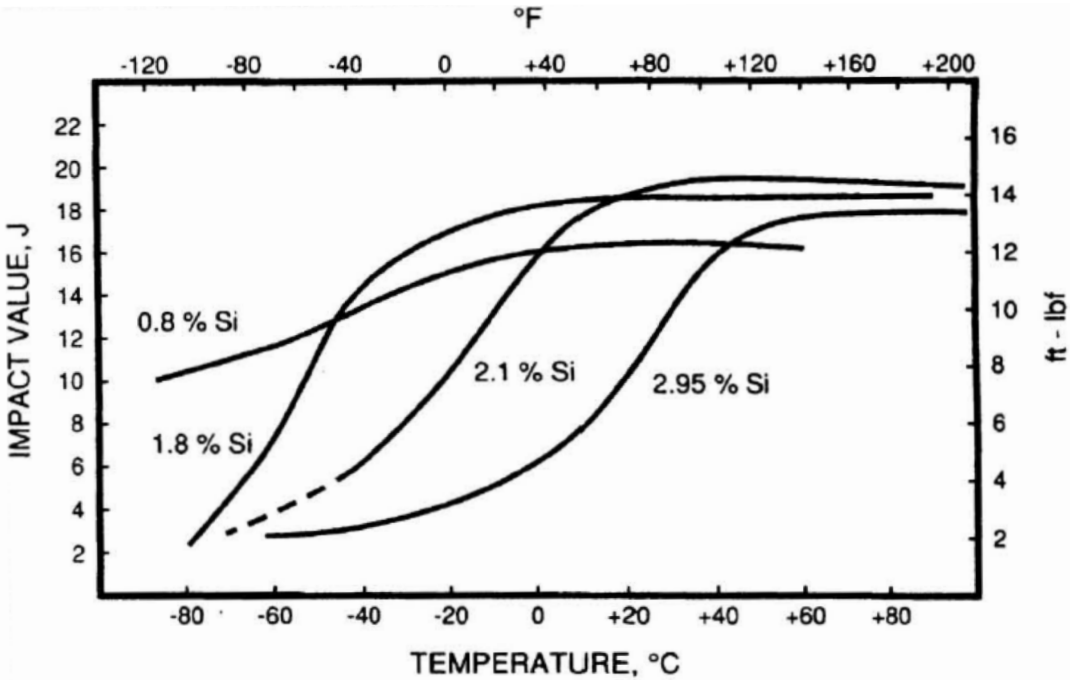


Figure 3.5: Influence of Si content on Charpy V impact energy of ferritic ductile iron (Labrecque and Gagne, 1998)

This study does however not view the possible changes to properties that could occur at lower temperature, and if the increasing amount of Si affects the ductile-to-brittle transition temperature in any way.

3.4 Effect of Ferrite and Pearlite on Impact and Fracture Properties

It is clear that the mechanical properties of ductile iron is largely controlled by the microstructure. The importance of the graphite nodules has been discussed and highlighted previously. The graphite structure is however not the only significant microstructural feature. The graphite is surrounded by a metallic matrix, which is in the case of ductile iron, normally ferrite or pearlite. This matrix structure has the ability to affect the mechanical properties in both a positive or negative manner, and are crucial to control. Hafiz et al. (2005) published a research performed on the effect ferrite and pearlite have on the impact properties in ductile iron. The materials experimented on, all had the same chemical composition but went through different controlled cooling rates and/or heat treatment to promote different matrix structures. 5 materials with matrix structures ranging from fully ferritic to fully pearlitic were tested with a V-notched Charpy test to measure the impact value followed by a fracture surface analysis.

Ferrite is originally known to be a more ductile structure than pearlite. But the direct effect on the impact resistance and the crack development through the two structures is important to understand when talking about ductile iron.

The result was plotted with regards to 3 different parameters. The fracture initiation energy (E_i), the fracture propagation energy (E_p) and the total fracture energy (E_t) – illustrated in Figure 3.6. All the five materials had similar values regarding the recorded fracture initiation energy, which can be interpreted as that matrix structure does not have a clear affect on resisting crack initiation. The crack propagation energy, on the other hand, had a clear increasing effect with a higher amount of ferrite. Confirming ferrite as a structure with higher ability to absorb energy and deform plastically.

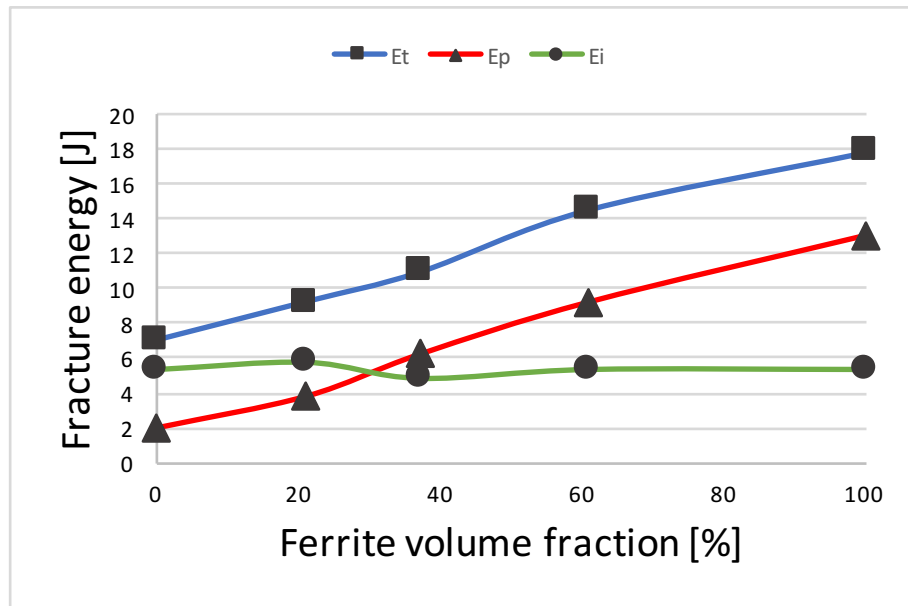


Figure 3.6: Impact properties on ductile iron with increasing volume of ferrite (Hafiz et al., 2005)

The fully ferritic material exhibits the highest fracture energy of 18 J. It can be assumed that the large difference regarding crack propagation energy is a result of ferrite's ability to absorb energy through plastic deformation, which pearlite does not possess. With a ferrite volume below 30% the fracture initiation energy is larger than the crack propagation energy. This is due to the presence of the more brittle pearlite phase. This is another confirmation that a value of fracture toughness will most likely be larger in a fully ferritic material than a fully pearlitic. Hafiz et al. (2005) also studied the ferritic and pearlitic effect on the crack propagation through the material. This study observed extensive nodule decohesion, not only ahead of the crack tip, but in a larger area affected by the applied stress. This process of decohesion transforms the ferritic matrix from a solid solution to a matrix containing holes, acting as stress concentrators. The plastic deformation in the ferritic material occurs to relieve the stress concentration caused by these voids.

This development is not favorable in the way that it creates porosity in the material, lowering its resistance to fracture. Despite this feature, the fully ferritic material expressed a different crack propagation than the pearlitic material, characterized by direction changes and ductile fracture characteristics. With increasing amount of pearlite, the crack experienced a more straight path sensitive to microcracks appearing ahead of the crack tip creating a cleavage fracture.

The results from the fracture propagation study correlates well with the results from the impact tests. Where the high energy of fracture propagation in the ferritic material is mostly controlled by ferrite's ability to absorb energy and deform plastically (Hafiz et al., 2005). These results show the clear difference in ferrite and pearlite's ability affect the properties of ductile iron regarding impact toughness. It can be safe to assume that to achieve high impact toughness, a ferritic matrix is favorable.

3.5 Mechanical Behavior of Graphite Nodules

One of the features that make ductile iron different from other material, such as steel or aluminum, is definitely the graphite nodules. These spheres are a key feature in how the material behaves when affected by stress and strain. Their shape and position in the matrix make them behave as stress arresters with the ability to stop the further development of a crack. The fracture propagation discussed by Hafiz et al. (2005) regarding decohesion around the graphite nodules are one of the mechanics that makes ductile iron special. The decohesion in front of the crack tip will in the case of a ductile matrix act positively, but can also negatively affect the fracture properties if the matrix is brittle and sensitive to crack development. Nodule decohesion is the mechanics of separation of the graphite nodule and the surrounding matrix. In the case of a slow developing crack, this decohesion can occur ahead of the crack tip due to the surrounding plastic zone.

A study conducted by (Cavallini et al., 2011) focus on the void formation and crack propagation around graphite nodules. In a ductile matrix, this reaction can happen in the formation of spherical voids around the nodules, illustrated in Figure 3.7. A developing crack will come upon this void and the sharp crack tip will be stopped temporarily. If there are no existing microcracks in this void, the crack is forced to restart from a blunt surface, which require a higher amount of stress. This mechanic will directly improve the material's resistance to fracture. On the other hand can this decohesion in a brittle material – pearlitic or embrittled ferritic – have a negative effect. If microcracks occur in the interface between nodules and matrix they can appear as stress concentrators instead of stress arresters, making crack propagation easier trough the material. Resulting in a lower resistance to failure.

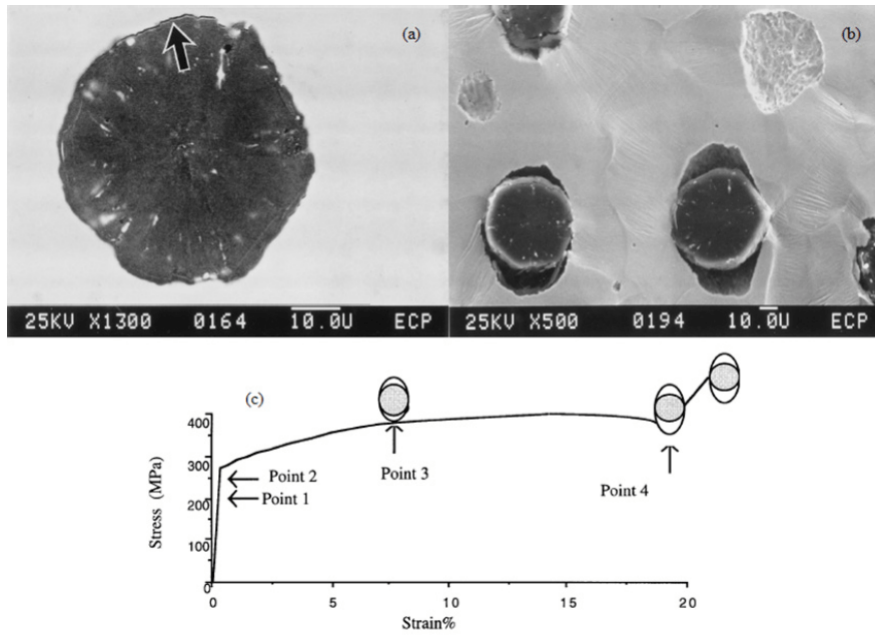


Figure 3.7: Decohesion of graphite nodule and matrix during tensile test. (a) Decohesion in the interface. (b) Void growth around nodules. (c) Stress-strain curve with connecting void growth. (Cavallini et al., 2011)

Whether decohesion is occurring in all types of ductile iron or not, or if Si has any direct impact on this feature is not sufficiently studied, and can not be confirmed. But it would seem that decohesion is mostly occurring when the material is subjected to fatigue crack growth rather than a sudden impact force.

4. Fracture Surface Study

This report was originally intended to be based on three different types of ductile iron – presented in Chapter 5. Due to unexpected delays concerning the production of the three materials and machining of test specimens, it was decided that the fracture surface analysis should be conducted on four separate materials. These materials are chosen based on their ductile iron quality is the same as the three main materials, as well as being realistic substitutes regarding microstructure. This makes this analysis realistic with regards to highlighting the effect of different matrix structure and increasing Si content, ultimately being sufficient to discuss the fracture behavior of the three main materials.

This chapter will view and discuss how different amount of Si, as well as varying mechanical properties, affects the fracture surface of ductile iron. This is done to highlight what makes ductile iron behave in a brittle or ductile manner. What characteristic fracture properties that occur in materials with increasing amount of Si and/or high and low value of elongation. The study will focus on four already fractured tensile bars, and specimens will be viewed in a SEM to illustrate the microstructural difference on the fracture surface.

4.1 Materials

The materials studied in this chapter has been produced by Elkem, tested at a certified lab and delivered with adjacent test result on mechanical properties and chemical analysis. This study has been limited to 4 materials with different wt% Si and elongation listed in Table 4.1. The materials targeted quality is 700-2, 600-10, 600-10, and 400-18, but will, due to simplification purposes, be mentioned in this report as FR1, FR2, FR3 and FR4, respectively.

Table 4.1: Mechanical properties of tensile tested materials

Material	FR1	FR2	FR3	FR4
Tensile strength [MPa]	694	596	614	484
Yield strength [MPa]	453	503	503	321
Elongation [%]	2	9	17	21

There are large variations regarding elongation for these four materials. The common assumption of strength and elongation being opposing values are not that clearly visible since FR3 have a larger strength than FR2 even though the elongation is greater in FR3. This could be because of variations in the chemical composition (Table 4.2) or difference in the casting process.

Table 4.2: Chemical composition of tensile tested materials

Material	FR1	FR2	FR3	FR4
C [%]	3.5	3.1	2.83	3.5
Si [%]	2.6	4.3	4.4	2.5
Mn [%]	0.90	0.33	0.32	0.32
P [%]	0.0260	0.0250	0.0260	0.0239
S [%]	0.00970	0.0090	0.010	0.0099
Mg [%]	0.0478	0.0460	0.0460	0.0480

From Table 4.2 it is clear that FR1's pearlite matrix most likely is originating from the high amount of Mn. FR2 and FR3 have both a high amount of Si but FR2 have a larger quantity of C which also can affect the microstructure.

Figure 4.1 illustrates the 4 tensile bars used in the study. FR1 did not break inside the preferred area. This could affect the mechanical properties, meaning the values listed in Table 4.1 may not be realistic. The specimen is chosen to be studied anyway to highlight the microstructural effect of pearlite. The main focus in this study will be the difference between FR3 and FR4; these two materials have not so different value of elongation but different content of Si. The effect Si have on the fracture surface is relevant this report. Seen on Fig-

ure 4.1, the most ductile materials, FR3 and FR4, have experienced some sort of necking during the tensile testing process. However, the feature does not appear as clearly as in some steels, illustrated in Figure 2.10(a). With a closer look, the more dominant feature in the plastic zone is the propagation of microcracks.

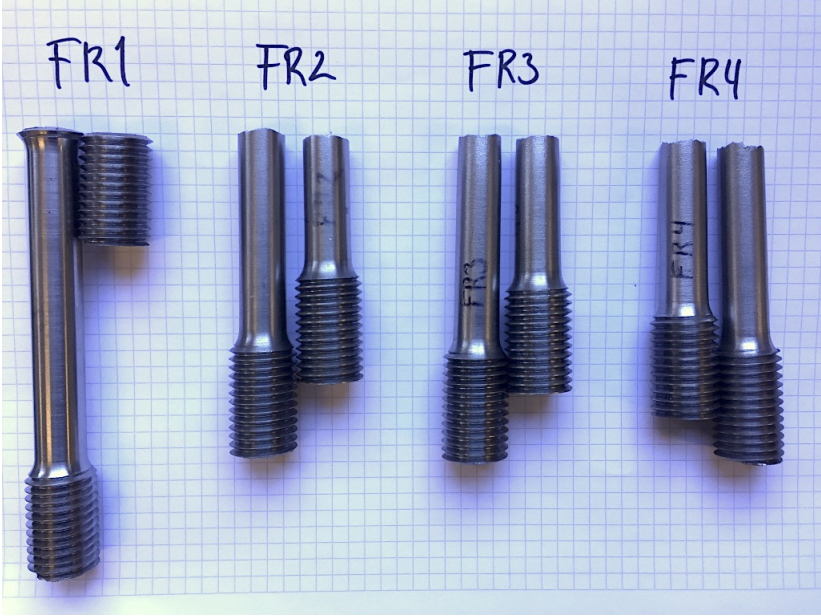


Figure 4.1: 4 tensile bars used in fracture surface study



Figure 4.2: Fracture surface of the 4 cut tensile bars

By studying Figure 4.2 the most ductile material (FR4) exhibit a darker fracture surface than the others. This is most likely because of a higher concentration of graphite, however, this

feature will be evaluated through the SEM images in Section 4.3.2. FR2 and FR3 do also contain this darker surface feature, though only locally, as seen in the center of FR3. FR1 and FR2 have a reflective fracture surface which is clearly visual without magnification. This is, as mentioned in Section 2.4.1, a clear sign of a brittle transgranular fracture. This feature is not visual in either FR3 or FR4, which make sense looking at the value of elongation for these test specimens.

4.2 Experimental

The microstructure was examined at Elkem Foundry Products' laboratory for determination of graphite structure and amount of ferrite and pearlite.

The microstructural analysis of the fracture surface was conducted at a ZEISS Supra 35VP SEM. The samples required no custom preparation before being placed under the electron beam. Ductile iron is a ferromagnetic material which will not cause disturbance to the electron beam or the magnetic lenses. The signals used for the image generation are secondary electron due to their ability to generate more detailed topographic images.

4.3 Results

4.3.1 Microstructure

The microstructural analysis showed variation in graphite formation and matrix structure. Images of etched samples are shown below to visualize the distribution of the two matrix structures as well as the graphite structure of each material. These values are listed in Table 4.3 to clearly illustrate the main differences.

Table 4.3: Microstructural characteristics of the FR-materials

Material	FR1	FR2	FR3	FR4
Nodularity [%]	87.0	-	72.0	83.0
Average nodule size [μm]	33.4	-	27.6	32.4
Number of nodules	1392	-	1796	1663
Ferrite [%]	3.4	100	100	78.0
Pearlite [%]	96.6	0	0	22.0

Note that FR2 have not listed values regarding graphite structure. The reason for this is that the automatic image analysis of the graphite structure is not feasible when there is chunky graphite present. It will potentially give an incorrect high number of nodules but with low nodularity. This structure is clearly visible in Figure 4.3(b). The other materials have a acceptable value of nodularity. Regarding the distribution of ferrite and pearlite, it is clear that Si is a strong ferrite promoter – the two high Si material are both fully ferritic. The critical effect of Mn is clearly visible from this table, most likely being the factor that makes FR1 close to fully pearlitic.

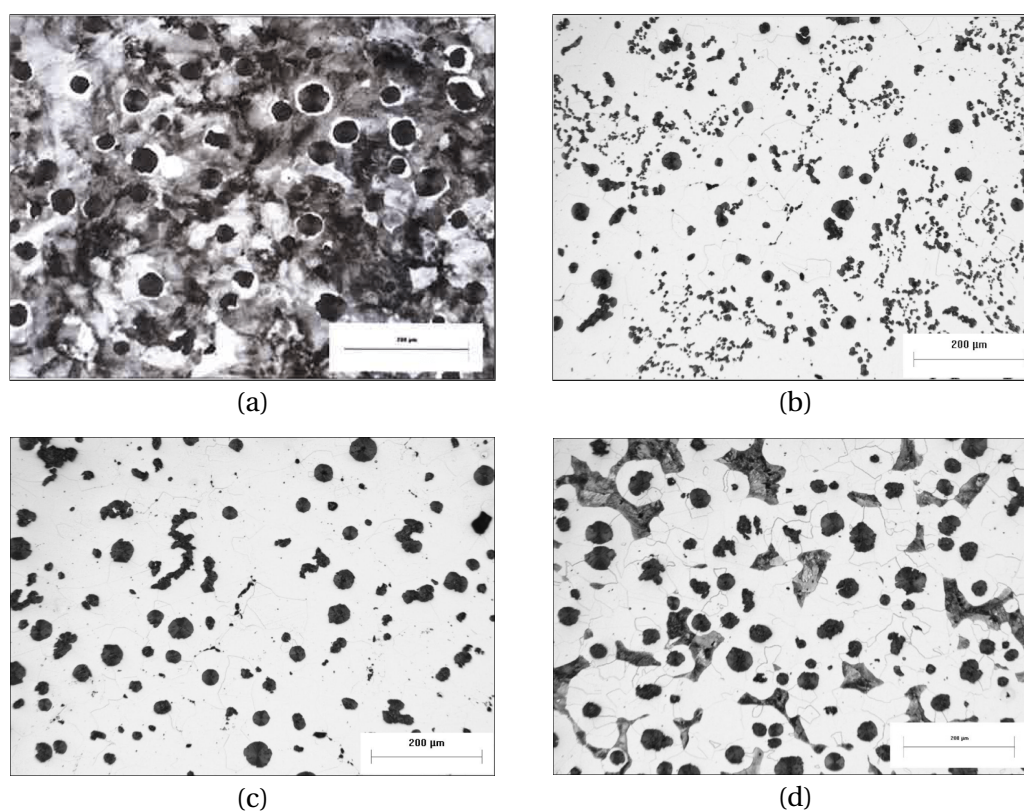


Figure 4.3: Microstructure. (a) FR1, (b) FR2, (c) FR3, (d) FR4

The images in Figure 4.3 show plane samples etched in Nital (acid mix of 5% nitric acid and 95% alcohol). The Nital is what makes it possible to visually be able to see the different microstructures. Visually there is a large difference in the ferrite and pearlite. The ferrite being clear white, only showing the grain boundaries and the pearlite appearing as dark areas.

Figure 4.3(b) does consist of a chunky graphite structure, which is not preferable. From Table 2.2 it's stated that this structure could be a result of high Si content. On the other hand, does FR3 have a larger amount of Si without experiencing the formation of chunky graphite. It could be other individual difference that causes this outcome like the purity of the charge, various cooling rates or poor inoculation. It is known that FR2 and FR3 had the same target grade, but are treated with different inocuants, which could assume that inoculation is the main reason for the chunky graphite formation. Figure 4.3(d) being the low Si material does consist of 22% pearlite, which is most likely due to the low Si content, or traces of pearlite promoting elements.

4.3.2 Fracture Surface

Images in Figure 4.4 are all captured at a magnification of 200X to focus on the difference in graphite concentration and formation.

It looks like the concentration of graphite is substantially larger in FR4 than the other materials. Without knowing the carbon content or the nodule characteristics it could be assumed that these values would be larger in FR4. However, this is not the case, clearly illustrated in Table 4.3. The reason for the this more likely due to the crack propagation through this material, exposing the graphite nodules through nodule cohesion.

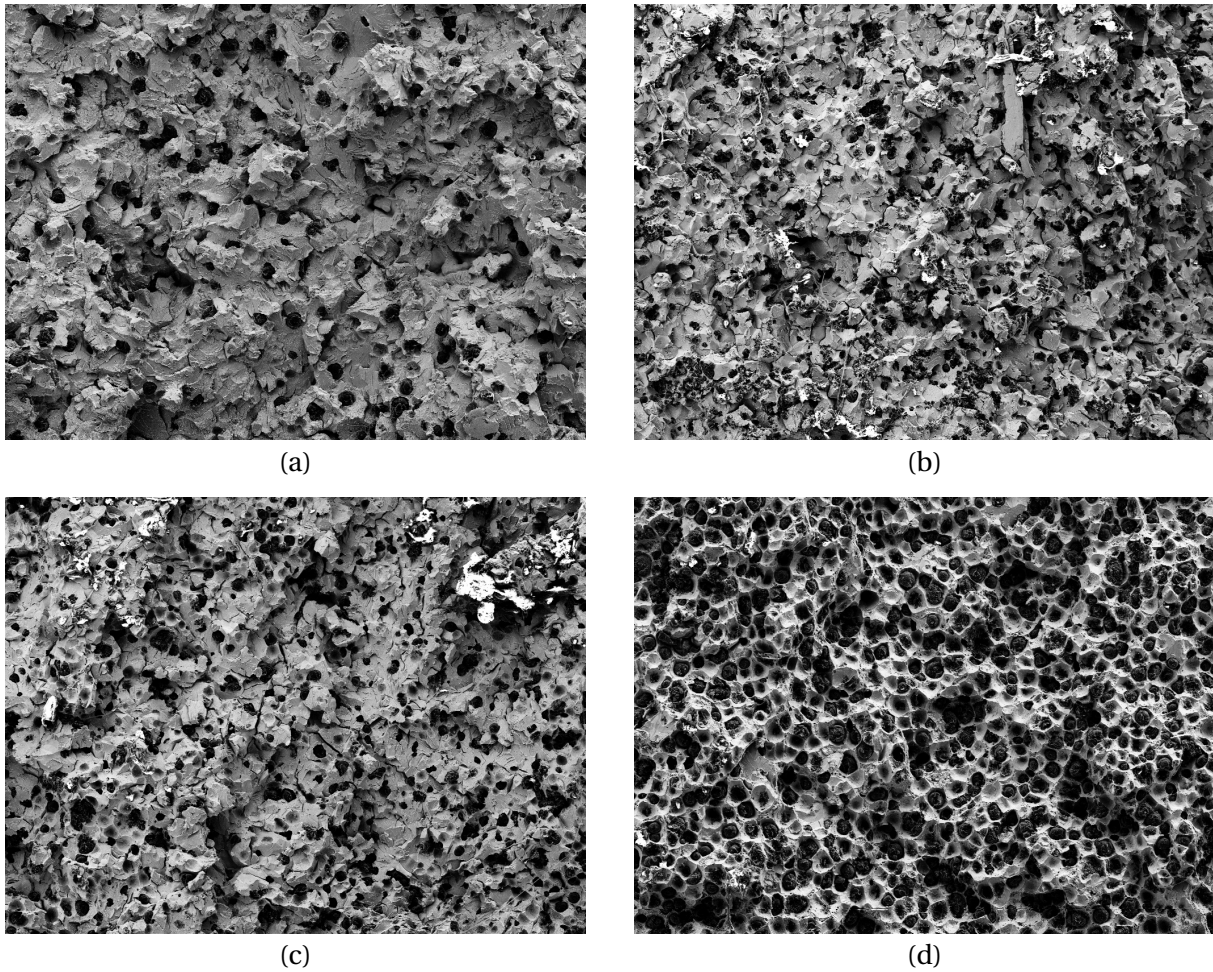


Figure 4.4: Fracture surface at a magnification of 200x. (a) FR1, (b) FR2, (c) FR3, (d) FR4

It is clear that the concentration of graphite is substantially larger in FR4 than the other materials. This is not surprising considering this material's high value of elongation and relatively low content of Si – preventing Si embrittlement of the ferritic matrix. This will naturally also negatively affect the strength, which is the lowest of the four, illustrated in Table 4.1. By looking at Table 4.2 the only difference between FR1 and FR4 regarding chemistry is the amount of Mn. This has clearly a damaging effect, not only by creating a fully pearlitic matrix but also on the formation of graphite nodules. From a visual perspective, the graphite concentration in FR1 is by far the lowest, even though the C content is similar to FR4. FR2 and FR3 exhibit similar values for both strength and chemical composition but a large difference in the value of elongation. This seems to be because on the formation of chunky graphite, showing the importance of spheroidal nodules to achieve high ductility. FR3, which possess superior mechanical properties, shows a smaller graphite concentration, on the surface, than FR4. This outcome could have materialized from the strength-

ened ferritic matrix dominating the fracture propagation.

When studying these surfaces at a higher magnification the nature of the fracture development is easier to characterize. The images in Figure 4.5 are all taken at a magnification of 1000x.

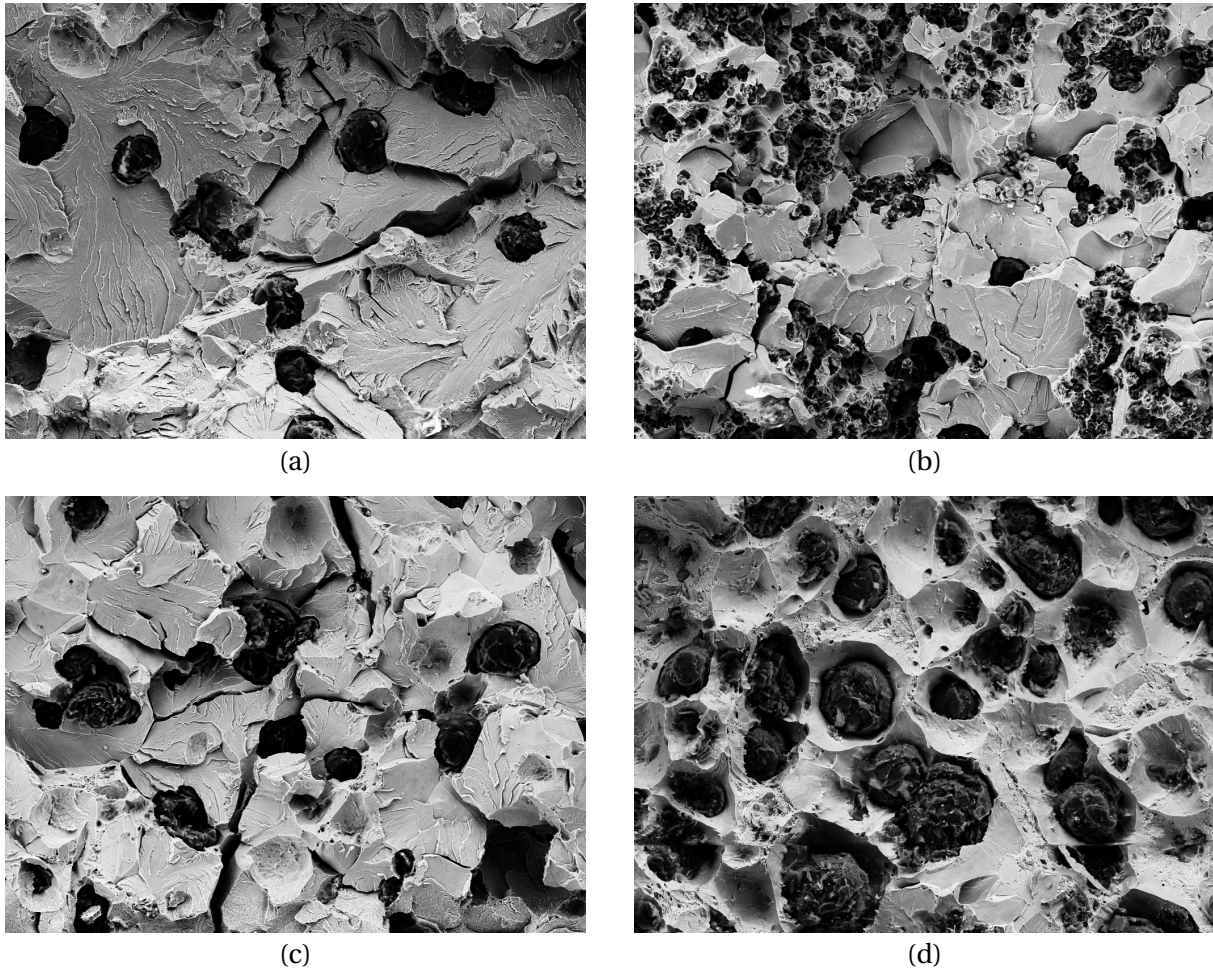


Figure 4.5: Fracture surface at a magnification of 1000x.
(a) FR1, (b) FR2, (c) FR3, (d) FR4

The most brittle material, FR1 (Figure 4.5(a)), clearly display a characteristic feature for a brittle fracture, known as river patterns. Succeeding this observation, it can be assumed that the crack propagation through this material is of a transgranular nature – crack development through the interior of grains. The grainy or faceted texture of the fracture surface is another confirmation that this is a characteristic brittle fracture. The relative large flat surfaces, creating reflections are also visible in this image. The microstructural features of this material is not unexpected considering the known characteristics of a predominant pearlitic matrix.

FR2's damaging graphite structure is more visible at this magnification, clearly showing areas of high accumulation of coarse graphite particles. This fracture surface does also show signs of intergranular crack propagation – crack development along grain boundaries – as well as transgranular fracture. The same trend is witnessed in FR3 which features intergranular fracture, visible at the top right corner of Figure 4.5(c). More intergranular fractures are most likely the outcome of embrittlement of the ferrite caused by high Si. Results of embrittlement are also visible from the development of microcracks in the matrix. These cracks are most likely not a result of the tensile tearing mechanism since these crack are developed perpendicular to tearing angle. Development of these types of microcracks is not optimal for the integrity of the material and is crucial to be controlled in a production phase.

FR4 shows the characteristics of a ductile fracture. The fracture surface consist mostly of graphite nodules, or areas that nodules have been teared of from. Areas with some distance between nodules show signs of transgranular brittle fracture. When studying the matrix around the graphite nodules, it is clear that it exhibit characteristics of a ductile fracture. Mostly in the shape of micro dimples and areas with height difference. These ductile feature seem to appear mostly close the graphite particle and at a certain distance between the borders of two or more graphite nodules, visible in the center of Figure 4.5(d).

4.4 Discussion

The silicon content in ductile iron clearly has a large impact on both the mechanical properties and visual fracture surface characteristics. The most surprising result is the impressive mechanical of FR3 with both high strength and elongation, despite the fact that the embrittling effect in the matrix is clearly visible in the microstructure, in the shape of inter- and transgranular fractures. This backs up the theory that high content of Si is not necessarily related to low elongation – at least up to 4.40 wt%. The difference in elongation between FR2 and FR3 is a good confirmation of the damage caused by an unwanted graphite formation. Regarding the visual aspect, a high value of Si in a ferritic matrix can cause similar fractographic appearance as a pearlitic matrix, but when comparing the mechanical properties, embrittled ferrite have a superior ductility and larger yield strength, meaning it is challenging to determine mechanical properties by just studying the fractographic fea-

tures of ductile iron.

One of the clear disadvantages of high Si content is the development of microcracks in the embrittled ferrite matrix. This is a consequence of embrittlement and is a dangerous feature that can be difficult to determine without this type of fracture surface analysis. It is likely to be damaging regarding impact properties as well.

The main reason for the reduced elongation experienced in FR2 is likely due to the undesired graphite structure. The graphite exists as smaller and coarser in this structure, leading to a smaller surface area bound to the surrounding matrix. This results in a lower amount of stress needed to tear the matrix and graphite apart, which will affect the elongation.

It can be assumed that fracture surfaces of ductile iron mostly exhibit brittle fracture features, even though the elongation, determined from a tensile test, is large. FR4 do express some ductile characteristic, however, not comparable to a ductile fracture of steel. By studying Figure 4.5(d) it can be concluded that the ferrite existing closely around the graphite nodules are more ductile than areas further away from the graphite. This could have a connection with the growth of the graphite nodules during solidification. The ferrite surrounding the graphite nodules is the first microstructure developed during solidification – assuming the cooling is relatively slow. It is a known fact that slow cooling rate promotes grain growth and reduce dislocations within the grains in iron, which will lead to a more ductile ferrite. From the theory of nucleation and grain growth, it can be suggested that the ferrite existing around the graphite have fewer dislocation and therefore exhibit a more ductile behavior. This could be the case in FR4. The cooling rate of this material is unknown, but the fracture surface is probably not abnormal for a low silicon alloyed ferritic ductile iron. The areas of FR4 that exhibit features of brittle fracture – as seen at the bottom of Figure 4.5(d) – could be due to the local formation of pearlite in the matrix. The occurrence of pearlite in the microstructure (4.3(d)) does seem to correlate well with the occurrence of areas of brittle fracture in FR4.

5. Materials

This thesis will focus on three specific types of ductile iron. The standard designation of ductile irons starts with EN-GJS, according to NS EN1563 (Standard Norge, 2011). The first number following the material specification name represents the material's minimum tensile strength and the last number corresponds to the material's minimum elongation. The three types of ductile iron are listed in Table 5.1. Note that the materials will be mentioned without the material specification EN-GJS throughout this report.

Table 5.1: 3 different grades of ductile iron

Types of ductile iron
EN-GJS-400-18LT
EN-GJS-500-14
EN-GJS-500-7

400-18LT is a standardized material used a variety of applications the last years, among other, in the wind turbine industry, where it is used as a construction material for hubs, main frames and bearing housing (Shirani and Härkegård, 2014). The materials 400-18LT and 500-14 were produced at Mandal Castings specifically for this thesis. The 500-7 material was provided by a producer of lifting appliances for offshore applications. This material is currently under evaluation for use in offshore application which has to comply with DNVGL-OS-E101.

The original plan was to use two other materials, including 400-18LT and 500-7, named 450-18 and 500-14. To study the effect of Si in the range from ca 2.0%, ca 2.5%, ca 3.0% to ca 3.5% on mechanical properties and fracture behavior. Due to time constraint, the 450-18 material was taken out, and it was decided to focus the studies on the 500-14 material as it has the same tensile strength as 500-7, which is currently in use for the application in question. 500-14 is categorized as a solution strengthened ferritic iron with an intermediate Si content.

5.1 Mechanical properties

The standardized minimum mechanical properties for the materials examined, according to Standard Norge (2011), are listed in Table 5.2. The minimum values are read from a relevant wall thickness (t) of $30 < t \leq 60$ mm. Be aware that these properties are not necessarily equivalent to the actual properties of the casting component as the actual section size might be different.

Table 5.2: Minimum requirements for given materials (Standard Norge, 2011)

Material	Tensile strength [MPa]	Yield strength	Elongation [%]
400-18LT	380	230	15
500-14	480	390	12
500-7	450	300	7

These minimum properties are the values a foundry will have to document that the reference casting used, is complying with. Actual properties may exceed and differ from these minimum properties significantly. One of the goals of this report is to examine the possibility of obtaining high ductile properties at lower temperatures with a higher amount of Si and high strength.

5.2 Chemical composition

The 3 different material listed in Table 5.1 have a different chemical composition that affects the behavior of the materials regarding microstructure and mechanical properties. The biggest difference in chemical composition in the materials is the amount of Si. One of the main objectives of this report is to study the effect of varying Si. A chemical analysis of all the materials studied was provided by Elkem Foundry Products. The analysis provides the exact compositions of the casted materials. Table 5.3 highlights the standardized wt% Si and C in the given materials.

Table 5.3: Standard amount of Si and C (vonRoll casting, 2017), (Standard Norge, 2011)

Material	wt% Si	wt% C
400-18LT	2.30-2.60	3.20
500-14	3.40-3.80	3.80
500-7	2.30-2.60	3.50-3.70

500-14 are, according to NS-EN1563, categorized as solution strengthened ferritic grade of ductile iron. These grades are strengthened by silicon and as a guidance value, the approximate amount of Si for these materials are listed as 3.80%.

5.3 Microstructure

The three given materials are all preferably predominantly ferritic. Due to the high value of Si in 500-14 will this material most likely have the highest ferrite distribution. To achieve good toughness properties, pearlite should be kept at a minimum. Preferably with a maximum content of 10% to be regarded as sufficient for offshore application, as stated by SHI (Ko, 2012).

6. Experimental

This chapter focus on the practical experimental methods used to both produce the iron, machining the test specimens and perform the mechanical testing methods. It also contains information on the presentation of results presented in Chapter 7.

6.1 Casting

As casting to produce samples for examination a standardized cast on sample with the dimensions 200x40x55mm was used. This cast on samples is produced using a core shooter and the core is under normal conditions placed on the casting on agreed positions. These cast-on samples are based on the relevant wall thickness (t) of $30 < t \leq 60$ specified in chapter 8.3 in NS-EN1563 (Standard Norge, 2011). To ensure a sufficient number of samples available for examination the mould as, seen in the sketch in Figure 6.1, was produced. Each sample was given a specific marking to ensure traceability of location in case of deviating results, and in total 16 samples from each material produced at Mandal Castings was available for subsequent examinations.

Along with the rectangular cast samples, two round bar-shaped samples for mechanical testing according to Type A in NS-EN1563 (Standard Norge, 2011), were produced. These four cylindrical bars were later machined to tensile bars and tested accordingly.

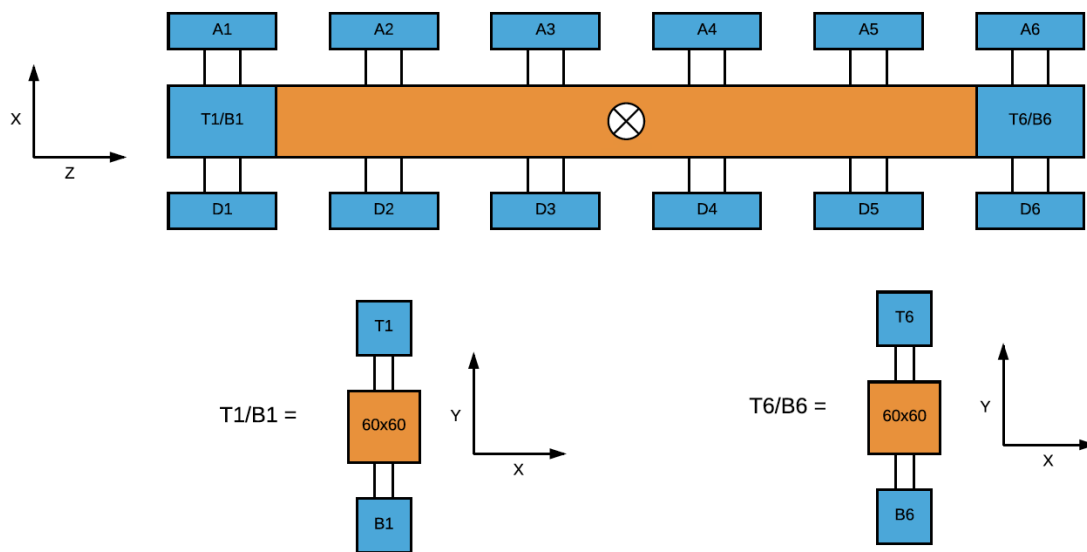
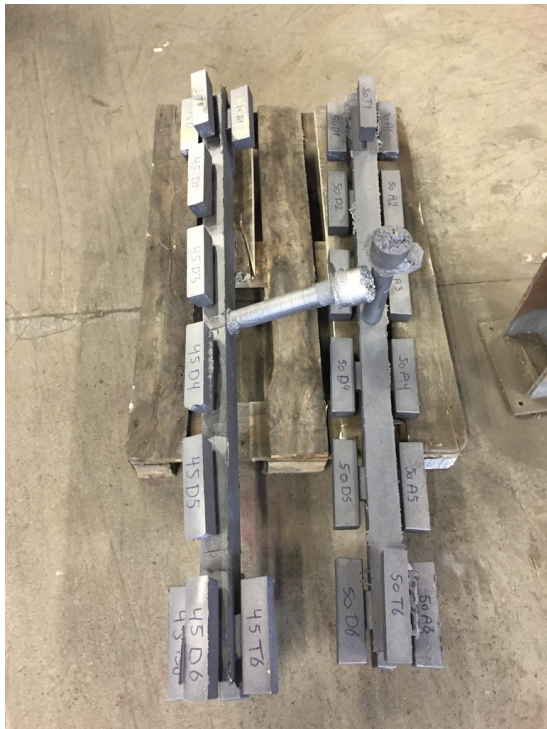


Figure 6.1: Sketch illustrating placement of the given number of samples in the cast mould

400-18 and 500-14 are produced by melting a charge consisting of a mixture of scrap iron, steel scrap and pig iron in an induction furnace with a capacity of 3 tons. Adjustments are made with alloying additions such as FeSi, FeS, FeMn etc. to give the target base iron chemistry. Once the target chemistry is achieved the melt is heated up to 1500°C. The melt is then tapped into an open ladle where MgFeSi/nodulariser has been added to the bottom and covered with steel chips. When 2/3 of the target iron volume has been tapped into the ladle tapping is stopped and the ladle is covered to allow for the reaction with Mg to subside. To the last 1/3 of iron tapped into the ladle, inoculant is added. The slag is then removed from the ladle and temperature and chemistry sample is collected prior to pouring of the mould. The addition rates and types of products are proprietary to the foundry and Elkem Foundry Products. The casting was cooled in room temperature overnight and removed from the mould the next day. Figure 6.2 shows the finished cast.



(a)



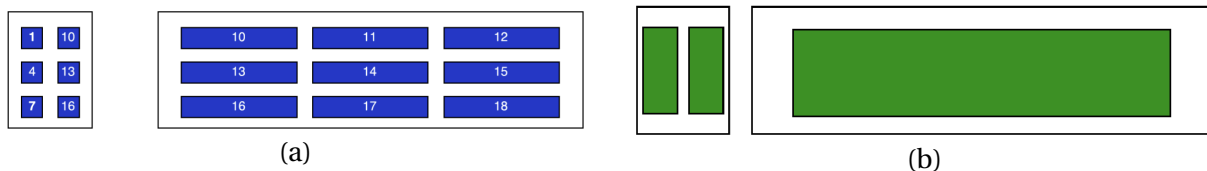
(b)

Figure 6.2: Finished cast sample

The casting process of 500-7, regarding melt composition, cooling time and procedure is not known and can therefore only be assumed when discussing the results.

6.2 Machining

The standardized test specimens casted was machined to tensile bars, fracture toughness bend specimens and Charpy test specimens. From each cast bar it is possible to get 18 Charpy test specimens and 2 bend specimens, illustrated in Figure 6.3.



(a)

(b)

Figure 6.3: Model for machining the different test specimens. (a) Charpy specimens, (b) Bend specimens.

The V-notch was produced at UiS after the specimens had been machined. A total of 2 cast bars was used to produce 36 Charpy specimens and 3 bars for the bend specimens. Due to

different factors such as time schedule and availability where two different workshops and machining techniques used. The test specimens retrieved from 400-18LT and 500-7 were machined using a CNC machine. The test pieces from the 500-14 material were machined using EDM. The bend specimens produced through CNC machining were also in need of an EDM machining process to add the notch for the fracture toughness test.

6.3 Tensile testing

The tensile test were preformed on a INSTRON 600LX with a capacity of 600 kN. The tensile bars was machined from a standardized cylindrical cast sample and tested according to ISO 6892-1 (ISO, 2009)(Appendix C).

6.4 Charpy Testing

Two types of Charpy test specimens have been used in this experiment. V-notched samples and un-notched samples. The V-notched samples' purpose is to map the ductile-to-brittle transition temperature – if possible. But most of all, to highlight the difference regarding impact properties as well as fracture behaviour between 20° and -20°C. It is stated in NS-EN1563 Standard Norge (2011) that un-notched Charpy samples are being increasingly used for as-cast ductile irons. It is also concluded that for equal values of tensile strength, Si-solution strengthened ferritic cast irons normally possess higher values of un-notched impact energy. The V-notched test specimens are, as mentioned, not values to be used in design calculations. However, they can give valuable information about the change in fracture mode at different temperatures. They can also together with un-notched samples and fracture toughness tests give a larger understanding of transition temperature. The values gathered could also be the basis of correlating and developing an equivalent value of fracture toughness together with the K_{Ic} values.

6.5 Fracture Toughness Testing

The test method of determining fracture toughness is described in ASTM E 399 - Standard test method for plain strain fracture toughness of metallic materials. It is chosen to use a three-point bend specimen presented in Section 2.5.1 (ASTM, 2012). Standardized fracture toughness specimens consist of a machined notch as well as a sharp pre-crack developed from fatiguing the test specimen. The process of pre-cracking a specimen is time-consuming and requires controlled supervision. With the restricted timeframe of this report and the large number of test specimens planned, it was decided that the fracture toughness test would be completed by a simplified test procedure. Where the normally fatigued pre-crack is substituted with a crack machined with an electrical discharge machine (EDM). An EDM have the ability to machine extremely small cuts. The EDM used in this case had the ability to machine a notch with a length of 0.36mm. A report published by Madyira and Akinlabi (2015) tested the validity of using a machined notch instead of a fatigued pre-crack when determining the fracture toughness of titanium. They concluded that using a simplified EDM notch is sufficient when determining fracture toughness on the basis that the result had a deviation of only 4.4% from results using a fatigued pre-crack.

The notch dimensions and geometry were designed from specifications listed in ISO 12135 (ISO, 2016). The test specimens were originally set to be in the shape of SE(20), with the measurements of 40x20x180mm. 400-18LT, being the first material machined had these measurements. Later it was determined that SE(15) specimens should be used instead, to follow the SHI report that focused on fracture toughness of similar materials. The 500-14 and 500-7 material will be tested with SE(15) specimens measuring 30x15x160mm. Since K_{Ic} is a size insensitive quantity, the difference in test geometry should not be an issue regarding the obtained results.

The test was performed on a INSTRON universal testing machine with a capacity of 250kN. The test specimens were tested and both room temperature (20°C) and at -20°C. Test specimens tested at -20°C was cooled in liquid, using a Julabo refrigerated circulator. Each test ran until critical fracture in she shape of a pop-in or a stable crack growth occurred. This test resulted in a graph listing the applied load versus the crack tip opening displacement

measured by the clip gauge – visible in Figure 6.4.

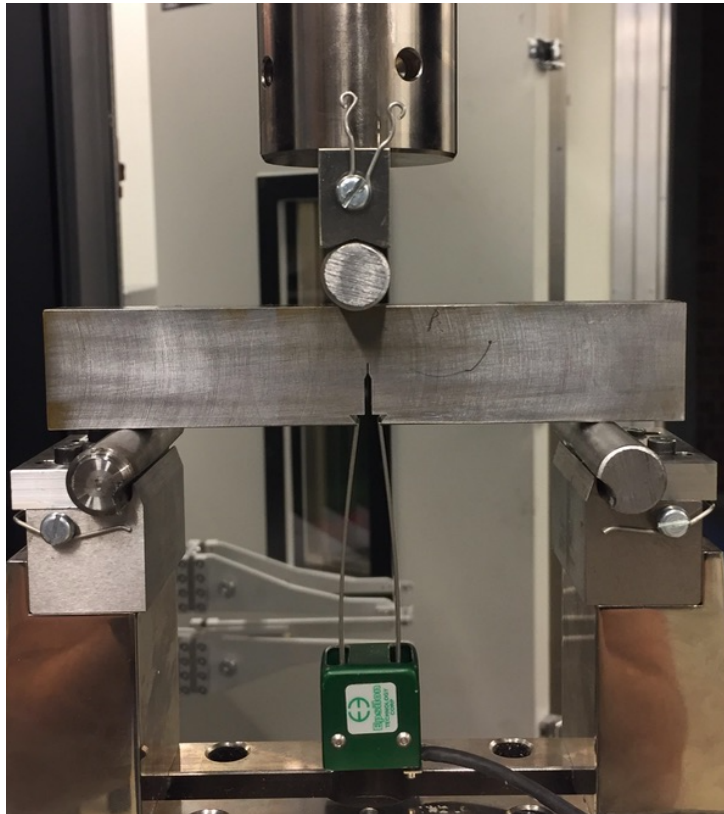


Figure 6.4: Fracture toughness test setup

6.6 Microstructural Analysis

The microstructural analysis was performed on a representative test piece taken from the same cast as the test specimens. It was polished to the point when no critical scratches or other disturbing features were visible on the surface. This process is described more in detail in Section 2.5.2.

7. Analysis

This chapter will present the results from the different mechanical tests conducted.

7.1 Mechanical, Chemical and Microstructural Properties

Here, the mechanical properties and microstructural features will be presented and discussed with relation to the chemical composition of each material.

Results from the materials tensile test are listed in Table 7.1. The results presented is the average of three samples.

Table 7.1: Results from tensile test (Appendix C)

Material	Tensile strength [MPa]	Yield strength [MPa]	Elongation [%]
400-18LT	476 ± 5.6	289 ± 2.2	17 ± 0.8
500-14	529 ± 0.7	418 ± 2.5	20 ± 1.7
500-7	682 ± 0	455 ± 31	5.7 ± 2

The resulting values are all within the minimum requirements mentioned in Section 5.1, except the elongation of 500-7. This result will be discussed later.

One of the known effects of increasing Si in ductile iron is that it increases the yield strength. When designing mechanical components, the yield strength is usually the max strain the component should be exposed to before onset of plastic deformation.

The materials highlighted in Table 7.2 are the most important elements in a ductile iron composition.

Table 7.2: Chemical analysis (Appendix B)

Material [%]	400-18LT	500-14	500-7
C	3.70	2.90	3.49
Si	2.0	3.68	2.62
Mn	0.30	0.11	0.359
P	0.020	0.017	0.029
S	0.007	0.008	0.003
Mg	0.032	0.048	0.036
Cu	0.045	0.008	0.30
Ni	0.044	0.013	0.38
Sn	0.002	0.002	0.016
CE	4.4	4.1	4.4

Results from the microstructural analysis are listed in Table 7.3.

Table 7.3: Microstructural analysis (Appendix A)

	400-18LT	500-14	500-7
Total area [mm²]	14.2	14.2	14.2
No. of particles	3360	3397	1341
No. of nodules	2890	2836	1013
Nodule density [# /mm²]	203	199	71
Nodularity [%]	86	81	84
Graphite [%]	11.5	8.5	8.9
Ferrite [%]	100	100	14.9
Pearlite [%]	0	0	85.1
Particle size [μm]	26.5	23.2	36.7
Nodule size [μm]	25.7	21.8	37.6

The microstructural analysis indicates only minor differences between 400-18 and 500-14. However, there is a substantially large difference between these two materials and 500-7 when it comes to the number of nodules, which are fewer and larger in 500-7 and the dominant matrix which is predominantly pearlitic in 500-7. This can be seen clearly in Figure 7.1(c) below.

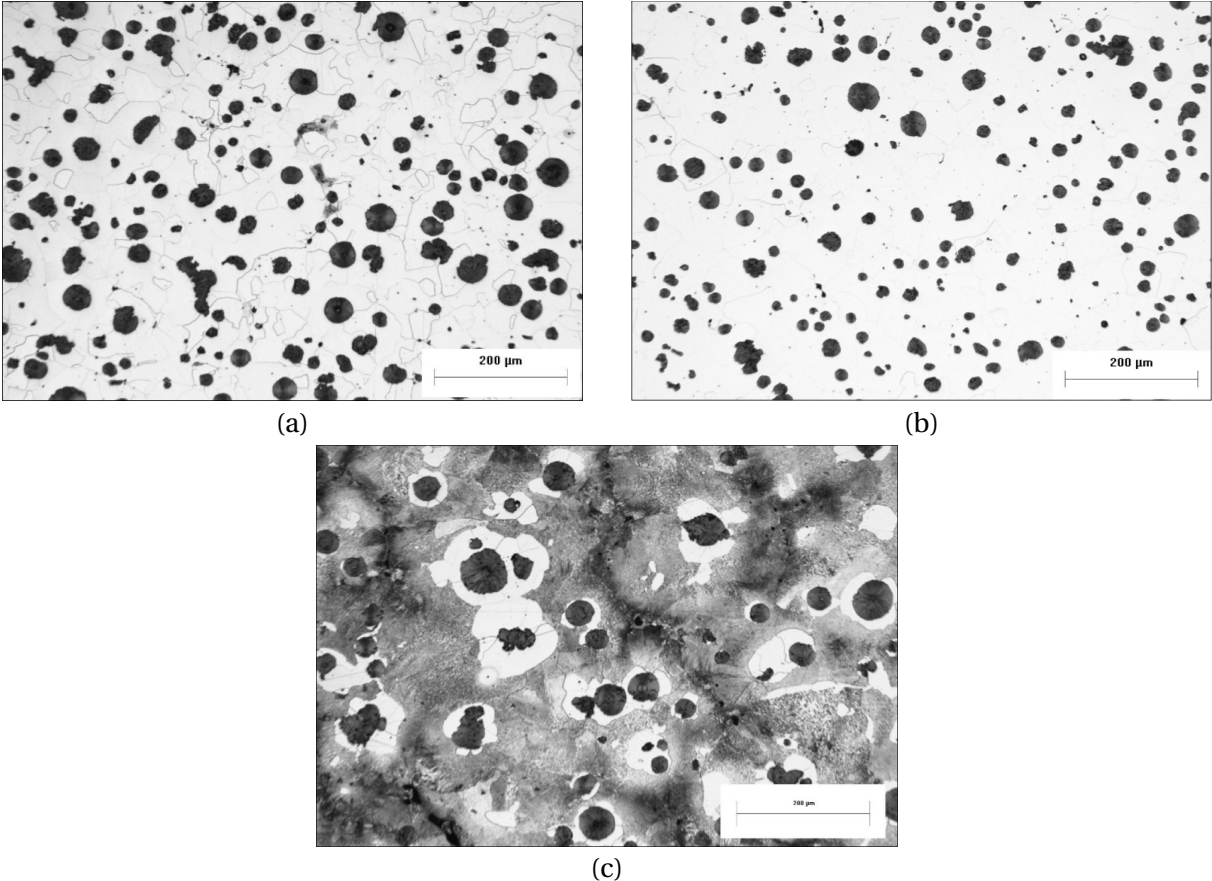


Figure 7.1: Representative image of the microstructure of the three materials. (a) 400-18LT, (b) 500-14, (c) 500-7

Figure 7.1(a) shows minor traces of pearlite in the matrix. This is, however, too little to be measured against the dominant ferrite, and still, less than 5% which is normally the maximum allowed for this material.

The values listed in Table 7.3 illustrates large similarities between 400-18 and 500-14 concerning microstructural features. This is most likely an affect of them both being produced at the same foundry. They have, however, been treated with slightly different inoculants, which might be the reason 400-18's graphite nodules seem to be of a lower shape grade, generally. From Figure 7.1 it can seem that 500-14 have a more consistent roundness of its

nodules.

The chemical composition of 500-14 illustrates values within the recommended ranges. It has a high amount of Si, with a subsequently slightly lower amount of C. The elements that preferably is kept at a minimum – explained in Section 2.2.4 – are also achieved. The combination of these element's wt% in the material is the reason for the matrix structure becoming fully ferritic, illustrated in Table 7.3. Based on the theory of how different alloying materials affects the mechanical properties, the observed strength values are in line with what is expected. The elongation, however, is significantly higher than the required minimum and in line with the required minimum for 400-18LT. The study presented in Section 3.3 shows mechanical properties similar to 500-14 at the same wt% Si. The higher elongation could be an effect of higher quality inoculants and/or lower amount of embrittling elements. Si is known to increase the yield strength without necessarily decreasing the elongation, which is evident for the 500-14 material produced and tested here. Whether the slightly lower nodularity visible in 500-14 compared to 400-18 is an effect of the increasing Si is hard to determine, but it is likely when knowing the effect Si has on the promotion of ferrite.

500-7 does not meet the minimum requirements of elongation defined in NS-EN-1563 for relevant thickness (t) $30 < t \leq 60\text{mm}$. The strength is higher than the standard values and is more in line with what is expected for EN-GJS-600-3 according to NS-EN-1563 (Standard Norge, 2011). This will nevertheless not affect the further discussion of this material, and it will keep on being named 500-7, since the material in question has been supplied as this.

7.2 Charpy Impact Test

The results from Charpy impact test, performed on both V-notched and unnotched specimens at 20° and -20°C are listed and evaluated in this chapter. Both the actual impact values and the visual fracture appearance will be presented.

7.2.1 V-notched Test Samples

The average V-notch impact results for the 3 tested materials are presented in Table 7.4 along with the standard deviation. The result is the average and standard deviation of 9 samples tested.

Table 7.4: V-notched impact test results

Material	Temperature [°C]	Impact energy [J]
400-18LT	20	19.03 ± 0.5
	-20	16.76 ± 3.2
500-14	20	5.02 ± 0.2
	-20	4.00 ± 0
500-7	20	4.60 ± 0.6
	-20	4.05 ± 0.1

The average values in Table 7.4 are presented graphically in Figure 7.2 while the visual appearance of the individual samples are presented in Figure 7.3.

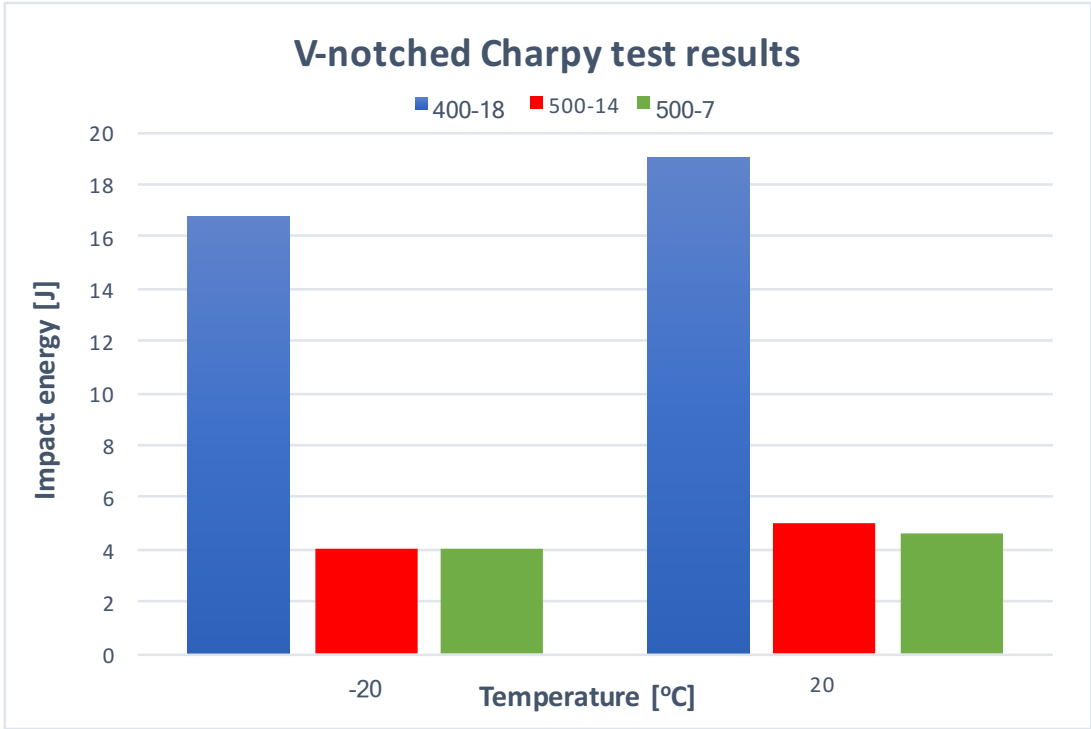


Figure 7.2: V-notched test results

400-18, expressing the highest values of impact energy in this test, are not the material with the highest elongation from the tensile test, which are two parameters that are usually connected. 500-14 which exhibit a very good ductility in the tensile test performs poorly in this V-notched test. This outcome emphasize the effect that strain rate has on the behavior of the material, especially when strengthened by Si. 400-18 decrease slightly from 20°C to -20°C – naturally. From the impact value seen for this material it can be assumed that this temperature range lies in the upper half of the ductile-to-brittle transition curve and that the actual transition temperature is below -20°C. The recorded impact energy value of 500-14 are not surprising, when comparing it against the trend illustrated in Figure 3.5 with its high Si value. The brittle pearlite structure in 500-7 is, not unlikely, the main contributor to the low values obtained in this test. Both the 500 materials are assumed to exist in the lower shelf of the ductile-to-brittle transition curve in this temperature range, based on the result from this specific test. It can be said that the low impact energy experienced by 500-7 is expected when looking at the low elongation. However, the equally low value exhibited by 500-14 highlights how notch sensitive this material is.

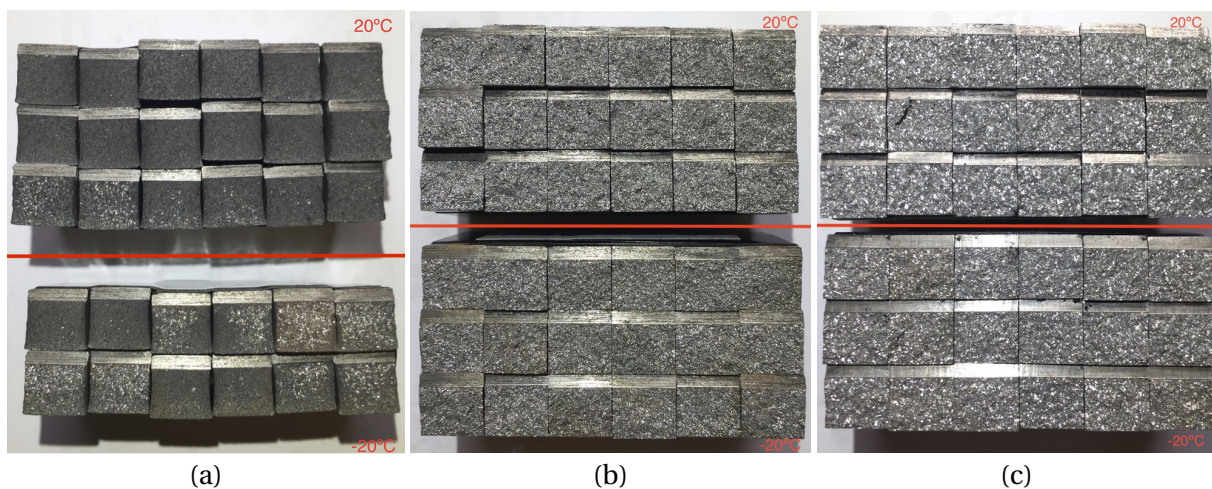


Figure 7.3: Image of the V-notched impact test specimens. Top specimens tested at 20°C, bottom at -20°C. (a) 400-18LT, (b) 500-14, (c) 500-7.

Figure 7.3 illustrate clear visual differences between the three materials regarding fracture surface appearance. 400-18LT feature a dark surface, that implies ductile fracture behavior – as seen in FR4 discussed in Section 4. This dark surface is a consequence of ductile fracture behavior, exposing a much larger amount of the graphite nodules on the surface than in a brittle fracture. 500-14 expresses a lighter color with small, but clearly visible, light reflections. This emphasize a fracture behavior dominated by embrittled ferrite cleavage,

not exposing the same amount of graphite in the fracture surface as 400-18. The fracture surface is most likely comparable to that of FR3 illustrated in Figure 4.5(c). Similar brittle features are seen in 500-7, only exhibiting a much coarser surface. This surface is most likely dominated by transgranular fracture – similar to the pearlitic material FR1 in Chapter 4 – exposing larger, light reflecting surfaces than seen in 500-14. The visible surface in Figure 7.3(b) and (c) are most likely comparable to the difference in the fracture surface seen for FR1 and FR3. Where both materials express brittle fracture behavior and the main difference lies in the larger occurrence of intergranular fracture in the ferritic material, altering the direction of the crack development, creating smaller light reflecting surfaces.

7.2.2 Unnotched Test Samples

The average V-notch impact results for the 3 tested materials are presented in Table 7.5 along with the standard deviation. The result is the average and standard deviation of 9 samples tested.

Table 7.5: Unnotched impact test results

Material	Temperature [°C]	Impact energy [J]
400-18LT	20	106 ± 21
	-20	112 ± 22
500-14	20	95.30 ± 38
	-20	20.20 ± 4.9
500-7	20	22.84 ± 1.9
	-20	10.50 ± 4.2

The average values in Table 7.5 are presented graphically in Figure 7.4 while the visual appearance of the individual samples is presented in Figure 7.5.

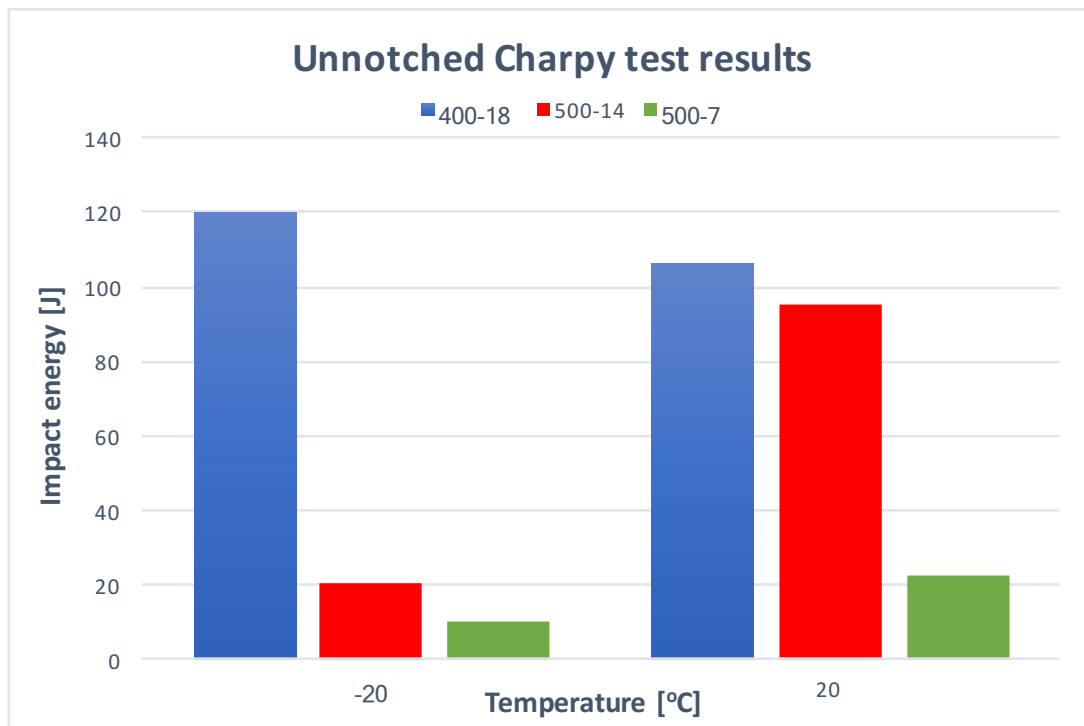


Figure 7.4: Unnotched test results

Test results from the unnotched Charpy specimens are not directly comparable to the V-notched test results. 400-18 express a surprising result by having a lower impact value at 20°C than -20°C. With that in mind, the impact energy is expected, with similar value as other ferritic ductile irons. This outcome can only be explained by the fact that this material performs in the upper region of the ductile-to-brittle transition curve and that this test method, without a notch, is possibly influenced by differences in the microstructure such as degenerated graphite, presence of pearlite, or micro-porosities. These varying results are consistent with all the test specimens. 500-14 express a large variation between the two temperatures, which is slightly unexpected when comparing the results from the V-notched specimens. This is another confirmation of the notch sensitivity present in this material.

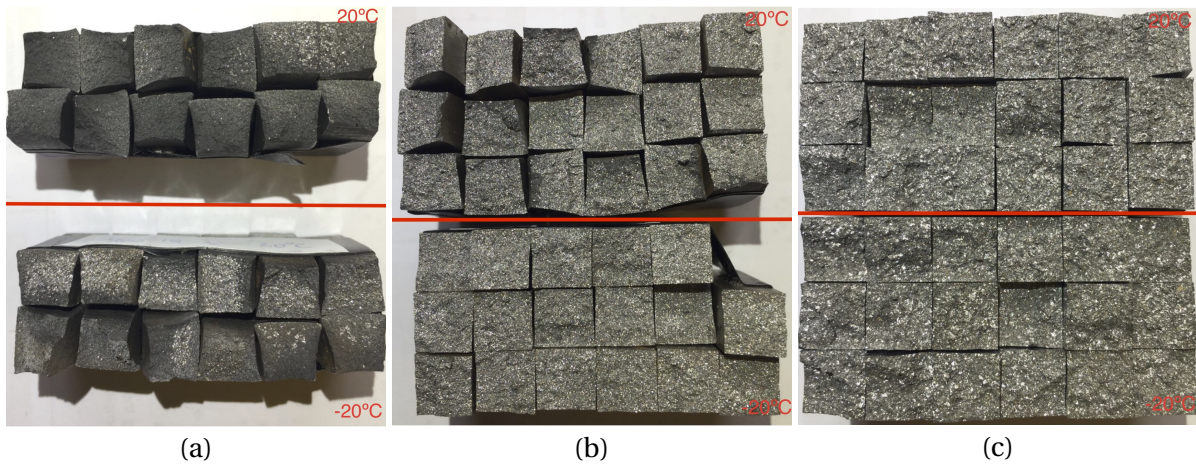


Figure 7.5: Image of the Unnotched impact test specimens. Top specimens tested at 20°C, bottom at -20°C. (a) 400-18LT, (b) 500-14, (c) 500-7.

The visual deformation observed for the different test specimens correlates well with the amount of impact energy recorded. The high values listed in Table 7.5 are all a product of plastic deformation, specifically for 400-18LT and 500-14 – seen in Figure 7.5. The lowest values are clearly a product of brittle cleavage fracture, causing no deformation to the test specimen and leaving a flat fracture surface, as seen in Figure 7.5(c) for 500-7. Regarding the fracture surface itself, are the visual characteristics mostly the same with and without the V-notch. Some lighter areas are imminent in 400-18 at -20°C, which could indicate an effect of ferrite embrittlement at the lower temperature. This has nevertheless not negatively affected the results as shown in Figure 7.4. The characteristic dark fracture surface is also visible in minor areas in the 500-14 plastically deformed test specimens, indicating that ductile fracture behavior is still possible in solution strengthened ferrite. 500-7 is still dominated by brittle behavior, confirming yet again how sensitive a pearlitic matrix is to a high impact force.

7.3 Fracture Toughness

In this section, the calculated values of K_{Ic} is presented in addition to the associated load vs. CTOD graph gathered from the fracture toughness test. The values in Table 7.6 are determined from the mean value of three tests. The K_{Ic} value are calculated using Eq. 2.5 with the values of F_Q gathered from the load vs. CTOD graph and the geometrical constants of the test specimens. All results were tested to meet the requirements stated in Eq. 2.6

and Eq. 2.7 and declared sufficient K_{Ic} values. Figure 7.6 displays the calculated fracture toughness values with a line marking $50 \text{ MPa}\sqrt{\text{m}}$, which is the limit for this material to be approved as a construction material for offshore application, determined by SHI.

Table 7.6: Fracture toughness test results

Material	Temperature [°C]	K_{Ic} [$\text{MPa}\sqrt{\text{m}}$]
400-18LT	20	49.60 ± 1.8
	-20	49.35 ± 1.5
500-14	20	64.84 ± 0.3
	-20	60.75 ± 5.4
500-7	20	51.08 ± 5.3
	-20	36.96 ± 1.2

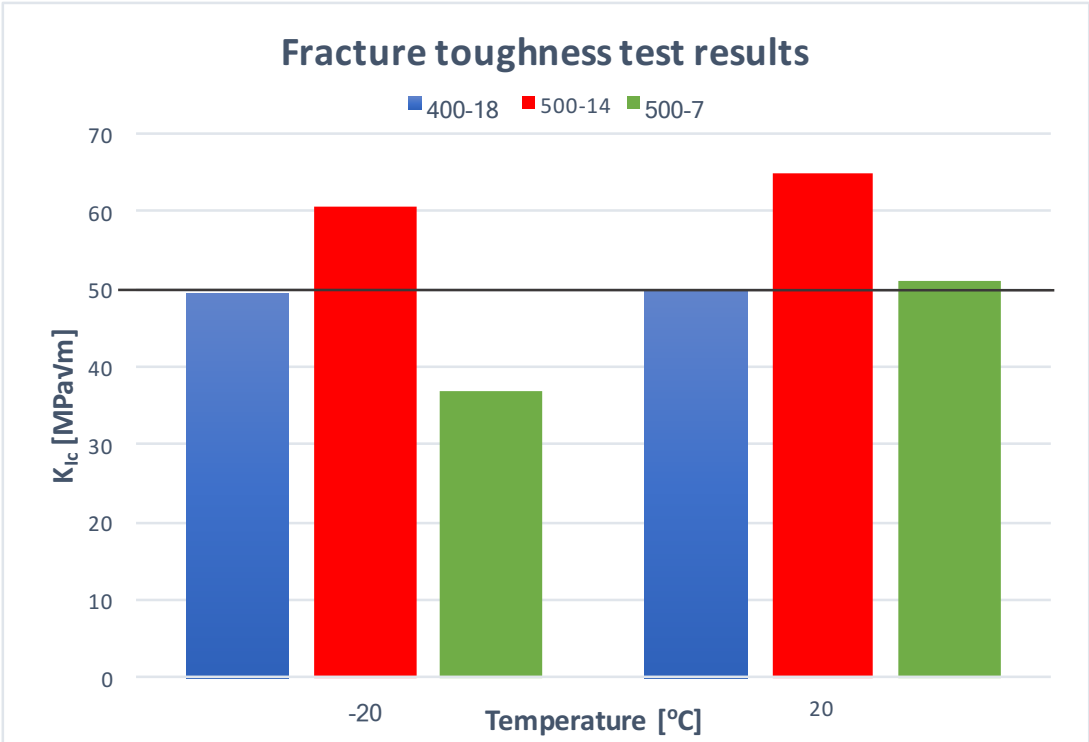


Figure 7.6: Fracture toughness at the two temperatures

The fracture toughness results confirm the question of reliability of toughness properties gathered from Charpy tested ductile iron, discussed in Section 3.1. 500-14, which performed poorly in the V-notch Charpy test, express impressive results in the fracture tough-

ness test. Clearly being sufficient according to the requirements used by Samsung of minimum $50 \text{ MPa}\sqrt{\text{m}}$. However, the results indicate that the fracture toughness is decreasing with decreasing temperature for 500-14, which is not imminent for 400-18. This is a confirmation of Silicons influence on increasing the ductile-to-brittle transition temperature. If the reduction in fracture toughness seen for 500-14 between 20°C and -20°C is maintained between -20°C and -40°C the target K_{Ic} value of $50 \text{ MPa}\sqrt{\text{m}}$ can likely be maintained even at -40°C .

400-18 performs with values close to $50 \text{ MPa}\sqrt{\text{m}}$. These results are lower than expected, knowing that this is a material is often used for offshore windmill applications. It is also lower than what is stated in NS-EN-1563, illustrated in Figure 3.2. It should be noted that these results, being as stable as they are, probably lies in the top half of the transition curve. This could mean that this is the largest value achievable for this test method, for this specific material (chemistry, production method and microstructure). Where 500-14 could have a higher max value since this transition curve is not possible to establish with the current set of available data.

500-7 exhibits the overall lowest results but the value of $51.08 \text{ MPa}\sqrt{\text{m}}$ at 20°C is surprisingly higher than 400-18. However, the significantly lower value observed at lower temperature shows that this material has a definite weakness when it comes to toughness, at low temperatures. Which is also confirmed by the results from the impact tests, both notched and unnotched. 500-7 did also fracture at the lowest CTOD value of 0.3 mm. These results demonstrate the effect pearlite has on the toughness properties in this type of material.

To emphasize the effect the two different temperatures has on the materials load vs. displacement curve from the fracture toughness test, the recorded graphs are included below in Figure 7.7, 7.8 and 7.9. Note that the x-axis is scaled differently for each diagram, which needs to be taken into consideration when evaluating the graphs against each other.

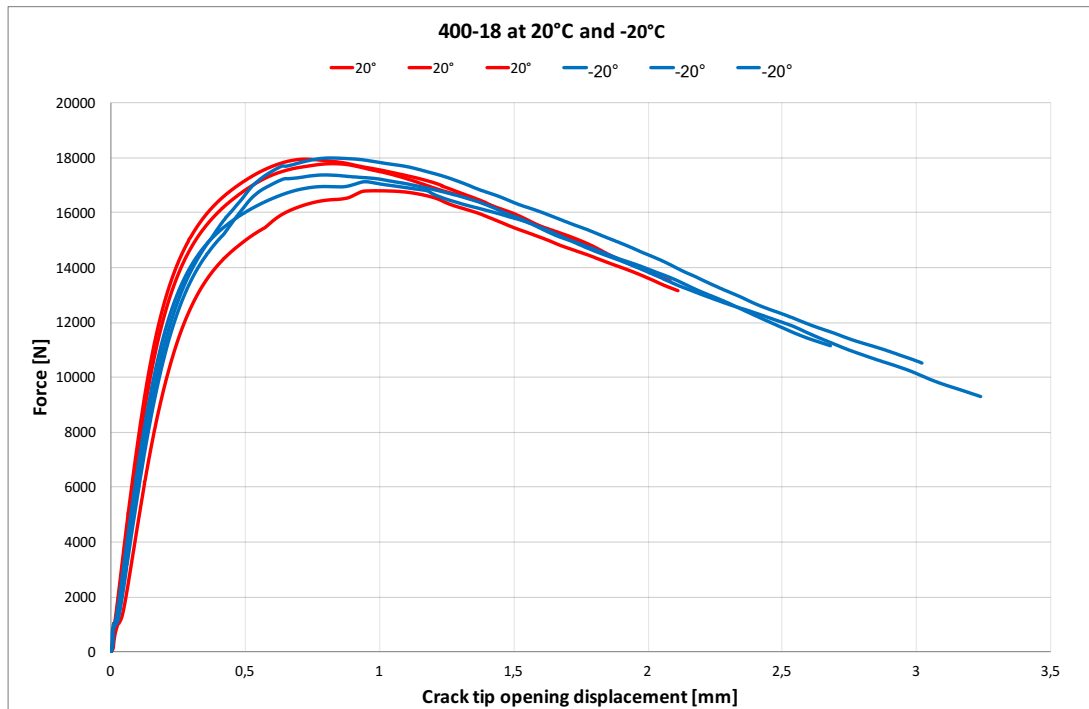


Figure 7.7: Load vs. displacement curve of 400-18 at two temperatures

During the fracture toughness bend test, 400-18 behaved with the characteristics of a ductile material with a slow, tearing crack propagation dominated by plastic deformation. The test was stopped before the test specimen was completely broken in two, due to the limited range of the clip gauge, which is why the curve stops before reaching the bottom. As seen in Figure 7.7 the material experienced a large maximum CTOD value, however at the point of maximum load (16-18 kN) the displacement was only at about 0.8 mm. This is the critical yield point for this specific material, where the crack is fully developed and will continue to propagate until the part is fully fractured. This crack propagation, controlled by plastic deformation, was only observed in this material. It should be noted that even though the maximum force is higher for 400-18 than the other material, the K_{Ic} value is lower due to the larger geometry of the test specimens.

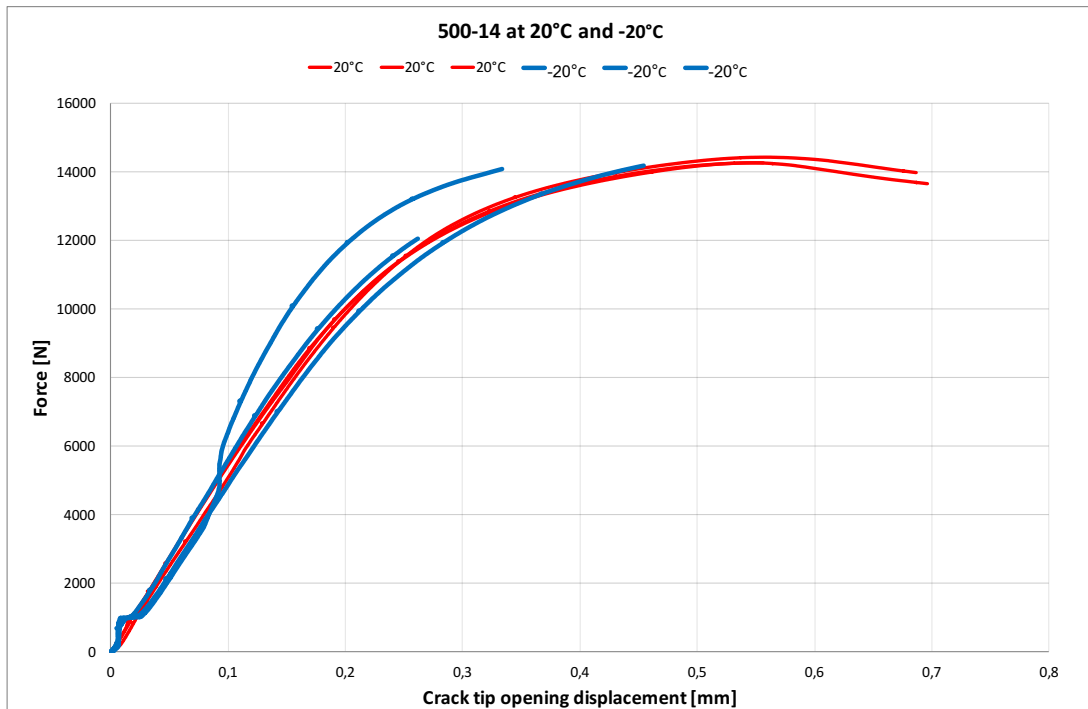


Figure 7.8: Load vs. displacement curve of 500-14 at two temperatures

The 500-14 test specimens did not experience plastic deformation like 400-18 did. The fracture test ended with brittle fracture behavior, visible from the sudden stop of the graphs in Figure 7.8. The biggest difference between behavior at the different temperatures is the CTOD which was about 0.35 mm at -20°C and 0.69 mm at 20°C.

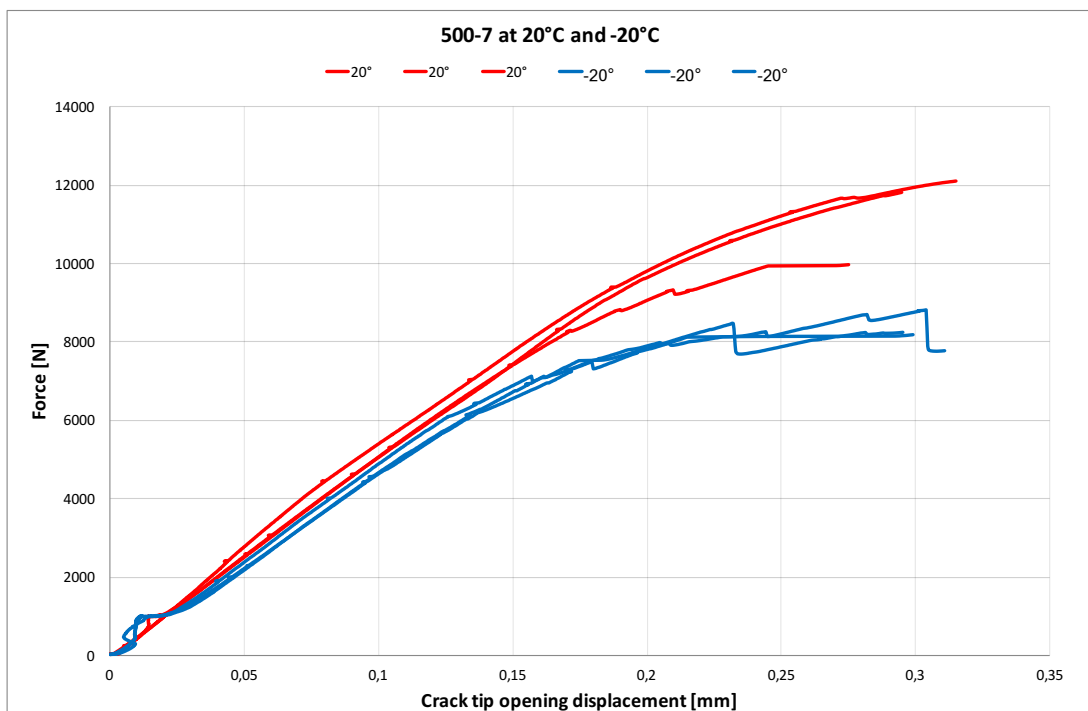


Figure 7.9: Load vs. displacement curve of 500-7 at two temperatures

500-7 displayed the largest difference between the two temperatures. However, the CTOD were not affected by lowering the temperature, only the maximum fracture load. This development is the opposite of 500-14, approximately displaying similar max load value, but different CTOD, at the two temperatures. One characteristic that is clearly imminent in this material is the occurrence of minor pop-ins before full fracture, which can be related to a more unstable crack propagation than what is visible in 500-14.

7.3.1 Relationship Between Charpy-V and Fracture Toughness

In Section 3.2 is the relationship between fracture toughness and impact energy for steel, presented. The general trend here is that the fracture toughness values are about 10-90% larger than the impact energy for, non-specified, general grades of steel. However, the relationship most interesting to compare against, are the values gathered from the same types of tests for welded S355 steel. Figure 7.10 illustrate the this relationship for the three grades of ductile iron and welded S355 steel. Where each material is presented with K_{Ic} and Charpy-V impact energy values at 20°C. This will create a basis for comparison of this specific relationship between ductile iron and steel.

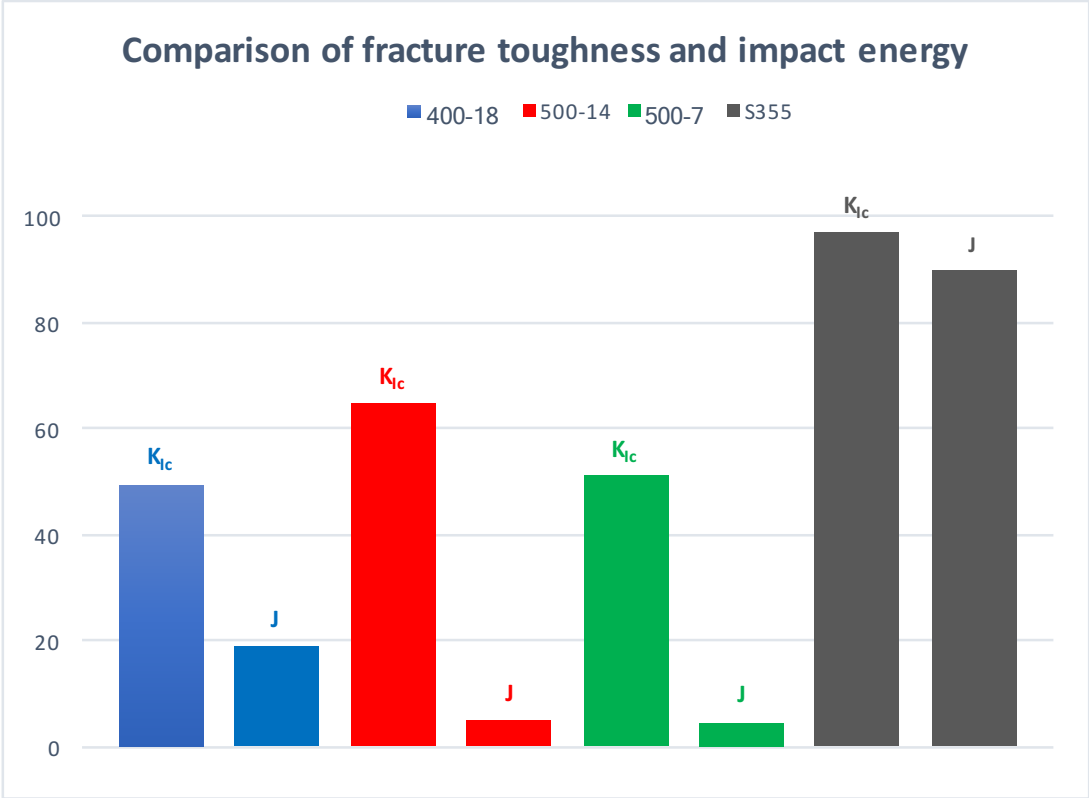


Figure 7.10: Comparison of fracture toughness and impact energy at 20°C

The relationship will also be presented in the table below to emphasize the percentage of increasement from Charpy-V to fracture toughness.

Table 7.7: Percentage difference between Charpy-V impact values and K_{Ic}

Material	Impact energy [J]	K_{Ic} [MPa\sqrt{m}]	Difference [%]
400-18	19.03	49.60	160
500-14	5.02	64.84	1191
500-7	4.60	51.08	1010
S355	90	97	7.8

Table 7.7 shows there is a large difference in the relationship between Charpy-V impact values and fracture toughness. Especially for the solution strengthened 500-14 and the pearlitic 500-7. This table is another confirmation that ductile iron is much more sensitive to strain rate than steel. It can be assumed that the microstructural features that make the ductile iron perform relatively well in the fracture toughness test, does not get the time to really make an impact on the toughness when subjected to a high strain rate. Especially when contemplating the notch sensitivity that has clearly been established based on the results from the two impact tests conducted. The substantial difference when compared to S355 steel is another confirmation that ductile iron and steel should not be evaluated on the same basis of toughness.

8. Discussion

This chapter will discuss the results presented in Chapter 7, implementing the background theory discussed in Chapter 2 and link it towards the original problem definition. Each of the three materials will be discussed separately.

8.1 EN-GJS-400-18LT

For a material often being used in the wind turbine industry, for both on and offshore applications, it is surprising that it does not perform with a higher K_{Ic} . By looking at the fracture toughness values presented Figure 3.2 from NS-EN1563 it would suggest that this material would achieve a higher value in this specific test. K_{Ic} at both temperatures were lower than the stated requirement of $50 \text{ MPa}\sqrt{\text{m}}$. The observed impact energy values from this material were more as expected based on similar tests of the same material. Based on the toughness test it can be assumed that this temperature range lies in the upper region in the ductile-to-brittle transition curve, meaning that these values are the highest that can be gained from this material. However, this is not to be taken as a fact, considering how difficult it is to establish a definite transition curve for ductile iron with the given tests and temperature range.

Reasons for the observed results for this material is difficult to define. The slightly lower amount of Mg, compared to 500-14, could be an indication of a declining inoculation effect. This can develop if too long time has passed from the inoculant being added, to the melt being poured. This would also cause a development of larger sized nodules, being the case in this specific material (average $25.7 \mu\text{m}$ against 500-14's $21.8 \mu\text{m}$). The representative image of the microstructure in Figure 7.1(a) seem to consist of some irregular shaped nodules. This could be – as mentioned in Table 2.2 – a result of poor inoculation or high holding time, which again is a confirmation of inaccurate inoculation process being imminent in the production of 400-18.

Another explanation could be related to the crack development in the ductile matrix imminent in 400-18. Based on the silicon content, the ductile deformation witnessed in both the Charpy and fracture toughness and the dark colored fracture surface, it is likely that the matrix is dominated by plastic deformation around the nodules and the fracture surface is similar to that illustrated in Figure 4.5(d). Based on the theory of crack tip plasticity and nodule decohesion in front of the crack tip, it can be assumed that this type of test method could cause a porosity to the material. This porosity would normally create a larger resistance to crack propagation in ductile iron, but if many of the nodules express a coarser surface they can potentially create microcracks at the nodule matrix debonding, ahead of the crack tip. This will cause a clear weakness in the decohesion process, where the developing crack will not be arrested, but rather have an easier path through the matrix. Especially when considering plastic deformation that has already occurred ahead of the crack tip at this point in the process. This process is more likely to happen in the case of a fracture toughness test, with its relatively low strain rate. In a Charpy impact test will this process most likely not get the time to develop due to high strain rate. This could be the explanation on the low difference between the values gathered from the two toughness tests for 400-18, illustrated in Figure 7.10. It can be assumed that the graphite nodules plays a more direct role in affecting the tearing properties in this type of ductile iron, dominated by plastic deformation.

As a note to this, the microstructural report shows a trend of low consistency regarding nodule density in 400-18. Some areas display a larger nodule density and nodularity than others. In a case of irregular shaped nodules, causing damage to the toughness, high nodularity could potentially be damaging. As would a nodule density varying over a larger area.

8.2 EN-GJS-500-14

There is no doubt that 500-14 is a material with some clear advantages when it comes to strength, elongation and fracture toughness. It is the only material that passes the required K_{Ic} value of $50 \text{ MPa}\sqrt{\text{m}}$ at both temperatures. The high Si content has resulted in similar values to what presented in Section 3.3. Where the ferrite strengthening mechanism is the dominant force resulting in the combination of high strength and elongation.

When it comes to the microstructural behavior of 500-14, do FR3, presented in Chapter 4, provide similarities enough to create a basis of comparison, based on Si content and mechanical properties. By studying the SEM image in Figure 4.5(c) it is clear that solution strengthened ferrite will be dominated by brittle fracture appearances, with traces of both trans- and intergranular fractures. This will, however, not directly mean that it will perform worse regarding ductility, than a material such as 400-18, expressing ductile fracture behavior on the microstructural level. As mentioned early in the report, ductility is a relative term being difficult to define. This fact has shown to fit well with this material, showing signs of being brittle when studying the fracture surface but still performs with an elongation of 20% and a plastic deformation in the unnotched impact test.

Using the Charpy impact test method to establish the transition temperature have shown to work well with steel. In this high Si material, on the other hand, it has shown to be difficult. Studying the results from the unnotched impact test it can be suggested that the temperature range (-20°C to +20°C) lies exactly around the transition temperature, assumed to be around 0°C, in this case. This is however not consistent with the results from the V-notched test, making it challenging determining the exact ductile-to-brittle behavior of this material. With that being said, the fact that this material deforms plastically at 20°C, without the added weakness of a notch, is an interesting development. Especially contemplating that this unnotched state is more realistic when considering this for being used as a construction material. The high value recorded in the unnotched impact test is also a verification of the notch sensitivity imminent in ductile iron, confirming the theory discussed in Section 3.1.

For 500-14 to achieve its full potential, it can be suggested that it behaved with similar features of plastic deformation as 400-18, being a material normally performing with higher values of fracture toughness (Figure 3.2). The most obvious solution to this is to lower the Si content decreasing the embrittlement of ferrite, allowing more plastic deformation to occur. Based on the presented theory of ductile iron behavior, will a reduction of Si result in a reduction of strength. To achieve the optimal combination of strength, ductility and fracture toughness this material needs to be researched further with a focus on establishing the optimal Si percentage for offshore applications.

8.3 EN-GJS-500-7

500-7 is the material with the lowest average value of K_{IC} , with a particularly low value at low temperature. This is, according to the requirements targeted in this evaluation, not sufficient to be considered as a reliable construction material for offshore applications. The test specimen failed in the fracture toughness test by a sudden fracture, likely as a product of the brittle pearlitic matrix. Even though it has been established that the Charpy impact test is not a reliable test type for ductile iron, did 500-7 illustrate some clear weaknesses. Where 500-14's low Charpy-V impact test results could be related to the notch sensitivity, is this not as evident in 500-7. Its unnotched test results did show a slight increase in absorbed energy, but in the context with the other materials, it is not comparable. The low impact energy is also related to the fracture surface, undoubtedly dominated by brittle cleavage fracture, showing no signs of plastic deformation.

The reason for the poor results in the toughness test is evidently the high pearlite content in the matrix. When contemplating the documented effect pearlite have on this type of material, the result is not surprising. 500 grade ductile irons should ideally not have this high pearlite content, and the outcome is possibly a product of too high content of pearlite promoting elements. When comparing the pearlite promoting element distribution with 500-14, are these elements considerably larger in 500-7. The sum of pearlite promoting elements in 500-7 is 1.94 times larger than the content in 400-18, and 4.92 times larger than in 500-14.

As stated in Section 2.2.4 are Ni and Cu categorized being both graphitizers and weak pearlite promoters. Since the original casting thickness, this material originates from, is unknown, the high Ni and Cu content is most likely intentional. Being graphitizers, they are elements often used in large thickness casts to control the nucleation and formation of graphite. In castings consisting of varying thicknesses, these elements can cause pearlite to form if not controlled.

Regarding the microstructure is there also a substantially large difference in the number of nodules in 500-7 compared to the two other materials investigated. This has however not affected the nodularity which is as high as 84%. Even though the carbon content is high and the amount of graphite in the microstructure are similar to the other materials, the nodule

density is low, naturally affecting the nodule size being 72.4% larger than the nodules appearing in 500-14. This development of nodule characteristics is likely related to cooling time and wall thickness of the original casting. It could be a case of flotation, however, the CE value is not especially high and this is hard to determine without examining the full cast sample. Most likely, this formation of large nodules is a consequence of slow cooling time and fading of inoculation effect.

8.4 Offshore Application

One of the main objectives is to, based on the results from the testing conducted, evaluate if any of the 3 materials fulfill the minimum requirements for use in offshore applications. In Table 8.1 the requirements are listed along with the relevant results for the 3 materials evaluated at -20°C. The evaluation is based on the minimum value of strength, elongation and matrix structure defined by NS-EN1563, and the minimum value of K_{Ic} as defined by SHI for approving the material for being used in the wind turbine industry, being $50 \text{ MPa}\sqrt{\text{m}}$. These minimum requirements are listed in the parentheses beside the actual determined value. If the result is presented in green it indicates that it is achieving the minimum and if it is presented in red, it is not. As can be seen from the table, 500-14 is passing on all listed requirements, while 400-18 is only marginally below on fracture toughness, while 500-7 fail on both elongation and fracture toughness.

Table 8.1: Evaluation of mechanical properties to be evaluated for offshore application

Material	Tensile strength [MPa]	Yield strength [MPa]	Elongation [%]	Fracture toughness [MPa√m]
400-18	476 (380)	289 (230)	17 (15)	49.35 (50)
500-14	529 (480)	418 (390)	20 (12)	60.75 (50)
500-7	682 (450)	455 (300)	5.7 (7)	36.96 (50)

9. Conclusion

The objective of this thesis has been to evaluate 3 cast iron materials with the purpose of being used in offshore applications. Possibly as a substitute material for similar strength, welded steel. The materials in question have been examined with respect to chemistry, microstructure, mechanical properties and fracture toughness, where the main interest has been to investigate and understand the difference in fracture behavior.

Regarding microstructural features is ductile iron a material that can have a high ductility despite fracturing with brittle characteristics. Especially when it comes to high Silicon, solution strengthened ductile iron, displaying definite advantages over other cast irons.

Ductile irons mechanical properties are highly dependent on microstructural features such as graphite and matrix structure. High nodularity, optimal shape and distribution of graphite nodules, as well as carefully controlled chemical composition and production process, is imperative for the material to reach its full potential. It is clear that to achieve sufficient properties regarding toughness, a ferritic matrix is necessary. This can be accomplished by the addition of Silicon due to its ferrite promoting abilities together with its capability of increasing the strength while preserving the ductile properties.

500-7 is a good example of the damaging effects caused by a high pearlite content. A ductile iron with this high pearlite content has proved to be not acceptable for offshore application, based on its low elongation, brittle fracture behavior and value of K_{Ic} at -20°C .

400-18 is the material showing the best performance with high Charpy impact values and ductile fracture behavior. Although this was not confirmed by the fracture toughness results. The most likely solution to improving the fracture toughness results lies in optimizing the production process and taking special care to avoid inoculant fading. This would result in 400-18 reaching a higher K_{Ic} value and the material fulfilling the requirements for offshore application.

500-14, performing with the highest elongation and fracture toughness is found to be the best fitted material for offshore application in this work. The Silicon content of 3.68 % have

been proven to result in a unique combination of high strength and elongation, and not causing a too critical embrittling effect to the ferritic matrix. The fracture surface in a solution strengthened ductile iron is concluded to be dominated by brittle fracture behavior of both trans- and intergranular nature, despite its high ductility. Regardless of this material's crack propagation being dominated by matrix cleavage, it is still dependent on good nodule formation. Irregular shaped nodules can potentially lead to microcracks which again can lead to inferior fracture toughness.

Regarding the reliability of using Charpy-V impact test to categorize ductile iron in the same manner as steel, it can be concluded that this test does not provide enough accuracy to determine a valid value of toughness, nor a transition temperature. This is clearly illustrated by the relationship between V-notch test values and K_{Ic} – where K_{Ic} has been proved to give a more realistic value of toughness. This development is a product of notch- and strain rate sensitivity present in ductile irons, especially in solution strengthened ferrite. Unnotched Charpy tests provide a larger understanding of plastic behavior and deformation, but is largely affected by uncertainties giving unrealistic values of toughness.

It is concluded that ductile iron can be regarded as a reliable construction material for offshore applications based on the specific requirements used in this evaluation. Given that the production process is being sufficiently controlled, especially the inoculation process.

10. Further Work

While the work conducted in this report can be evaluated sufficiently for the objective at hand, there will always be some unanswered questions in need of further research. Suggested topics to be evaluated further are listed below.

- Based on the fact that the solution strengthened 500-14 material performed with the best results in the fracture toughness test, can it be suggested that this material makes the basis of evaluation the optimal Silicon content in ductile iron, to achieve the ultimate combination of strength, ductility and fracture toughness.
- A study focusing on the microstructural features visible on the fracture surfaces, on three specific materials used in this report.
- An evaluation of the reliability of using an EDM machined notch as a substitute for a fatigued pre-crack in a fracture toughness test.
- An extensive investigation on the unexpected low values of fracture toughness observed for 400-18LT in this report.

Bibliography

- Al-Ghonamy, A., Ramadan, M., Fathy, N., Hafez, K., and El-Wakil, A. (2010). Effect of graphite nodularity on mechanical properties of ductile iron for waterworks fittings and accessories. *Int J Civil Environ Eng*, 10:1–5.
- Anderson, T. L. (2005). *Fracture mechanics: fundamentals and applications*. CRC press, third edition.
- ASTM (2012). Standard test method for linear-elastic plane-strain fracture toughness K_{Ic} of metallic materials. ASTM E399.
- Bannister, A. (1998). Determination of fracture toughness from charpy impact energy: procedure and validation. *British Steel plc*.
- Blair, M. and Monroe, R. (2017). Steel fabrication vs. castings. [Online] Available from: <http://www.afsinc.org/content.cfm?ItemNumber=6931> [Accessed 28.04.17].
- Bradley, W. and Srinivasan, M. (1990). Fracture and fracture toughness of cast irons. *International Materials Reviews*, 35(1):129–161.
- Callister, W. D. and Rethwisch, D. G. (2011). *Materials science and engineering*, volume 5. John Wiley & Sons NY, 8th edition.
- Cavallini, M., Di Cocco, V., Iacoviello, F., and Iacoviello, D. (2011). Ductile irons damaging micromechanisms: graphite nodules role investigated by means of image processing procedures. In *Convegno IGF XXI Cassino 2011*.
- Di Cocco, V., Iacoviello, F., and Cavallini, M. (2010). Damaging micromechanisms characterization of a ferritic ductile cast iron. *Engineering Fracture Mechanics*, 77(11):2016–2023.
- DNV-GL (2015). Drilling plant. DNVGL-OS-E101.
- Double, D. and Hellawell, A. (1995). The nucleation and growth of graphite—the modification of cast iron. *Acta metallurgica et materialia*, 43(6):2435–2442.

- Ductile Iron Society (2013). Ductile iron data for design engineers. [Online] Available from: <<http://www.ductile.org/didata/Section3/3part1.htm>> [Accessed 14.02.17].
- Elkem AS (2011). Inoculation of cast iron. [PDF] Retrieved from: Elkem AS.
- Elkem AS (2017). Chemical composition of ductile iron. [Powerpoint presentation] Retrieved from: Elkem AS.
- Forrest, D. R. (2006). Meeting low temperature property specifications in ductile iron. *Sorelmetal, Suggestions for Ductile iron Production*.
- Glavas, Z., Strkalj, A., and Stojakovic, A. (2016). The properties of silicon alloyed ferritic ductile irons. *Metalurgija*, 55(3):293–296.
- Guo, X., Stefanescu, D., Chuzhoy, L., Pershing, M., and Biltgen, G. (1998). A mechanical properties model for ductile iron. *TRANSACTIONS-AMERICAN FOUNDRYMENS SOCIETY*, pages 47–54.
- Hafiz, M., Hammouda, A., and El-Gemae, S. (2005). Impact properties and fractography of spheroidal graphite cast irons. *Transactions of the American Foundry Society, Vol. 113*, 113:625–636.
- Hechler, O., Axmann, G., and Donnay, B. (2015). The right choice of steel—according to the eurocode. In *Economical Bridge Solutions based on innovative composite dowels and integrated abutments*, pages 21–43. Springer.
- Hesse, A.-C., Nitschke-Pagel, T., and Dilger, K. (2016). Fracture toughness of electron beam welded fine grain steels. *Procedia Structural Integrity*, 2:3523–3530.
- ISO (2009). 6892-1. metallic materials-tensile testing-part 1: Method of test at room temperature. *International Organization for Standardization*.
- ISO (2016). 12135. metallic materials-unified method of test for the determination of quasistatic fracture toughness. *International Organization for Standardization (ISO)*.
- Khursheed, A. (2011). *Scanning electron microscope optics and spectrometers*. World scientific.

- Ko, K. (2012). Selection of ductile cast iron from a fracture toughness point of view in colde climate project. *Samsung Heavy Industries - Technical Documentation*.
- Labrecque, C. and Gagne, M. (1998). Ductile iron: fifty years of continuous development. *Canadian Metallurgical Quarterly*, 37(5):343–378.
- Madyira, D. M. and Akinlabi, E. T. (2015). Influence of wire edm on fracture toughness of ti6al4v. In *Transactions on Engineering Technologies*, pages 147–161. Springer.
- Materials Evaluation and Engineering, Inc. (2017). Quantitative chemical analysis. [Online] Available from:
<<http://www.mee-inc.com/hamm/quantitative-chemical-analysis/>>
[Accessed 19.05.17].
- Mathers, G. (2017). Ctod testing. TWI. [Online] Available from:
<<http://www.twi-global.com/technical-knowledge/job-knowledge/ctod-testing-076/>> [Accessed 24.03.17].
- McEvily, A. J. (2013). *Metal Failures: Mechanisms, Analysis, Prevention*. John Wiley & Sons, 2nd edition.
- Oaks, M. (2012). Letting mr. charpy die - evaluating the usefulness of charpy impact testing on ductile iron. Holiday Inn-Muskegon Harbor, OH.
- Penticton Foundry (2015). Ductile iron vs steel. [Online] Available from:
<<http://www.pentictonfoundry.com/news/ductile-iron-vs-steel/>>
[Accessed 04.03.17].
- Reardon, A. C. (2011). *Metallurgy for the Non-metallurgist*. ASM International, 2nd edition.
- Riposan, I., Chisamera, M., and Stan, S. (2010). Performance of heavy ductile iron castings for windmills. *China Foundry*, 7(2):163–170.
- Shirani, M. and Härkegård, G. (2014). A review on fatigue design of heavy section en-gjs-400-18-lt ductile iron wind turbine castings. *Energy Equipment and Systems*, 2(1):5–24.

- Skaland, T. (2005). Nucleation mechanisms in ductile iron. In *Proc. AFS Cast Iron Inoculation Conference*, pages 13–30.
- Standard Norge (2011). Founding – spheroidal graphite cast irons. Norsk Standard NS EN1563.
- TWI (2017). Mechanical testing - notched bar or impact testing. [Online] Available from: <http://www.twi-global.com/technical-knowledge/job-knowledge/mechanical-testing-notched-bar-or-impact-testing-071/> [Accessed 23.03.17].
- vonRoll casting (2017). Cast iron. [PDF] Available from: <http://www.vonroll-casting.ch/Public/De/03.Technologie%2020Fertigung/02.Werkstoffe/Werkstoffe%20Eisenguss.en.pdf> [Accessed 04.03.17].
- Wallin, K. R. (2014). Equivalent charpy-v impact criteria for nodular cast iron. *International Journal of Metalcasting*, 8(2):81–86.
- Williams, M. L., Meyerson, M. R., Kluge, G. L., and Dale, L. R. (1949). Investigation of fractured steel plates removed from welded ships. Technical report, DTIC Document.

A. Microstructural Reports

A.1 EN-GJS-400-18LT



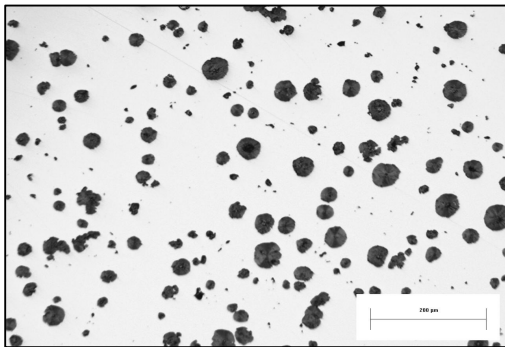
Microstructure report

Based on ASTM E2567

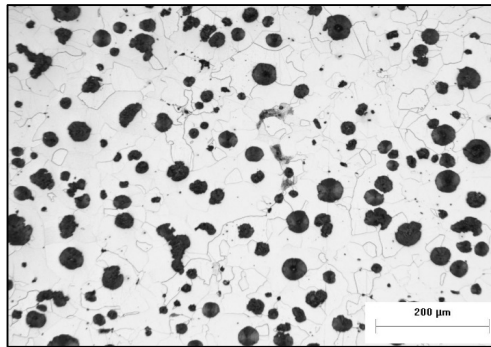
Sample description: Sample 400-18LT

Lab. Ref. No: M217-145

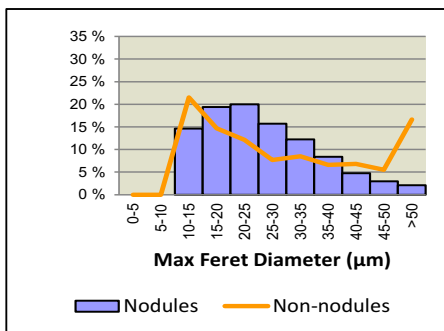
	Total area (mm ²)	No. of fields	No. of particles	No. of nodules	Nodule density ⁽¹⁾ (#/mm ²)	Nodularity by count (%)	Nodularity by area ⁽¹⁾ (%)	Graphite (%)	Ferrite (%)	Pearlite (%)
Average values	14.2	25	3360	2890	203 ± 11	86 ± 1.4	86 ± 1.5	11.5 ± 0.4	-	-
The image below	0.6	1	133	113	198	85	87	11.4	-	-



Micrograph showing the nodule structure in a position in the sample (polished condition) *



Micrograph showing the microstructure in a position in the sample, full-ferritic (etched condition) *



Analysis conditions				
Size limit; Feret(max)	> 10 µm			
Shape factor	≥ 0.6			
Calibration Factor	0.68 µm/pixel			
Objective magnification	10x			
Total magnification	100x			
Statistics	min	max	average	Std Dev
Particle size (µm)	10.1	144.0	26.5	11.9
Limited by size				
Nodule size (µm)	10.1	73.3	25.7	10.2
Limited by size and shape				

Kristiansand 04.05.2017

Approved:

B.Kroka

R.Gundersen

* The images shown are representative to the average of the 25 examined fields, but individual values may be outside the 95% confidence interval for the average without this being an error.

(1) The error is calculated as the 95% confidence level based on the individual analysis of 25 fields

A.2 EN-GJS-500-14



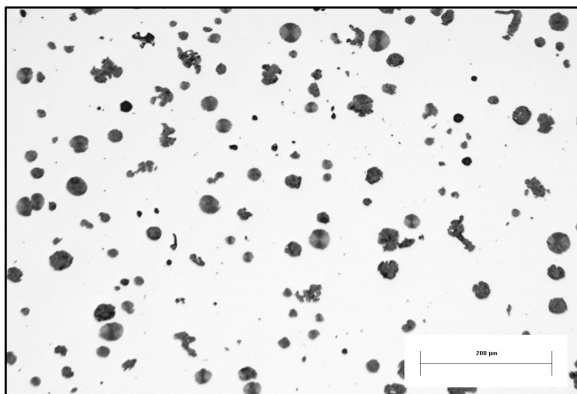
Microstructure report

Based on ASTM E2567

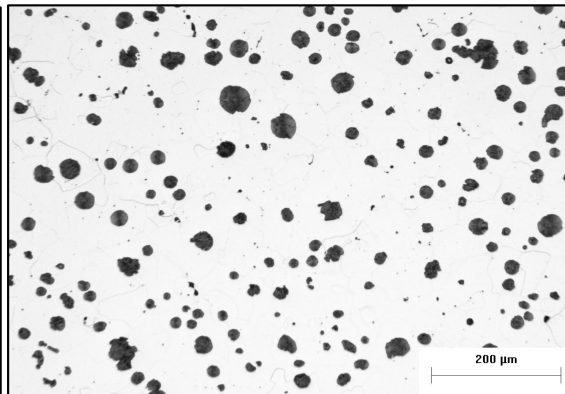
Sample description: Sample 500-14

Lab. Ref. No: M217-142

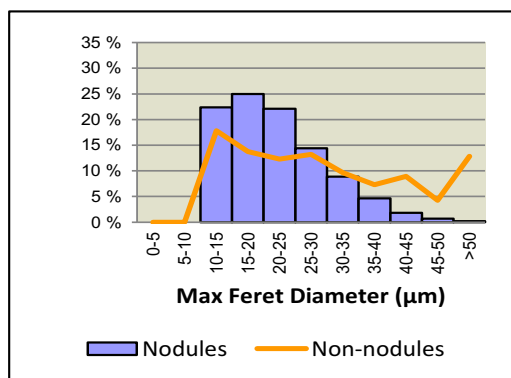
	Total area (mm ²)	No. of fields	No. of particles	No. of nodules	Nodule density ⁽¹⁾ (#/mm ²)	Nodularity by count (%)	Nodularity by area ⁽¹⁾ (%)	Graphite (%)	Ferrite (%)	Pearlite (%)
Average values	14.2	25	3397	2836	199 ± 8	83 ± 1.4	81 ± 2.1	8.5 ± 0.3	-	-
							Ferrite + pearlite = 100%:		-	-
The image below	0.6	1	134	113	198	84	79	8.7	-	-



Micrograph showing the nodule structure in a position in the sample (polished condition) *



Micrograph showing the microstructure in a position in the sample, full-ferritic (etched condition) *



Analysis conditions				
Size limit; Feret(max)	> 10 µm			
Shape factor	≥ 0.6			
Calibration Factor	0.68 µm/pixel			
Objective magnification	10x			
Total magnification	100x			
Statistics	min	max	average	Std Dev
Particle size (µm)				
Limited by size	10.1	103.5	23.2	10.4
Nodule size (µm)				
Limited by size and shape	10.1	53.3	21.8	8.0

Kristiansand 27.04.2017

Approved:

B.Kroka

R.Gundersen

* The images shown are representative to the average of the 25 examined fields, but individual values may be outside the 95% confidence interval for the average without this being an error.

(1) The error is calculated as the 95% confidence level based on the individual analysis of 25 fields

A.3 EN-GJS-500-7



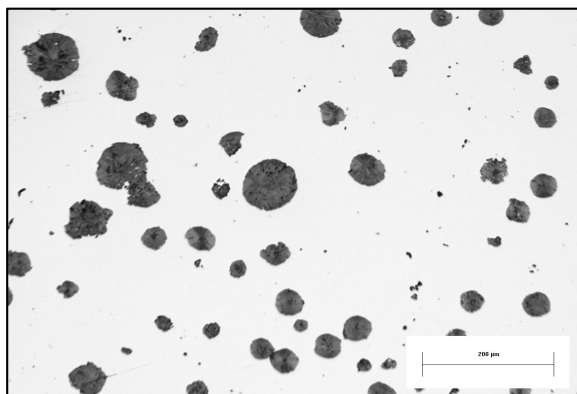
Microstructure report

Based on ASTM E2567

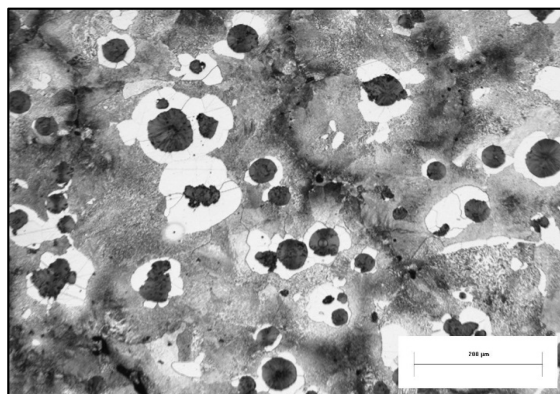
Sample description: Sample 500-7

Lab. Ref. No: M217-157

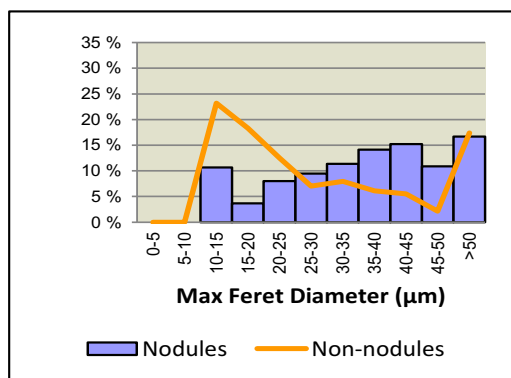
	Total area (mm ²)	No. of fields	No. of particles	No. of nodules	Nodule density ⁽¹⁾ (#/mm ²)	Nodularity by count (%)	Nodularity by area ⁽¹⁾ (%)	Graphite (%)	Ferrite (%)	Pearlite (%)
Average values	14.2	25	1341	1013	71 ± 5	76 ± 2.4	84 ± 3.1	8.9 ± 0.6	13.6 ± 0.7	77.5 ± 0.8
							Ferrite + pearlite = 100%:		14.9	85.1
The image below	0.6	1	49	40	70	82	82	9.0	13.2	77.8



Micrograph showing the nodule structure in a position in the sample (polished condition) *



Micrograph showing the microstructure in a position in the sample (etched in Nital) *



Analysis conditions				
Size limit; Feret(max)	> 10 µm			
Shape factor	≥ 0.6			
Calibration Factor	0.68 µm/pixel			
Objective magnification	10x			
Total magnification	100x			
Statistics	min	max	average	Std Dev
Particle size (µm)				
Limited by size	10.1	170.5	36.3	19.1
Nodule size (µm)				
Limited by size and shape	10.1	113.2	37.6	16.7

Kristiansand 23.05.2017

Approved:

B.Kroka

A.H.Amundsen

* The images shown are representative to the average of the 25 examined fields, but individual values may be outside the 95% confidence interval for the average without this being an error.

(1) The error is calculated as the 95% confidence level based on the individual analysis of 25 fields

B. Chemical Analysis Reports

B.1 EN-GJS-400-18LT



Commission: 2017-00401
To: Cathrine Hartung, Elkem AS HK
Address: Postboks 372 Skøyen, 0213 Oslo
From: Mariann Synstad
Copy: , ,
Date: 12.06.2017

ACTIF - MANDAL

Sample ID: M217 - 157
400 Jern
Approved: 12.06.17
Wilab no: A217-01628-1
Instrument Gnist
Method STOPEJERN

Unit	Parameter	Analysis
%	C	3,67
%	C (Eltra)	3,70
%	Si	1,99
%	Mn	0,296
%	P	0,020
%	S (Eltra)	0,007
%	Mg (AAS)	0,032
%	Ce	0,007
%	La	0,001
%	Cu	0,045
%	Ni	0,044
%	Cr	0,019
%	Al	0,0075
%	Ti	0,0055
%	V	0,0046
%	Mo	<0.0007
%	Zr	0,0005
%	Sn	0,0023
%	Sb	0,0012
%	Nb	0,0011
%	As	0,0025
%	Zn	0,001
%	Se	<0.0006
%	Te	0,0011
%	W	<0.003
%	Pb	<0.003
%	Bi	0,0011
%	Co	0,0072
%	B	0,0004
%	Y	0,0002
%	N*	0,0036
%	O*	0,013

*)Elements are not validated. Are therefore considered as guidance.

B.2 EN-GJS-500-14



Commission: 2017-00311
To: Cathrine Hartung, Elkem AS HK
Address: Postboks 372 Skøyen, 0213 Oslo
From: Mariann Synstad
Copy: , ,
Date: 28.04.2017



Mandal Castings 500-14 forsøk

Sample ID:	Forprøve	Sluttprøve
	-	-
Approved:	28.04.17	28.04.17
Wilab no:	A217-01246-1	A217-01247-1
Instrument	Gnist	Gnist
Method	STOPEJERN	STOPEJERN

Unit	Parameter	Analysis	Analysis
%	C	3,28	2,98
%	Si	2,53	3,68
%	Mn	0,089	0,110
%	P	0,017	0,017
%	S	0,010	0,008
%	Mg	0,0003	0,048
%	Ce	0,0020	0,0091
%	La	0,0002	0,0017
%	Cu	0,0074	0,0084
%	Ni	0,012	0,013
%	Cr	0,009	0,013
%	Al	0,0034	0,013
%	Ti	<0.0002	0,0028
%	V	0,0016	0,002
%	Mo	<0.0007	<0.0007
%	Zr	<0.0004	0,0005
%	Sn	0,0024	0,0035
%	Sb	0,0014	0,0011
%	Nb	0,0004	0,0007
%	As	0,0024	0,0024
%	Zn	<0.001	<0.001
%	Se	0,0006	<0.0006
%	Te	0,0013	0,001
%	W	<0.003	<0.003
%	Pb	<0.003	<0.003
%	Bi	0,0012	0,0007
%	Co	0,0055	0,0053
%	B	0,0005	0,0007
%	Y	0,0002	0,0002
%	N*	0,0037	0,0069
%	O*	0,0084	0,0079
%	C (Eltra)	-	3,06
%	S (Eltra)	-	0,011

*)Elements are not validated. Are therefore considered as guidance.

B.3 EN-GJS-500-7



Commission: 2017-00366
To: Cathrine Hartung, Elkem AS HK
Address: Postboks 372 Skøyen, 0213 Oslo
From: Ida Therese Gloppen
Copy: ,,
Date: 30.05.2017

Actif-W.Gierisen 500-7

Sample ID: 1 2


Approved: 30.05.17 30.05.17
Wilab no: A217-01525-1 A217-01526-1
Instrument Gnist Gnist
Method STOPEJERN STOPEJERN

Unit	Parameter	Analysis	Analysis
%	C	3,51	3,46
%	Si	2,63	2,60
%	Mn	0,360	0,357
%	P	0,029	0,029
%	S	0,003	0,003
%	Mg (AAS)	0,037	0,036
%	Ce	0,013	0,011
%	La	0,004	0,002
%	Cu	0,299	0,307
%	Ni	0,323	0,327
%	Cr	0,037	0,036
%	Al	0,019	0,019
%	Ti	0,007	0,007
%	V	0,007	0,007
%	Mo	0,002	0,001
%	Zr	0,007	0,006
%	Sn	0,017	0,016
%	Sb	<0.0005	<0.0005
%	Nb	0,001	0,001
%	As	0,003	0,003
%	Zn	0,003	0,003
%	Se	0,0006	0,0007
%	Te	0,0013	0,0013
%	W	<0.003	<0.003
%	Pb	<0.003	<0.003
%	Bi	0,0013	0,0013
%	Co	0,0081	0,0082
%	B	0,0006	0,0006
%	Y	0,0002	0,0002
%	N*	0,005	0,005
%	O*	0,010	0,010
%	S (Eltra)	0,0043	0,0038
%	C (Eltra)	3,59	3,58


C. Tensile Testing Reports

A tensile test report for EN-GJS-500-7 has not been received and is not included in the following Appendix.

C.1 EN-GJS-400-18LT



TEST REPORT



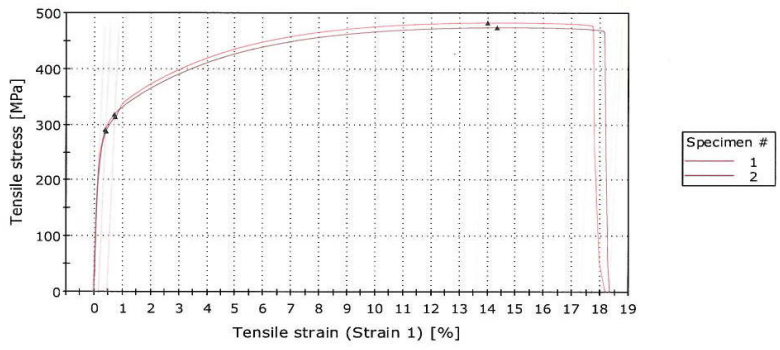
Test Standard: ISO 6892-1:2009 Method B

Customer	Elkem Foundry Products
Report no.	17-054
Task no	317-20230.01
Tester	ABR
Machine data	INSTRON 600LX
Speed to yield	30, MPa/s
Speed through yield region	0,00250 mm/mm/s
Speed after yield	0,00670 mm/mm/s

Test results

	Specimen ID	Diameter [mm]	Area [mm ²]	L0 [mm]	Rp0,2 [MPa]	FRp0,2 [kN]	Rm [MPa]	Fm [kN]	A5.65 [%]	Break Location
1	400-1	14,015	154,268	69,74	291,16	44,92	482,46	74,43	17,28	Inside GL
2	400-2	14,008	154,114	69,60	288,09	44,40	473,93	73,04	17,67	Inside GL
3	400-3	14,015	154,268	69,63	286,82	44,25	471,86	72,79	16,05	Inside GL


Specimen 1 to 2



External Inspection Signature

4. april 2017

FORCE Technology
Authorised Response Signature
TEST 269



FORCE Technology Norway
Mjovannsveien 79
4628 Kristiansand
Tel: +47 64 00 35 00
Fax: +47 64 00 37 71
info@forcetechnology.no
www.forcetechnology.no

C.2 EN-GJS-500-14



TEST REPORT



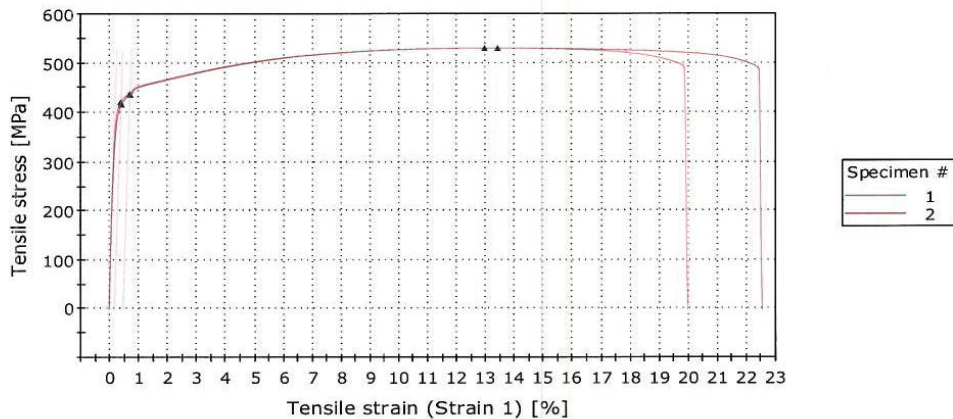
Test Standard: ISO 6892-1:2009 Method B

Customer	Elkem Foundry Products
Report no.	17-075-1
Task no	317-20230.01
Tester	ABR
Machine data	INSTRON 600LX
Speed to yield	30, MPa/s
Speed through yield region	0,00250 mm/mm/s
Speed after yield	0,00670 mm/mm/s

Test results

	Specimen ID	Diameter [mm]	Area [mm ²]	L0 [mm]	Rp0,2 [MPa]	FRp0,2 [kN]	Rm [MPa]	Fm [kN]	A5.65 [%]	Break Location
1	1B	14,076	155,614	70,29	420,95	65,51	528,97	82,31	19,54	Inside GL
2	2A	14,069	155,459	70,31	416,18	64,70	529,08	82,25	22,07	Inside GL
3	2B	14,057	155,194	70,34	417,29	64,76	527,84	81,92	18,88	Inside GL

Specimen 1 to 2



External Inspection Signature

FORCE Technology
 Authorised Respons. Signature
 TEST 269

10. mai 2017

FORCE Technology Norway
 Mjovannsveien 79
 4628 Kristiansand
 Tel +47 64 00 35 00
 Fax +47 64 00 37 11
 info@forcetechnology.no
 www.forcetechnology.no